Development and Application of Functional Magnetic Resonance Imaging in Paediatric Focal Epilepsy

Tim M. Tierney

University College London

Developmental Imaging and Biophysics,

UCL Great Ormond Street Institute of Child Health

London, U.K.

PhD Thesis

Submitted for Doctor of Philosophy Degree

November 2016

I, Tim Tierney, confirm that the work presented in this thesis is my own. Where information has been derived from other sources, I confirm that this has been indicated in the thesis.

Abstract

There are two major applications of fMRI in paediatric focal epilepsy. The first is mapping of eloquent cortex. The second is the use of simultaneous EEG-fMRI to map the epileptogenic zone. The main methodological issues faced by these fMRI applications are: motion, physiological noise, quality assurance, and statistical analysis. To address the issues of subject motion and physiological noise we constructed a simple analytical biophysical model of Blood Oxygenation Level Dependent (BOLD) signal capable of identifying and correcting these artefacts (named FIACH). This model was validated in a sample of children performing a language task with high motion levels. FIACH outperformed 6 other competitive methods of noise control. In the second study, we characterized how metrics of quality assurance could predict the clinical utility of EEG-fMRI. We also quantified the impact of a natural stimulus (a cartoon) on reducing subject motion. During this analysis it was noted that the corrections for multiple comparisons employed using Random Field Theory (RFT) at an individual level were overly conservative. This led to an exploration of RFT sensitivity and its relationship to image smoothing and degrees of freedom. By reviewing over 150 papers published in 2016 it was possible to estimate that 80% of studies suffer from a similar loss in sensitivity. Simulations are provided to help identify and prevent this loss in sensitivity. In the final study we sought to use EEG-fMRI to characterize the relationship between the brain's functional organization and Interictal Epileptiform Discharges (IEDs) in paediatric focal epilepsy. Interestingly, we identified increasing connectivity of the piriform cortex and caudate to the default mode network as a function of IEDs. This suggested a mechanism by which IEDs may propagate through functional networks in the brain.

Acknowledgements

This completion of this thesis would not have been possible were it not for the help and support of so many people.

Firstly, I would like to thank my supervisor David Carmichael who not only taught me all I know about MRI but also made it a thoroughly enjoyable experience. He always supported me in the development of my own ideas and assisted me in their execution. I also would like to thank my supervisor Chris Clark without whom I would not have even started the PhD. I was never very good with deadlines but Chris happily edited my PhD application on New Year's Eve 2012 for submission on New Year's Day 2013.

I also was incredibly lucky to be surrounded by a great group of people all working together in the Developmental Imaging Biophysics Section and the Cognitive Neurosciences and Neuropsychiatry Section of the Institute of Child Health. Ellie Shamshiri, Suejen Perani, Maria Centeno, Fabio Nery, Danilo Maziero, Torsten Baldeweg and Louise Weiss-Croft have all been fantastic colleagues and friends to work with over the course of my PhD (even when that "work" involved hiking up a hill at 1 in the morning inside the Arctic Circle).

Most importantly, I would like to thank my family. My Mom and Dad have always been my biggest champions. I can't begin to express how much that means to me and can only apologize for my infrequent trips home. I've only ever wanted to follow in your footsteps and push myself to the full extent of my abilities.

My brother Sean has been my idol as far back as I can remember and has always been a source of inspiration and drive. When I come home the highlight of my time is usually waiting up until 2/3 AM for him to get back from work so we can chat about nothing in particular. My sister Muireann has, more often than not, been a source of frustration in my life. However, now more than ever than ever I find myself looking forward to her screaming at me when I come home because I know it will have nothing to do with my PhD. And finally I would like to thank Roger, Raffa, Ben, Steffi, Fiach and Sam for listening to me ramble when no one else would.

List of Publications

Tierney T.M., Weiss-Croft L.J., Centeno M., Shamshiri E.A., Perani S., Baldeweg T., Clark C.A., Carmichael D.W. (2016): FIACH: A biophysical model for automatic retrospective noise control in fMRI. Neuroimage 124:1009–1020.

Tierney, T. M., Clark, C. A., & Carmichael, D. W. (2016). Is Bonferroni correction more sensitive than Random Field Theory for most fMRI studies? *arXiv*. Applications; Medical Physics. Retrieved from http://arxiv.org/abs/1607.08205

Shamshiri, E. a., Tierney, T. M., Centeno, M., St Pier, K., Pressler, R. M., Sharp, D. J., … Carmichael, D. W. (2016). Interictal activity is an important contributor to abnormal intrinsic network connectivity in paediatric focal epilepsy. *Human Brain Mapping*, *00*(August), 1–16.

Murta, T., Chaudhary, U., Tierney, T.M., Dias, A., Leite, M., Carmichael, D., … Lemieux, L. (2016). Phase-amplitude coupling and the BOLD signal: A simultaneous intracranial EEG (icEEG) - fMRI study in humans performing a finger-tapping task. *NeuroImage*.

Murta, T., Hu, L., Tierney, T.M., Chaudhary, U., Walker, M., Carmichael, D., … Lemieux, L. (2016). A study of the electrohaemodynamic coupling using simultaneously acquired intracranial EEG and fMRI data in humans. *NeuroImage*.

Centeno, M., Tierney, T. M., Perani, S., Shamshiri, E. a, StPier, K., Wilkinson, C., … Carmichael, D. W. (2016). Optimising EEG-fMRI for Localisation of Focal Epilepsy in Children. *PloS One*, *11*(2),

Contents

Table of Figures

Table of Tables

Table of Abbreviations

fMRI	Functional Magnetic Resonance Imaging
EEG	electroencephalogram
BOLD	Blood Oxygenation Level Dependent
FIACH	Functional Image Artefact Correction Heuristic
RFT	Random Field Theory
IED	Interictal Epileptiform Discharge
MRI	Magnetic Resonance Imaging
NMR	Nuclear Magnetic Resonance
RF	Radiofrequency
EMF	electromotive force
FOV	Field of View
EPI	Echo Planar Imaging
HRF	Haemodynamic Response Function
FC	Functional Connectivity
ILAE	International League Against Epilepsy
PDS	Paroxysmal Depolarisation Shift
FCD	Focal Cortical Dysplasia
PMG	Polymicrogyria
HS	Hippocampal Sclerosis
NOS	Nitric Oxide Synthase
NO	Nitric Oxide
GLM	General Linear Model
rs-fcMRI	Resting State Functional Connectivity MRI
TR	Repetition Time
RP	Realignment Parameter
ICA	Independent Component Analysis
PCA	Principal Component Analysis
TE	Echo Time
rTSNR	Robust Temporal Signal to Noise Ratio
PCs	Principal Components
aCompCor	Anatomical Component Correction
tCompCor	Temporal Component Correction
RPE	Realignment Parameter Expansion
MFP	Motion Fingerprint
RWLS	Robust Weighted Least Squares
PET	Positron Emission Tomography
FD	Framewise Displacement
MFD	Mean Framewise Displacement
SPM	Statistical Parametric Mapping
FWHM	Full Width at Half Maximum
FLAIR	Fluid Attenuated Inversion Recovery
SPECT	Single-photon emission computed tomography
MEG	Magnetoencephalography
SD	Standard Deviation
SE	Standard Error
IQ	Intelligence Quotient
DMN	Default Mode Network
ICN	Intrinsic Connectivity Network
Fps	Frames per second

1. Theory of NMR, MRI and fMRI

The main method utilised in this thesis is functional Magnetic Resonance Imaging. Therefore prior to discussing the issues surrounding this method's application I give a brief overview of the signal's origin.

Declaration of Contribution: This Theory section was written by Tim Tierney and was largely adapted from a combination of sources (Gadian, 1982; Haacke, Brown, Thompson, & Venkatesan, 1999)**.**

1.1 From NMR to MRI

Magnetic Resonance Imaging (MRI) is fundamentally the spatial localisation of the Nuclear Magnetic Resonance (NMR) signal. The theoretical underpinnings of MRI are therefore also shared with NMR and a certain level of understanding of NMR is required before an adequate treatment of MRI can be given. NMR is essentially the frequency selective process by which nuclei respond to magnetic fields.

This phenomenon was initially discovered by bombarding a molecular beam of Lithium with oscillating magnetic fields at the appropriate frequency (Rabi, Zacharias, Millman, & Kusch, 1938). These findings were expanded upon by demonstrating the feasibility of NMR in liquids and solids (Bloch, Hansen, & Packard, 1946; Purcell, Torrey, & Pound, 1946). This posed a major advance in the study of naturally occurring substances as the method was not restricted to work solely with atoms or molecules. Concurrently a general theory of how the NMR signal changes following the application of oscillating magnetic fields termed “Nuclear Induction” was proposed (Bloch, 1946). This laid the foundation for the understanding and theoretical treatment of MRI.

Nearly thirty years later NMR was used to create an image of water in two separate capillary tubes by linearly varying the magnetic field across the image in different directions (Lauterbur, 1973). This was in part inspired by the multiple projection approach that was used in the development of x-ray computed tomography. The method was, at the time, termed “zeugmatography”.

Even at this early stage the clinical ramifications were already apparent as it was suggested that the method could be used for the study of malignant tumours as their NMR signal was fundamentally different to that of normal tissue (Lauterbur, 1973). A number of years later the first image of a human was produced, albeit a finger (Mansfield & Maudsley, 1977). As many of the principles of MRI had been elucidated and medical interest was rising clinical trials commenced (Gadian, 1982). The use of MRI became widespread and now an estimated 2.5 million MRI examinations are carried out in the UK each year (OECD, 2015).

1.2 Nuclear Spin

1.2.1 Spin

The concept of magnetic resonance has already been introduced but not how this process arises. It arises through the quantum properties of atomic nuclei (which is why it is termed *nuclear* magnetic resonance). All fundamental particles, composite particles and atomic nuclei exhibit a property called “spin”. Spin can be *conceptualized* but not realised as magnetic dipole arising from a charged particle’s rotation around its principal axis. The behaviour of spin is therefore often mathematically described using classical mechanics and is often referred to as spin angular momentum. In contrast to classical depictions of momentum, spin angular momentum can only take on discrete values in the presence of an external magnetic field (when measurement takes place). This was illustrated by demonstrating that silver beams were deflected in the presence of a magnetic field in two directions as opposed to a continuum of possible momentums (Stern & Gerlach, 1922). However, in this thesis we adopt the classical interpretation of NMR by *conceptualising* spin as a magnetic dipole arising from a charged particle’s rotation around its principal axis.

1.2.2 The Nucleus

The nuclei of atoms are not fundamental particles and are in fact composed of protons and neutrons (collective term: nucleons) which are fundamentally composed of quarks. The spin of these quarks adds up to give a “net spin” of the nucleon referred to as “isospin”. All nucleons have isospin *(I = ½ h).* The net sum of the isospins gives the net spin angular momentum (h is Planck’s constant).

In the case of the hydrogen atom I = ½ h as the atom contains only one nucleon. However, as well as a net spin angular momentum nuclei can also have an orbital angular momentum due to the motion of the electrons. With regards to hydrogen this form of momentum is zero so the total angular momentum (J) in hydrogen is +/-½ h. This makes hydrogen an ideal system to study as its total angular momentum has a simple form.

1.3 Magnetic Moments

If a particle has a non-zero angular momentum (J) it also has a non-zero

magnetic moment (μ). In fact the magnetic moment is directly proportional to the angular momentum.

$$\mu = \gamma J = \gamma h/2 \qquad 1$$

γ is a constant of proportionality (gyromagnetic ratio). This gyromagnetic ratio is inversely proportional to the atom's mass (m) and proportional to the atom's charge (c).

$$\gamma \propto \frac{c}{2m} \qquad 2$$

When an external magnetic field (B) is applied the magnetic moment experiences a torque (N). This torque can represented as the crossproduct ($\times$) of the moment with the field.

$$N = \mu \times B \qquad 3$$

If the system experiences nonzero torque it implies that the total angular momentum of the system is changing over time.

$$N = \frac{dJ}{dt} \qquad 4$$

If the total angular momentum is changing over time it also implies that the magnetic moment is changing over time.

$$\frac{d\mu}{dt} = \gamma \frac{dJ}{dt} \qquad 5$$

By combining the information of (*3*) and (*4*) the expression for the change in magnetic moments can be formulated in a more intuitive form.

$$\frac{d\mu}{dt} = \gamma\mu \times B \qquad 6$$

This is the equation of motion for a dipole in a magnetic field and demonstrates the relationship between field strength, gyromagnetic ratio and magnetic moment.

1.4 Resonance

NMR has previously been described as the frequency selective process by which matter responds to oscillating magnetic fields but the conditions under which this phenomenon occurs have not been described.

Due to the discrete nature of spin the moments can be oriented in a fixed number of directions with respect to the magnetic field (2I +1 directions). These directions are often referred to as spin eigenstates. In the case of the hydrogen atom there are two, commonly named “spin up” and “spin down”, states. The transition between these states is accompanied by an emission of energy. This is resonance.

$$\Delta E = h\omega_0 \qquad 7$$

Where ΔE = is the change in energy, h is Planck’s constant and ω_0 is the frequency at which the magnetic moment rotates around its axis. From this equation it is important to note that, as the spin states are discrete, the frequencies at which energy will be emitted are also discrete (i.e. to observe a change in energy the applied magnetic field must oscillate at frequency ω_0). Therefore if resonance is to occur ω_0 must be known.

1.5 Precession

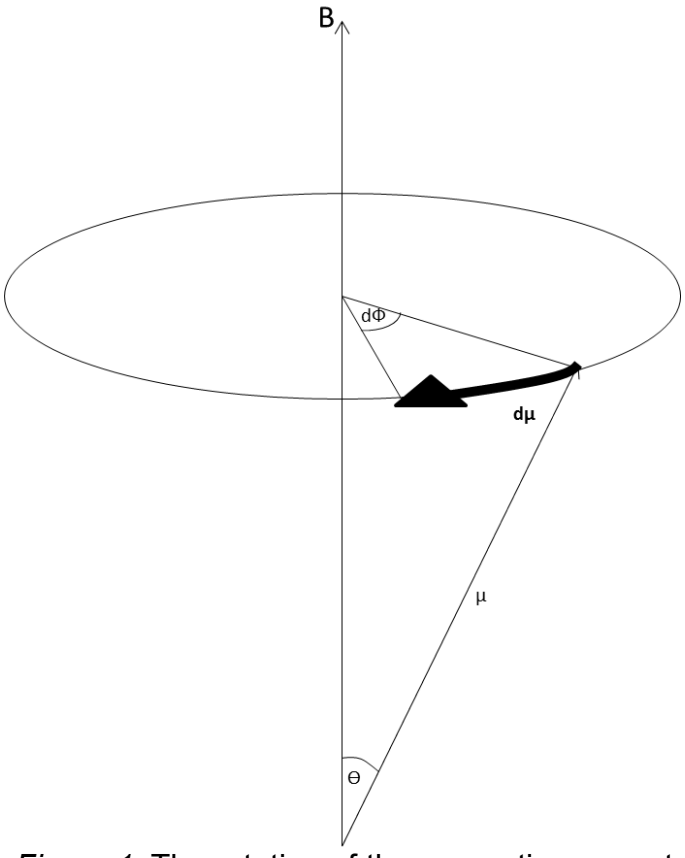

Precession in the context of NMR can be conceptualised as the rotation of the magnetic moment about its axis (a classical description). By using the laws of angular momentum we can derive the frequency at which the magnetic moment will rotate around its axis. An illustration of the system is given in *Figure 1*.

Figure 1. The rotation of the magnetic moment (μ) about the magnetic field (B).

The magnitude of $d\mu$ can be found by computing the arc length. If the angle is measured in radians the arc length is only contingent upon the radius (r) and change in angle ($d\phi$).

$$d\mu = r\, d\phi \tag{8}$$

As the vector B and μ form a right angled triangle with the circle describing the rotation of the moment, the radius can easily be derived.

$$r = \mu \sin(\theta) \tag{9}$$

However, from (6) and the rules of cross products (|A x B| = |A||B|$\sin(\theta)$) we know that

$$d\mu = \gamma \mu B \sin(\theta)\, dt \tag{10}$$

Equating (*8*) and (*10*) we find the following

$$\mu \sin(\theta) d\phi = \gamma \mu B \sin(\theta)\, dt \tag{11}$$

By expressing (11) in terms of its angular frequency the following simplification is made.

$$\frac{d\phi}{dt} = \omega_0 = \gamma B \tag{12}$$

1.6 Magnetization

At this point a caveat must be made. While these rules successfully define the precession of a single magnetic moment in an external magnetic field, single moments are not subjected to external magnetic fields. Instead populations of spins or “ensembles” of moments are subjected to external magnetic fields. The discrete behaviour of the magnetic moment (μ) no longer holds. The individual moments are no longer oriented parallel or anti parallel (their eigenstates) to the main magnetic field. Instead the distribution of angles with which the moments orient with respect to the main magnetic field is near uniform (due to nuclear interactions). There is only a slight

tendency to be aligned with the field. In the quantum mechanical framework the individual spins are said to exist in a superposition of their eigenstates.

However, the average effect of the magnetic field on the population of spins can be described by still using the equation of motion described in (*6*) with a slight adjustment. This is because the magnetization (M) is just the sum of all resonating magnetic moments (n) per unit volume (V).

$$M = \frac{1}{V}\sum_{i=1}^{n}\mu_i \qquad 13$$

Because of this fact the equation of motion now changes from describing the rotation of the magnetic moment about its access to describing the rotation of the magnetisation vector about its axis.

$$\frac{dM}{dt} = \gamma M \times B \qquad 14$$

Unfortunately this magnetisation signal is weak due to the near uniform distribution of spins states with respect to the main magnetic field. However as the magnetisation is proportional to the number of spins in the sample resonance is feasible in realistic samples which contain large amounts of magnetic moment producing particles.

$$M = N/V\frac{\hbar^2\gamma^2 B_0}{4KT} \qquad 15$$

K is the Boltzmann constant; T is the absolute temperature in Kelvin, $\hbar$ is Planck's constant and N/V is the number of spins per unit volume.

1.7 The Rotating Frame

If the magnetisation precesses about the main magnetic field there is a periodic component to all calculations involving magnetisation. By adopting a rotating frame of reference (rotating the coordinate system around Z) this periodic motion can be effectively eliminated. For instance when the coordinate system rotates at an angular frequency (ω) the equation of motion changes as follows.

$$\frac{dM}{dt} = \gamma M \times B - \omega \times M \quad (16)$$

This simplifies to the following.

$$\frac{dM}{dt} = M \times (\gamma B + \omega) \quad (17)$$

Considering (12) and if ω is chosen to equal $-\omega_0$

$$\frac{dM}{dt} = M \times (\omega_0 - \omega_0) = 0 \quad (18)$$

The magnetisation is now no longer changing with respect to time in this frame of reference.

1.8 Radiofrequency Pulses

Radiofrequency (RF) pulses are magnetic fields oscillating at the larmor frequency of the sample under investigation in order to induce resonance. As they are a magnetic field (B_1) perpendicular to B_0 they add with the main magnetic field (B_0) to produce an effective magnetic field (B_{eff}).

$$B_{eff} = \sqrt{(B_0 + \frac{\omega}{\gamma})^2 + (B_1)^2} \quad (19)$$

If ω is chosen to equal $-\omega_0$ the effective field takes on a much simpler form.

$$B_{eff} = \sqrt{(B_0 - B_0)^2 + (B_1)^2} = B_1 \quad (20)$$

Now in this rotating frame the effect of B_0 vanishes and the magnetisation rotates about B_1 with angular frequency ω_0. The angle with which the magnetisation has been rotated away from the main magnetic field is given by the following formula.

$$\theta = \gamma B_1 t \quad (21)$$

Theta is the angle rotated in radians, γ is the gyromagnetic ratio, B_1 is the strength of the magnetic field and t is the duration of the RF pulse.

1.9 Bloch Equations

The equation of motion for the magnetisation (*16*) M has already been introduced as a macroscopic equivalent for the equation of motion for the magnetic dipole (*6*). Expanding (*16*) via the crossproduct leads to the following differential equations.

$$\frac{dM_x}{dt} = \gamma M_y B_z - \gamma M_z B_y = \gamma M_y B_z \quad 22$$

$$\frac{dM_y}{dt} = \gamma M_z B_x - \gamma M_x B_z = -\gamma M_x B_z \quad 23$$

$$\frac{dM_z}{dt} = \gamma M_x B_y - \gamma M_y B_x = 0 \quad 24$$

However this is an oversimplification that does not take into account the interaction of the spins with their local environment. Bloch (1946) introduced extra terms to the equation of motion to take account of these interactions.

$$\frac{dM_x}{dt} = \gamma M_y B_z - \frac{M_x}{T_2} \quad 25$$

$$\frac{dM_y}{dt} = -\gamma M_x B_z - \frac{M_y}{T_2} \quad 26$$

$$\frac{dM_z}{dt} = -\frac{M_0 - M_z}{T_1} \quad 27$$

By transforming (*25*) and (*26*) to the rotating reference frame the following simplification can be by assuming (*18*)

$$\frac{dM_{xy}}{dt} = -\frac{M_{xy}}{T_2} \quad 28$$

By solving (*27*) and (*28*) the equations for magnetisation in the longitudinal and transverse plane can be found.

$$M_{xy}(t) = M_{xy}(0)e^{-t/T_2} \quad 29$$

$$M_z(t) = M_o + (M_z(0) - M_o)e^{-t/T_1} \quad 30$$

1.10 Relaxation

It is necessary to add the terms T1 and T2 to the equations of motion as they

account for the changes in magnetisation due to the interactions of the magnetic moments with their local environment. The time constant T1 is related to the time taken for the magnetisation to return to thermal equilibrium. The time constant T2 is related to change in magnetisation due to the interaction of magnetic moments with each other.

As already stated the values of T2 and T1 are determined by the spin ensemble's interaction with the local environment. The interaction which dominates the change in T2 and T1 is molecular motion. The correlation time (τ) describes the time taken for a molecule to undergo one full revolution. The following two expressions relate molecular motion and relaxation.

$$\frac{1}{T1} \propto \frac{\tau \, B_{xy}^2}{1 + \omega_0^2 \tau^2} \qquad 31$$

$$\frac{1}{T2} \propto \tau \, B_z^2 \qquad 32$$

1.11 T1

The first equation captures the frequency sensitive nature of T1. In essence any molecular rotations that are at or near the larmor frequency will decrease T1. While any molecular motions further away from the larmor frequency will increase the T1 of the substance. This is because the rotating molecules are producing changing magnetic fields that oscillate at the larmor frequency and essentially function as RF pulses and induce resonance. As resonance has been induced energy is lost to the surrounding environment. This keeps occurring and causes M_z to approach M_o according to (*30*).

1.12 T2

While the effect on T1 of molecular motion is frequency specific the effect of molecular motion on T2 is not. The local magnetic field can be approximately considered a sum of the externally applied field and the contribution from the magnetic fields of the other neighbouring spins. This coupled with the oscillating fields experienced due to molecular motion cause the local magnetisation to precess at different frequencies. This "fanning out" of precessional frequencies in the transverse plane results in a decrease of the net magnetisation. As this continues to happen the magnetisation tends

towards its equilibrium value of 0.

1.13 T2*

In practice after an RF pulse the decay of the magnetisation in the transverse plane is not governed by the time constant T2 but is instead governed by molecular motion and changes in the local susceptibility (indicates degree of magnetisation in response to a magnetic field). This is T2* A simple substitution updates equation (*29*).

$$M_{xy}(t) = M_{xy}(0)e^{-t/T_2^*} \quad 33$$

Where T2* is simply the sum of the effects due to T2 and the change in susceptibility and local field inhomogeneities (T2')

$$\frac{1}{T2^*} = \frac{1}{T2} + \frac{1}{T2'} \quad 34$$

This is often expressed in a more simple form using the reciprocal of the above terms

$$R2^* = R2 + R2' \quad 35$$

As this is an additive effect it means that anything that increases the magnitude of $R2'$ will increase the rate of signal decay. While at first this may seem undesirable it can be taken advantage of for the study of human brain function using a technique called functional Magnetic Resonance Imaging (fMRI).

When the energy demand of the brain increases due to neural activity blood is delivered to the site of neural activity to increase the supply of oxygen. As oxygenated blood is diamagnetic and deoxygenated blood is paramagnetic when the tissue becomes more oxygenated the susceptibility increases in magnitude and so does the magnetisation (Ogawa, Lee, Kay, & Tank, 1990). This allows for magnetisation to dynamically change over time in response to brain function. This is the theoretical basis of fMRI (The Biological basis for this technique is discussed in chapter 2).

1.14 Imaging

We have introduced how the property of spin gives rise to a

magnetic moment and how the resulting moment behaves in a magnetic field. We have also described how multiple moments (which give rise to a net magnetisation) interact with their local environment (relaxation). It has not yet been described how we detect this change or we spatially encode this information (image creation). The purpose of this thesis is largely the application of MRI in epilepsy and not the development of MRI sequences so the imaging portion of MRI is given less weight then the signal origin itself.

1.15 Signal Detection

The time varying magnetisation produced by the resonating spins in the transverse plane causes an electromotive force (emf) to be induced in any nearby conductor. This emf is equal to the negative of the changing flux (ϕ) through the conductor.

$$emf = -\frac{d\phi}{dt} \qquad 36$$

The flux that the conductor experiences is directly related to the magnetisation and the magnetic field produced by the conductor.

$$\phi(t) = \iiint M(r,t)\, B_{Receive}(r)\, d^3r \qquad 37$$

The triple integral indicates that the flux at time t is equal to the integral of the magnetisation with respect to spatial position (r) across the three spatial dimensions (d^3r). This integral is modified by the $B_{Receive}(r)$ field which if non uniform causes the flux to deviate from the expected value. By placing a RF receive coil near the sample this dynamically changing flux produces a voltage in the coil that varies with time.

1.16 Spatial Encoding and k-Space

In order to spatially encode the induced voltage magnetic field gradients are employed. These gradients vary the magnetic field linearly (usually) with respect to space. As a result the precessional frequencies vary as a function of space.

If a RF pulse is applied to a sample all the on resonance spins will produce a signal that contributes to the magnetisation. However, if a constant linear gradient is turned on in a direction normal to the plane that is intended to be imaged the resonance frequency changes as a function of position.

$$\omega(z) = \gamma(B_0 + G(z)) \quad (38)$$

By applying a RF pulse which is frequency selective for the frequency at position z defined by (*38*) only the integral of the magnetisation in that plane contributes to the induced voltage.

Having selected a slice the flux is further encoded by applying frequency encoding and phase encoding gradients. These both are linearly varying magnetic field but have different shapes. Their shape can be related to the spatial frequencies they are sensitive to by the following relations.

$$k_x(t) = \gamma \int_0^t G_x(t)dt \quad (39)$$

$$k_y(t) = \gamma \int_0^t G_y(t)dt \quad (40)$$

Essentially these integrals produce the x and y coordinates in 2 dimensional Fourier space. This space is often referred to as k-space in MRI. Therefore at time (t) the induced voltage (*36*) in the receiver by the changing magnetic flux (*37*) will represent the integral of the magnetisation (modulated by the receive field) due to the spatial frequencies dictated by the integral of the gradient waveforms (*39*

and *40*).

1.17 Image Resolution

The image resolution in the frequency encoding direction is determined by the Field of View (FOV) and the desired number of samples (N_x).

$$\Delta x = \frac{FOV_x}{N_x} \quad (41)$$

The desired number of samples is limited by time taken to acquire that line of k-space (T_x). The user may wish to keep T_x small in order to increase the speed of the sequence. This then constrains the number of points that can be acquired for a fixed sampling rate.

$$T_x = N_x \Delta t_x \quad (42)$$

Where Δt is the time between samples of the induced emf. It is sometimes referred to as the dwell time. The inverse of the dwell time is the bandwidth (Δv)

$$\Delta v_x = \frac{1}{\Delta t} \quad 43$$

The bandwidth is determined by the field of view (FOV_x), gradient strength (G_x) and gyromagnetic ratio (γ)

$$\Delta v_x = \gamma G_x FOV_x \quad 44$$

Therefore if one wishes to keep scan time low while increasing resolution bandwidth needs to be increased. If the field of view is fixed this requires stronger gradients to be utilised. Importantly if the desired FOV_x is less than the length of the object being imaged aliasing can occur on the frequency encode direction. If this occurs an anti-aliasing filter must be used to correct the resulting artefact.

For determining resolution in the phase encoding direction similar strategy can be used.

$$\Delta y = \frac{FOV_y}{N_y} \quad 45$$

The total time for acquiring N_y points in the phase encoding direction is as follows.

$$T_y = N_y T_x \quad 46$$

This means that the effective bandwidth in the phase encoding direction is much lower than in the frequency encoding direction. Therefore the number of points acquired in the phase encoding direction is limited by the time taken to acquire 1 line in the frequency encoding direction.

1.18 EPI k-Space Trajectory

k-space has been described as the Fourier space in which signal is acquired. The coordinate is dictated by the gradients. The signal at that coordinate is dictated by the flux in the coil due to the magnetisation. There are a number of strategies for optimally filling k-space known as k-space trajectories. By way of example we describe a typical EPI trajectory used for

fMRI acquisition as fMRI is the primary imaging method used in this thesis.

EPI represented a crucial step forward in the application of MRI due to the increased speed at which images could be acquired. This increase in speed was brought about by utilising the frequency encode gradients to form echoes by reversing their direction rapidly and using phase encoding "blips" to jump lines in k space following a single radiofrequency pulse. A schematic of the pulse sequence is presented in Figure 2. as well as the k-space trajectory.

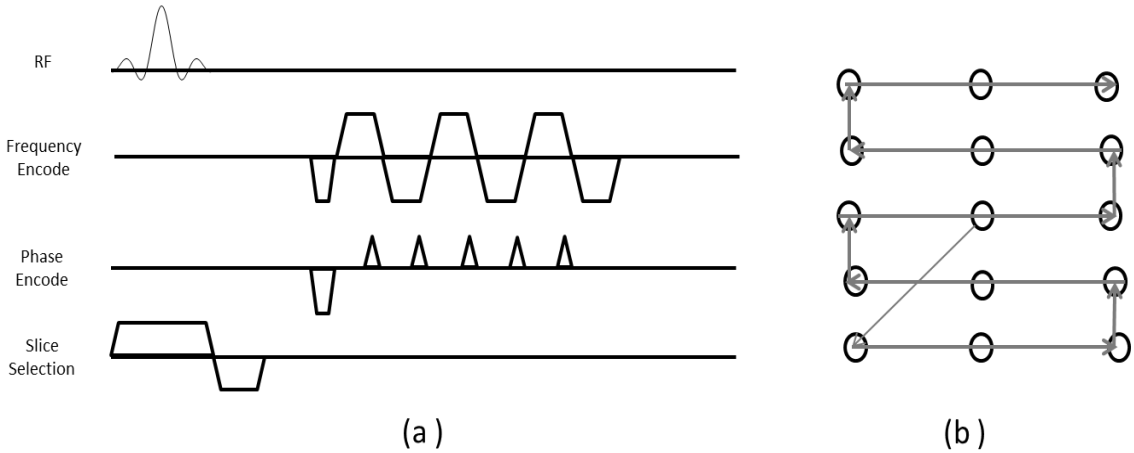

Figure 2. EPI pulse sequence diagram (a) and EPI k –space trajectory (b). In (b) circles represent sampling points

Initially the slice is excited with a frequency selective RF pulse. The positive portion of the slice selective gradient dictates the change in the resonant frequency across slices. The negative portion rephases magnetisation dephased by the gradient. The initial negative lobe of the frequency and phase encoding gradients initialise the k-space trajectory in (b) to the bottom left hand corner of k-space. The increasing integral of the frequency encode gradient waveform drives the trajectory to the right. When the integral is zero due the cancellation of the positive and negative waveform an echo is formed in the central circle of the current line of k-space. The integral then continually increases until the end of the line is reached. At this point the phase encoding blip increases the phase encode gradient integral and causes the trajectory to jump to the next line. At this point the integral of the frequency encode gradient begins to decrease due to

the negative portion of the gradient waveform and the trajectory is now sent from right to left. This zig-zag trajectory is continued until all lines of k-space are filled.

This rapid imaging is utilised in the acquisition of fMRI data to acquire T2* weighted images every few seconds which are sensitive to changes in oxygenation and therefore indirectlty to neural activity (see section 1.13 **T2**). We now give a brief overview of how fMRI is used to study nerual activity and how the data is processed.

1.19 Typical fMRI analysis pipelines

Typically fMRI data is acquired while a subject is performing a cognitive or behavioural task. As an example while in the scanner a subject may tap one of their fingers for 10-15 seconds then rest for 10-15 seconds and repeat for a predetermined amount of time (e.g. 3-10 minutes). However the signal changes in fMRI are typically small (a few percent) as T2* does not change drastically in response to neural activity. Therefore a rigorous statistical framework is employed to optimally detect these changes in neural activity. Prior to the statistical analysis a number of preprocessing steps are employed to ensure optimal analysis. There are a number of fMRI analysis strategies available in the literature but we briefly review one of the most popular: Statistical Parametric Mapping (Friston et al., 1995).

1.20 fMRI pre-processing

1.20.1 Realignment (motion correction)

As fMRI acquisition takes anywhere between 100ms and 3s per image subjects can move between acquisitions. This motion results in each successive image being out of alignment with respect to each other. However if the assumption is made that the differences between the images are purely the result of a transformation of space (and not intensity) this motion can be corrected for.

This is achieved by first calculating the partial spatial derivatives of the target image (the image we wish to be in alignment with) with respect to translation in x, y and z and rotation around the x, y and z axes (roll, pitch and yaw). These derivative images are then regressed on the difference

between the target and the source image (the image that has moved). The resulting parameter estimates define a transformation between source and target space that optimally aligns the images. If the motion is large this process is iterated using a Gauss-Newton optimisation scheme (Friston, Williams, Howard, Frackowiak, & Turner, 1996) until the desired accuracy is achieved.

1.20.2 Spatial Smoothing

Images in fMRI are often smoothed with an isotropic Gaussian kernel. This is done for three main reasons. The first is that it enhances the signal to noise ratio. Secondly it supresses the inherent anatomical variability between subjects if a group study is performed (requires averaging across subjects). The last reason smoothing is performed is that it makes the parametric assumptions of methods used to threshold statistical maps more tenable.

1.20.3 Spatial Normalisation.

If one wishes to analyse a group of subjects to determine the average neural response to a stimulus in a given population the subjects' brains must be warped into a common space. This is because neural anatomy is different between subjects making direct averaging of subjects' brains impossible. This transformation is conceptually identical to that of realignment. The only difference is that the difference between the source and target image is now modelled using non-linear warps parameterised by a basis set of 3D cosines. The Gauss-Newton optimisation is also employed in this case (Friston et al., 1995). This model can be improved by incorporating prior knowledge of the anatomy into the estimation procedure (Ashburner & Friston, 2005).

1.21 fMRI Analysis (The General Linear Model)

The analysis of a stimulus driven fMRI tells us where in the brain responded to our stimulus. Whether or not a particular brain region is declared to have been "activated" is dependent on the results of a null hypothesis significance test. This test is performed on a parameter estimate (B) obtained from a linear model. The linear model can be summarised in the following matrix equation.

$$Y = XB + \varepsilon \quad (47)$$

Essentially the data (Y) is considered to be a weighted (B) sum of independent variables (X) with additive noise (ε). The time course (X) that we fit to our data (Y) is obtained by convolving the stimulus timings with a Haemodynamic Response Function (HRF). This HRF captures how we expect the T2* weighted signal to change in response to a stimulus (Buxton, Uludağ, Dubowitz, & Liu, 2004) and is depicted in Figure 3.

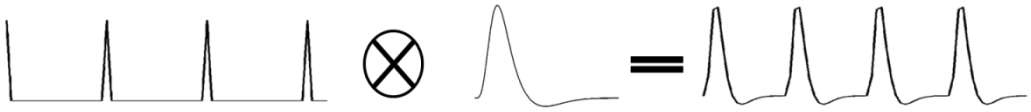

Figure 3. Convolution of stimulus with HRF.

1.21.1 Parameter estimation

It can be shown that that there is an analytical solution to estimating B if we choose to minimise the sum of square error ($\varepsilon^T\varepsilon$). This solution is as follows:

$$B = (X^T X)^{-1} X^T Y \quad (48)$$

However, this direct solution is numerically unstable as the formation of the inner product can be poorly conditioned. To avoid this decompositions of X are used to solve this equation instead of this direct solution. One highly stable method is the pseudo inverse method which is implemented by singular value decomposition of X. The pseudoinverse of X is often symbolised as X^+. Therefore to estimate B becomes

$$B = X^+ Y \quad (49)$$

1.21.2 Standard Error estimation

Once the parameter is estimated it is converted into t-value by dividing the parameter (B) by its standard error (SE)

$$t = \frac{B}{SE} \quad (50)$$

The standard error is computed as follow

$$SE = \sqrt{\frac{(X^T X)^{-1} \varepsilon^T \varepsilon}{df}}$$

The df term in the denominator represents the degrees of freedom. In the case where the matrix (X) is not rank deficient (columns are linearly independent) is simply the number of time points minus the number of parameters estimated.

1.21.3 Random Field Theory

This process of calculating t-values and standard errors is done at every voxel resulting in a large number of t values being computed. As such the chance of false positives is high. To control for these false positives a multiple comparisons correction procedure known as Random Field Theory is employed (Worsley, Evans, Marrett, & Neelin, 1992). This technique is unique in that it unites the fields of topology with probability by noticing that at high statistical thresholds the Euler Characteristic (a topological property) counts the number of local maxima in a statistical map. The Euler characteristic can therefore be thought of as asymptotically being a p-value as it calculates the expectation of the number of maxima above a given threshold. In one formalism (Adler, 1976) the Expectation (E) of the Euler characteristic ($\chi(A)$) for a zero mean, unit variance Gaussian Random Field of volume (V) can be calculated as follows

$$E\{\chi(A)\} = V(2\pi)^{-2} \, |A|^{\frac{1}{2}} \, (t^2 - 1) e^{\frac{-t^2}{2}} \qquad 52$$

Where $|A|^{\frac{1}{2}}$ is the square root of determinant the spatial covariance matrix and t is the statistical threshold. This work has been extended by (Worsley et al., 1996) who provide Euler characteristics for many different statistical fields (t, F, chi squared and Gaussian).

1.22 fMRI Analysis (functional connectivity)

Functional connectivity is a branch of fMRI analysis that aims to understand the functional organisation of the human brain. (Biswal, Yetkin, Haughton, & Hyde, 1995) reported that this was possible even in the

absence of an explicit task by demonstrating correlations between brain regions (which can be considered nodes in a network) when the subject was at rest. This was of great interest to the neuroscience community as it meant it was possible to probe neural function without an explicit task. This was advantageous for studying populations of wide age range and cognitive ability who may struggle to perform some tasks in the scanner. Subsequent studies have demonstrated that functional connectivity at rest is capable of explaining explain individual variability in brain activity, perceptual efficiency and IQ (Tavor et al., 2016; van den Heuvel, Stam, Kahn, & Hulshoff Pol, 2009)

1.22.1 Stationary connectivity

Stationary connectivity is the study of the brains functional connectivity over long time periods (5-10 minutes). This mode of analysis has found that the brain can be organised into Intrinsic Connectivity Networks (ICNs). These ICNs are characterised by a high degree of statistical similarity between the time courses of the brain regions that comprise the ICN (Smith et al., 2009).These brain regions can be thought of as nodes in a network. The similarity between these nodes is often measured with a correlation coefficient. If the correlation exceeds some predefined statistical threshold (e.g. using Random Field theory) we can conclude that these nodes are connected. Due to the linear nature of this analysis the general theory is exactly the same as that of the General Linear Model. The difference being that instead of X representing a stimulus X now represents a time course of neural activity obtained from fMRI.

1.22.2 Non stationary/dynamic connectivity

One of the limitations of the stationary approach to measuring functional connectivity is that it assumes that nodes in a network do not change their connectivity over time. Recent work has sought to explore whether it is possible for fMRI to explore the dynamics of functional connectivity (how connectivity changes over time). The use of dynamic connectivity (Zalesky, Fornito, Cocchi, Gollo, & Breakspear, 2014), typically involves windowing data into overlapping temporal segments and then calculating metrics of functional connectivity (again linear correlation).

However, it is debated as how data should be windowed to extract meaningful information (Lindquist, Xu, Nebel, & Caffo, 2014)

Techniques such as phase synchrony circumvent this issue by creating an instantaneous measure of synchrony within a network (Glerean, Salmi, Lahnakoski, Jääskeläinen, & Sams, 2012) which is claimed to be more sensitive than a sliding window based approach (Omidvarnia et al., 2016). These phase synchrony approaches typically utilise Hilbert transforms to transform the data into a space where the phase of a time course can be measured over time $(\theta_n(t))$. The synchrony (connectivity) between phase time courses is then easy established by performing a circular average across the phase time courses

$$R(t)e^{-i\phi(t)} = \frac{1}{N}\sum_{n=1}^{N} e^{-i\theta_n(t)} \quad 53$$

The parameter $R(t)$ then represents the synchrony over time with a value of 1 representing complete synchrony and 0 representing complete asynchrony.

The phase synchrony based approach has seen successful application in traumatic brain injury where the phase synchrony can be summarised with metrics such as metastability (Hellyer, Scott, Shanahan, Sharp, & Leech, 2015). This metric of metastability is simply the standard deviation of $R(t)$ In essence this metric directly measures the variability of functional connectivity over time with larger values indicating less temporally stable ICNs and lower values indicating more temporally stable ICNs.

1.23 References

Adler, R. J. (1976). On generalising the notion of upcrossings to random fields. *Advances in Applied Probability*, *8*(4), 789. http://doi.org/10.2307/1425934

Ashburner, J., & Friston, K. J. (2005). Unified segmentation. *NeuroImage*, *26*(3), 839–51. http://doi.org/10.1016/j.neuroimage.2005.02.018

Biswal, B., Yetkin, F. Z., Haughton, V. M., & Hyde, J. S. (1995). Functional connectivity in the motor cortex of resting human brain using echo-planar MRI. *Magnetic Resonance in Medicine : Official Journal of the*

Society of Magnetic Resonance in Medicine / Society of Magnetic Resonance in Medicine, *34*(4), 537–41. http://doi.org/10.1002/mrm.1910340409

Bloch, F. (1946). Nuclear induction. *Physical Review*, *70*(7-8), 460–474. http://doi.org/10.1103/PhysRev.70.460

Bloch, F., Hansen, W. W., & Packard, M. (1946). The Nuclear Induction Experiment. *Physical Review*, *70*(7-8), 474–485. http://doi.org/10.1103/PhysRev.70.474

Buxton, R. B., Uludağ, K., Dubowitz, D. J., & Liu, T. T. (2004). Modeling the hemodynamic response to brain activation. *NeuroImage*, *23 Suppl 1*, S220–33. http://doi.org/10.1016/j.neuroimage.2004.07.013

Friston, K. J., Ashburner, J., Frith, C. D., Poline, J.-B., Heather, J. D., & Frackowiak, R. S. J. (1995). Spatial registration and normalization of images. *Human Brain Mapping*, *3*(3), 165–189. http://doi.org/10.1002/hbm.460030303

Friston, K. J., Holmes, A. P., Worsley, K. J., Poline, J.-P., Frith, C. D., & Frackowiak, R. S. J. (1995). Statistical parametric maps in functional imaging: A general linear approach. *Human Brain Mapping*, *2*(4), 189–210. http://doi.org/10.1002/hbm.460020402

Friston, K. J., Williams, S., Howard, R., Frackowiak, R. S., & Turner, R. (1996). Movement-related effects in fMRI time-series. *Magnetic Resonance in Medicine*, *35*(3), 346–55.

Gadian, D. (1982). *Nuclear Magnetic Resonance and its Applications to Living Systems*. New York: Oxford University Press.

Glerean, E., Salmi, J., Lahnakoski, J. M., Jääskeläinen, I. P., & Sams, M. (2012). Functional Magnetic Resonance Imaging Phase Synchronization as a Measure of Dynamic Functional Connectivity. *Brain Connectivity*, *2*(2), 91–101. http://doi.org/10.1089/brain.2011.0068

Haacke, E. M., Brown, R. W., Thompson, M. R., & Venkatesan, R. (1999). *Magnetic Resonance Imaging: Physical Principles and Sequence Design*. Wiley-Blackwell.

Hellyer, P. J., Scott, G., Shanahan, M., Sharp, D. J., & Leech, R. (2015). Cognitive Flexibility through Metastable Neural Dynamics Is Disrupted by Damage to the Structural Connectome. *Journal of Neuroscience*, *35*(24), 9050–9063. http://doi.org/10.1523/JNEUROSCI.4648-14.2015

Lauterbur, P. C. (1973). Image Formation by Induced Local Interactions: Examples Employing Nuclear Magnetic Resonance. *Nature*. http://doi.org/10.1038/242190a0

Lindquist, M. A., Xu, Y., Nebel, M. B., & Caffo, B. S. (2014). Evaluating dynamic bivariate correlations in resting-state fMRI: A comparison study and a new approach. *NeuroImage*, *101*, 531–546. http://doi.org/10.1016/j.neuroimage.2014.06.052

Mansfield, P., & Maudsley, A. A. (1977). Medical imaging by NMR. *British Journal of Radiology*, *50*, 188–194. http://doi.org/10.1259/0007-1285-50-591-188

OECD. (2015). *"Medical technologies", in Health at a Glance 2015: OECD Indicators*. Paris: OECD Publishing.

Ogawa, S., Lee, T. M., Kay, A. R., & Tank, D. W. (1990). Brain magnetic resonance imaging with contrast dependent on blood oxygenation. *Proceedings of the National Academy of Sciences of the United States of America*, *87*(24), 9868–72.

Omidvarnia, A., Pedersen, M., Walz, J. M., Vaughan, D. N., Abbott, D. F., & Jackson, G. D. (2016). Dynamic regional phase synchrony (DRePS). *Human Brain Mapping*, *37*(5), 1970–1985. http://doi.org/10.1002/hbm.23151

Purcell, E., Torrey, H., & Pound, R. (1946). Resonance Absorption by Nuclear Magnetic Moments in a Solid. *Physical Review*, *69*(1-2), 37–38. http://doi.org/10.1103/PhysRev.69.37

Rabi, I., Zacharias, J., Millman, S., & Kusch, P. (1938). A New Method of Measuring Nuclear magnetic Moment. *Physical Review*, *53*(February), 318. http://doi.org/10.1103/PhysRev.53.318

Smith, S. M., Fox, P. T., Miller, K. L., Glahn, D. C., Fox, P. M., Mackay, C. E., … Beckmann, C. F. (2009). Correspondence of the brain's functional architecture during activation and rest. *Proceedings of the National Academy of Sciences of the United States of America*, *106*(31), 13040–5. http://doi.org/10.1073/pnas.0905267106

Stern, O., & Gerlach, W. (1922). Der experimentelle Nachweis der Richtungsquantelung im Magnetfeld. *Phyzik*, *9*, 349–352.

Tavor, I., Parker Jones, O., Mars, R. B., Smith, S. M., Behrens, T. E., & Jbabdi, S. (2016). Task-free MRI predicts individual differences in brain activity during task performance. *Science (New York, N.Y.)*, *352*(6282), 216–20. http://doi.org/10.1126/science.aad8127

Van den Heuvel, M. P., Stam, C. J., Kahn, R. S., & Hulshoff Pol, H. E. (2009). Efficiency of functional brain networks and intellectual performance. *The Journal of Neuroscience : The Official Journal of the Society for Neuroscience*, *29*(23), 7619–7624. http://doi.org/10.1523/JNEUROSCI.1443-09.2009

Worsley, K. J., Evans, A. C., Marrett, S., & Neelin, P. (1992). A three-dimensional statistical analysis for CBF activation studies in human brain. *Journal of Cerebral Blood Flow and Metabolism : Official Journal of the International Society of Cerebral Blood Flow and Metabolism*, *12*(6), 900–18. http://doi.org/10.1038/jcbfm.1992.127

Worsley, K. J., Marrett, S., Neelin, P., Vandal, A. C., Friston, K. J., & Evans, A. C. (1996). A unified statistical approach for determining significant signals in images of cerebral activation. *Human Brain Mapping*, *4*(1), 58–73.

Zalesky, A., Fornito, A., Cocchi, L., Gollo, L. L., & Breakspear, M. (2014). Time-resolved resting-state brain networks. http://doi.org/10.1073/pnas.1400181111

2. Epilepsy

This chapter gives a brief overview of epilepsy, its clinical presentation, aetiology, and neurophysiology. It also outlines the role MRI has in epilepsy and what needs to be improved in fMRI if the technique is to be clinically applied in the context of paediatric focal epilepsy.

Declaration of Contribution: This introduction was written by Tim Tierney.

2.1 Epilepsy

Epilepsy is described by the International League Against Epilepsy (ILAE) as a disease of the brain where at least one of the following conditions is met (Fisher, 2014):

1. At least two unprovoked (or reflex) seizures occurring >24 h apart,

2. One unprovoked (or reflex) seizure and a probability of further seizures similar to the general recurrence risk (at least 60%) after two unprovoked seizures, occurring over the next 10 years.

3. Diagnosis of an epilepsy syndrome

The exact world-wide prevalence of the disease is difficult to estimate (Bell, Neligan, & Sander, 2014). However, some estimates of prevalence lie between 1.5% and 5% (Sander & Shorvon, 1996) in the developed and developing world. This is slightly higher in comparison to (Ngugi, Bottomley, Kleinschmidt, Sander, & Newton, 2010) who estimate a median prevalence of approximately 5.8 per 1000 population in higher income countries, 10.3 per 1000 in the urban areas of lower income countries and 15.8 per 1000 in the rural areas of lower income countries. It is also notable that while incidence rates are higher in lower income countries lifetime prevalence is broadly similar across countries (Bell et al., 2014). This has been explained as a result of increased risk of premature death in lower income countries (Bell et al., 2014).

In the population of individuals who have seizures an estimated 30-40% will respond poorly to the medication designed to prevent seizures (Cascino, 2008). The increased burden seizures play in the lives of individuals who do not respond to medication can result in disruption to education and cognitive ability (Berg & Scheffer, 2011). Furthermore, everyday activities like crossing a road or driving a car can suddenly become incredibly dangerous if seizures are accompanied with loss of awareness or motor control.

These are not trivial issues and not only place a burden on the family caring for the individual with epilepsy (Jones & Reilly, 2016) but on the healthcare system trying to treat the individual. It was estimated in the United States that the direct cost of epilepsy per year per individual lies between

10000$ and 50000$ (Begley & Durgin, 2015). It has been further noted that these costs inflate when the individual does not respond to medication (Begley & Durgin, 2015) or has a comorbid condition (Wilner, Sharma, Thompson, Soucy, & Krueger, 2014). All these reasons motivate the need for research that can improve the effectiveness of current treatments. However, before we discuss the possibility of improvements we must first discuss in greater depth the aetiology and clinical presentation of an individual with epilepsy.

2.2 Seizures

A seizure is defined as “a transient occurrence of signs and/or symptoms due to abnormal excessive or synchronous neuronal activity in the brain” (Fisher, 2014). The terminology surrounding seizures and epilepsy has changed over the last few decades. Using terms such as “grand mal”, “catastrophic” and “complex partial” to describe seizures is no longer recommended (Fisher, 2016). The emotional undertone to these classifications is clear and the potential to mislead a patient into thinking their seizures are more complicated/harmful than others is not helpful. The ILAE has chosen to binarise their definition of the seizure into generalised and focal seizures (Fisher, 2016).The distinction made between generalised and focal is with regards to the origin of the seizure. If the seizure is regarded as having originated within brain networks limited to one hemisphere it is classified as focal (Berg & Scheffer, 2011). If the seizure is regarded as having originated within bilaterally distributed networks it is considered generalised (Berg & Scheffer, 2011).

Focal seizures can be further classified as to the extent they exhibit motor or non-motor symptoms. If motor symptoms are exhibited they can be described as tonic (stiffening of muscles), myoclonic (sudden and brief (<100 ms) contraction of muscles), atonic (loss of muscle tone without preceding myoclonic or tonic event), clonic (rhythmic contraction and relaxation of muscles), tonic-clonic (combination of tonic and clonic), epileptic spasms (flexion, extension or mixed flexion-extension of mainly truncal muscles (lasting longer than myoclonic but not as long as tonic)) or hypermotor (prominent bilateral motion, thrashing, kicking, hugging).

Non motor signs may also be present and should be described as sensory (e.g. auditory/olfactory/visual sensation), cognitive (e.g. aphasia, hallucinations, memory impairment), emotional (e.g. fear, laughter, pleasure, anxiety) or autonomic (nausea, vomiting, cold, hot). Lastly, the individual's awareness should be noted (aware/not aware/unknown awareness). As the purpose of this thesis regards the examination of children with focal epilepsy we will not consider generalised epilepsy further. The interested reader is directed elsewhere (Fisher, 2016) for a comprehensive overview of the classification of generalised seizures in non-focal epilepsy.

2.3 The Neurophysiology of Seizures, Interictal Epileptiform Discharges, and EEG

Seizures have already been described as a transient occurrence of "signs and/or symptoms due to abnormal excessive or synchronous neuronal activity in the brain" (Fisher, 2014). This definition clearly links abnormal neural behaviour to outwardly observable clinical correlates. However, isolated, brief and excessive synchronous brain activity can also occur in the absence of clinical correlates. This type of activity is not limited to individuals with epilepsy and is estimated to be observable in 1-5% of the normal population (Kasteleijn-Nolst Trenité & Vermeiren, 2005; Okubo et al., 1994). These events are referred to as Interictal Epileptiform Discharges (IEDs), in individuals with epilepsy, and have a controversial relationship to cognition and clinical treatment (Sanchez Fernandez, Loddenkemper, Galanopoulou, & Moshe, 2015). Regardless of whether the hypersynchronous activity has outward clinical correlates or not the origin of this synchrony is of interest as it may elucidate the mechanisms by which focal epilepsy can be treated.

Most theories concerning the neurophysiological underpinnings of epileptic events relate their occurrence to an imbalance of excitation and inhibition of neural activity. At a single cell level epileptic events are a result of a Paroxysmal Depolarisation Shift (PDS).

The following description of the PDS has largely been adapted from (Bromfield, Cavazos & Sirven, 2006). The PDS is the result of the sustained depolarisation of a neuron which allows a burst of action potentials to occur.

The burst of action potentials is a result of the influx of Ca^{++} from the extracellular environment. This then opens the voltage gated Na^{+} which allows for a sudden inflow of Na^{+} causing production of action potentials. Subsequently a rapid repolarisation occurs to restore the negative resting potential. However, this process overshoots resulting in a more negative potential than which the cell started with (this is termed hyperpolarisation). This is mediated by either the outflow of K^{+} ions or the inflow of Cl^{-} ions. The epileptic events can then spread to the rest of the brain by a number of mechanisms. This can be by accumulation of Ca^{++} in presynaptic terminals which causes excess neurotransmitter release or the excess K^{+} in the extracellular environment can result in depolarisation of neighbouring neurons.

It is worth noting that while the PDS is occurring at a cellular level in the clinical environment cellular level recordings are not made. Instead an Electroencephalogram (EEG) is used to measure the brain's electrical activity. The EEG was initially utilised in humans by Hans Berger in 1924 but published later (Berger, 1929). EEG utilises electrodes placed on the scalp to measure the brain's electrical activity. As the measurement takes place on the scalp we do not measure individual cells but the vector sum of the dipoles produced by the cells. The dipole produced by the cell is the difference in charge between the positively charged cell body and the negatively charged dendrites. The number of cells required to fire synchronously to get observable signal is on the order of 50000 cells (Da Silva, 2010). Furthermore, the ability to observe signal at the electrode site fades the further the source is from the scalp. EEG is therefore predominantly sensitive to neurons near the surface of the cortex. However, even with this limited spatial resolution EEG is of significant clinical value as it can assist in the detection of epileptic events, determine seizure type or help support diagnosis of epilepsy (Panayiotopoulos, 2010).

2.4 Epilepsy Aetiology

Up until now a descriptive account of epilepsy has been given by including the mechanisms by which seizures occur, their clinical presentation and the medical/financial ramifications they have. We have not described

what might cause these events. We now give an aetiological account of epilepsy with particular attention paid to some of the focal epilepsies that were studied in this thesis. Epilepsy is ultimately a disease defined by a common symptom: the seizure. However there are a wide variety of causes. The aetiologies advocated by the ILAE include the following: Genetic, Structural/Metabolic, Unknown (Berg et al., 2010). The children studied in this thesis largely fell under the categories of structural/metabolic (~50%) or unknown (~50%). The structural aetiologies largely consisted of focal cortical dysplasia, polymicrogyria, hippocampal sclerosis, and stroke.

2.4.1 Focal Cortical Dysplasia

Focal Cortical Dysplasia (FCD) is a malformation of cortical development that disrupts the typical layered structure of the cortex. The ILAE has proposed a three tiered structure for the classification of FCDs (Blümcke et al., 2011)FCD type I can be characterised by the presence of abnormal radial cortical lamination (type 1a), abnormal tangential cortical lamination (type Ib) or both (type Ic). Type II FCDs are defined by the presence of dysmorphic neurons (type IIa) or the presence of both dysmorphic neurons and balloon cells (type IIb). Type III FCD can be characterised by abnormal cortical lamination with an accompanying lesion (hippocampal sclerosis-Type IIIa, glial or glioneuronal tumour- Type IIIb, vascular malformation – Type IIIc, any other acquired lesion during the early life period – Type IIId).

2.4.2 Polymicrogyria

Polymicrogyria (PMG) is another cortical malformation that can be characterized by large quantities of small irregular gyri in the cerebral cortex. When viewed with MRI an abnormal appearance of the cortical surface is observed. It is thought that the onset of PMG is in the later stages of neuronal migration (Barkovich, Kuzniecky, Jackson, Guerrini, Dobyns, 2005) with causes linked to ischemia, infection and genetic mutation (Wang et al., 2015).

2.4.3 Hippocampal Sclerosis

Hippocampal Sclerosis (HS) is one of the most common histopathological findings when surgery is performed in adults (Blümcke et al., 2013). It has been found in a surgical series of over 5000 adult patients with drug resistant

epilepsy that over 33% had hippocampal sclerosis (Blümcke & Spreafico, 2012). HS is subdivided into three subtypes according to the ILAE (Blümcke et al., 2013) depending on the location of cell loss within the hippocampus. Type I is characterised by neuronal cell loss predominantly in CA1 and CA4 with accompanying gliosis. Type II is characterised by predominant cell loss in CA1 and gliosis. Type III is characterised by predominant cell loss in CA4 and gliosis.

2.4.4 Stroke

Post-stroke epilepsy is a common occurrence, particularly in older adults (Olsen, 2001). Seizures have been reported to occur in approximately 10% of patients following stroke (Burn et al., 1997). However, there are some subtleties to the presentation of seizures following stroke. Approximately 5% of patients will experience seizures within the first two weeks following stroke and a further 5% experience seizures after two weeks (Olsen, 2001). This does not mean however that all individuals who have seizures will go on to receive a diagnosis of epilepsy. Approximately 3.8% of individuals with stroke in one study (over a five year follow up period) had recurrent seizures and therefore qualified for a diagnosis of epilepsy (Burn et al., 1997). The mechanism that allows for seizures to occur in some stroke patients and not others is poorly understood but one hypothesis is that the surrounding area (the penumbra) containing excess excitotoxic glutamate may play a role in generating the early onset seizures (Olsen, 2001).

2.5 The contribution of MRI to Epilepsy

Many of the structural problems described would not be easy to diagnose were it not for MRI and as a result MRI is now considered mandatory for diagnosis (Cross et al., 2006). Advanced post processing methods have further helped with detection of structural abnormalities, particularly in FCD (Colliot et al., 2006; El Azami et al., 2016; Mellerio et al., 2014; Riney, Chong, Clark, & Cross, 2012) and HS (Maccotta, Moseley, Benzinger, & Hogan, 2015). However, there is currently very little agreement on the exact MRI sequences that should be used. Recent recommendations state that at a minimum a 3D T1-weighted gradient echo, coronal T2-weighted and axial Fluid Attenuated Inversion Recovery (FLAIR) should be

utilised (Mouthaan et al., 2016). That being said MRI is continually evolving and with the advent of higher field strengths (7 tesla) patients that were previously classified as being “MR-Negative” now can successfully have lesions identified that are histophatologically confirmed (De Ciantis et al., 2016). Once these lesions have been identified a neurosurgeon can resect the tissue in an attempt to alleviate the seizures.

In many cases traditional radiological review of MRI or advanced post processing of structural images can be uninformative. For instance, in the sample of patients with focal epilepsy included in this thesis nearly 50% (at the time of writing) do not have a known structural aetiology. In this sample it is clear that other methods for delineating the epileptic focus are required. In this case the use of simultaneous EEG and functional Magnetic Resonance Imaging (fMRI) has shown promise.

The goal of simultaneous EEG-fMRI is to harness both the strengths of EEG (high temporal resolution and direct measure of neural activity) with the strengths of fMRI (high spatial resolution and access to deep sources) to map the epileptic events observed with EEG. The combination of these two techniques has successfully allowed for the mapping of epileptic networks (Gotman & Pittau, 2011; Rosenkranz & Lemieux, 2010) and identification of the epileptic focus (Pittau, Dubeau, & Gotman, 2012; Salek-Haddadi et al., 2006; Thornton et al., 2010). There is also evidence that the combination of EEG-fMRI can result in the prediction of surgical outcome (Chaudhary et al., 2012; Fahoum et al., 2012).

The use of fMRI without EEG is capable of mapping the parts of the brain responsible for the production of meaningful speech (Duncan, Winston, Koepp, & Ourselin, 2016). This is important as careful tailoring of surgery, particularly in children, can have a positive impact on cognitive ability in the long-term (Skirrow et al., 2015). The procedure has been widely adopted across Europe with 20/22 centres (from a recent survey) reporting utilisation for the purpose of mapping eloquent cortex (Mouthaan et al., 2016). Previously the highly invasive Wada test has been utilised to map eloquent cortex but fMRI has shown high rates of concordance with Wada testing (Janecek et al., 2013) and does not come with the following risks: seizures,

status epilepticus, internal carotid artery vasospasm, inadvertent injection of anaesthetic in the external carotid artery (Beimer, Buchtel, & Glynn, 2015). It has been suggested by some that non-invasive methods such as fMRI should completely replace Wada testing (Papanicolaou et al., 2014). For all these reasons fMRI is clearly a valuable tool in the clinical care of individuals with epilepsy. However, fMRI is not without its drawbacks.

2.6 Problems with the Application of fMRI in the Context of Paediatric Focal Epilepsy

2.6.1 fMRI is an indirect Measure

The first problem associated with fMRI is that it is an indirect measure of neural activity. Before we describe why this is a problem it is worth reviewing the basic biological mechanism by which fMRI signal is determined.

The fMRI signal is weighted towards changes in magnetic susceptibility (a property of an object that determines the degree to which the object can be magnetised in an external magnetic field). These changes in magnetic susceptibility occur because the oxyhaemoglobin (a diamagnetic substance) concentration in the blood changes when neural activity increases. As oxyhaemoglobin concentration increases the fMRI signal increases also. The relationship between the activity of the neurons and the increase in oxyhaemoglobin is a complex one.

There are three primary mechanisms by which this interaction is mediated. The first is that glutamate released by excitatory neurons binds to interneurons containing Nitric Oxide Synthase (NOS) resulting in the opening of Ca^{++} channels. The influx of Ca^{++} causes the NOS to activate and produce Nitric Oxide (NO). NO then diffuses out of the cell and acts on smooth muscle cells of arterioles to produce vasodilation (Drake & Iadecola, 2007). This increase in vasodilation results in decreased vascular resistance which in turn gives rise to increased flow. This increase in blood flow means more oxygen is delivered to the site of neural activity and thus the fMRI signal increases. Another hypothesis is that astrocytes are activated by the excitatory neurons and release NO at their feet which are in contact with the

smooth muscle wall of the arterioles resulting in the vasodilation (Toda, Ayajiki, & Okamura, 2009). The last mechanism is more direct where nitrergic neurons can directly release NO and act directly on the vessel walls (Toda & Okamura, 2003).

This complex sequence of events that gives rise to fMRI signal is far removed from neural activity that generated it. Furthermore while neural activity can give rise to fMRI signal not all fMRI signal is related to neural activity. For instance changes in heart rate or respiration give rise to changes in blood flow and oxygen but are not necessarily associated with neural activity (Birn, Diamond, Smith, & Bandettini, 2006). This is further confounded in the paediatric context where variables such as Cerebral Blood Flow and haematocrit are different to adult populations (Hales, Kawadler, Aylett, Kirkham, & Clark, 2014; Hales, Kirkham, & Clark, 2015). Careful modelling of these effects is required to ensure that the application of fMRI in a clinical context is not confounded.

2.6.2 Motion and Quality Assurance

Motion is perhaps one of the biggest confounds experienced by researchers working with any age group (Friston, Williams, Howard, Frackowiak, & Turner, 1996; Lemieux, Salek-Haddadi, Lund, Laufs, & Carmichael, 2007; Wilke, 2012). This can be such a large confound in younger populations that scan success rate is very low (Yerys et al., 2009). In the research context exclusion of these subjects is suboptimal because it can lead to sampling bias (Wylie, Genova, DeLuca, Chiaravalloti, & Sumowski, 2014) where individuals with behavioural problems or low cognitive ability are never examined. In the clinical context this is not typically possible because the results from a single subject are of interest rather than a group or population. Furthermore with scan costs currently at approximately 500£ an hour a failed scan is a significant cost to the health service. It is therefore necessary to remedy this issue.

On a related note if a researcher/clinician is suspicious that the data is of poor quality and not of sufficient standard for inference to be made how do they objectively establish this without looking at their results first? Prior to this thesis no study utilising EEG-fMRI in a clinical context had ever

discussed this issue. Considering the variability in subject compliance in paediatric populations this is of crucial concern if EEG-fMRI is to be used clinically.

2.6.3 Statistical Analysis

There has, in the last few years, been considerable debate concerning the application/misapplication/validity of statistical inference in fMRI, particularly parametric statistical inference (Bennett, Baird, Miller, & Wolford, 2011; Bennett, Wolford, & Miller, 2009; Eklund, Nichols, & Knutsson, 2016; Flandin & Friston, 2016). This can have severe ramifications in the clinical environment as typically inference in the individual is required and increased false positive/false negative rates undermine the transition of the technique to the clinical environment. If statistical methods cannot be automated due to poor validity then the transition from fMRI being a research tool to clinical tool will halt. It is therefore necessary to characterise when these methods can and cannot be used in the application to clinical data.

2.6.4 The Effect of IEDs on the Brain's Functional Organisation.

It has previously been discussed that IEDs have a complex relationship to cognition (Sanchez Fernandez et al., 2015). They have an even more complex relationship to clinical treatment (Sanchez-Fernandez et al, 2015) yet these events have largely been ignored in the literature on EEG-fMRI in terms of their ability to disrupt the brains functional organisation (Centeno & Carmichael, 2014).

Typically reduced connectivity within ICNs and increased connectivity between ICNs is observed (Ibrahim, Morgan, et al., 2014) in patients with epilepsy. However this is often found when simultaneous EEG has not been acquired (Centeno & Carmichael, 2014). This is a prerequisite for accurate inference when studying ICNs using fMRI as IEDs can be an important contributor to abnormal ICN connectivity (Shamshiri et al., 2016) over long time scales in addition to their immediate effects on network topology (Ibrahim, Cassel, et al., 2014). However, the association between ICN connectivity and IEDs has previously been limited to stimulus driven connectivity (Shamshiri et al., 2016) and it is still uncertain how ICN connectivity may be modulated in the absence of stimuli. Furthermore

considering there is evidence of immediate changes in connectivity surrounding IEDs (Ibrahim, Cassel, et al., 2014) it would be appropriate not just to investigate the stationary connectivity of ICNs in focal epilepsy but also the dynamic connectivity.

2.7 Research Questions

Considering the issues raised in the previous section this thesis poses the following research questions.

For fMRI in a paediatric/clinical setting can we better address the issues of

1. Motion?

2. Physiological noise?

3. Data quality?

4. Poor sensitivity due to inappropriate use of parametric statistical inference?

5. Finally in the context of better control of data quality and analysis can we then explore the disruption of the brain's functional organisation in epilepsy and establish the role that IEDs might play therein?

2.8 References

Barkovich, A.J Kuzniecky, Jackson, G.D Guerrini, Dobyns, W. . (2005). A developmental and genetic classification for malformation sof cortical development. *Neurology*, *65*(12), 1873–1887. http://doi.org/10.1212/01.wnl.0000183747.05269.2d

Begley, C. E., & Durgin, T. L. (2015). The direct cost of epilepsy in the United States: A systematic review of estimates. *Epilepsia*, *56*(9), n/a–n/a. http://doi.org/10.1111/epi.13084

Beimer, N. J., Buchtel, H. A., & Glynn, S. M. (2015). One center's experience with complications during the Wada test. *Epilepsia*, *56*(8), e110–e113. http://doi.org/10.1111/epi.13046

Bell, G. S., Neligan, A., & Sander, J. W. (2014). An unknown quantity - The worldwide prevalence of epilepsy. *Epilepsia*, *55*(7), 958–962. http://doi.org/10.1111/epi.12605

Bennett, C. M., Baird, A. a, Miller, M. B., & Wolford, G. L. (2011). Neural Correlates of Interspecies Perspective Taking in the Post-Mortem

Atlantic Salmon: An Argument For Proper Multiple Comparisons Correction. *Journal of Serendipitous and Unexpected Results*, *1*, 1–5. http://doi.org/10.1016/S1053-8119(09)71202-9

Bennett, C. M., Wolford, G. L., & Miller, M. B. (2009). The principled control of false positives in neuroimaging. *Social Cognitive and Affective Neuroscience*, *4*(4), 417–422. http://doi.org/10.1093/scan/nsp053

Berg, A. T., Berkovic, S. F., Brodie, M. J., Buchhalter, J., Cross, J. H., Van Emde Boas, W., … Scheffer, I. E. (2010). Revised terminology and concepts for organization of seizures and epilepsies: Report of the ILAE Commission on Classification and Terminology, 2005-2009. *Epilepsia*, *51*(4), 676–685. http://doi.org/10.1111/j.1528-1167.2010.02522.x

Berg, A. T., & Scheffer, I. E. (2011). New concepts in classification of the epilepsies: Entering the 21st century. *Epilepsia*, *52*(6), 1058–1062. http://doi.org/10.1111/j.1528-1167.2011.03101.x

Berger, H. (1929). Uber das elektrenkephalogramm des menshen. *Archiv Für Psychiatrie and Nervenkrankheiten*, *278*(1875), 87: 527– 570. http://doi.org/10.1007/BF01797193

Birn, R. M., Diamond, J. B., Smith, M. A., & Bandettini, P. A. (2006). Separating respiratory-variation-related fluctuations from neuronal-activity-related fluctuations in fMRI. *NeuroImage*, *31*(4), 1536–1548. http://doi.org/10.1016/j.neuroimage.2006.02.048

Blümcke, I., & Spreafico, R. (2012). Cause matters: A neuropathological challenge to human epilepsies. *Brain Pathology*, *22*(3), 347–349. http://doi.org/10.1111/j.1750-3639.2012.00584.x

Blümcke, I., Thom, M., Aronica, E., Armstrong, D. D., Bartolomei, F., Bernasconi, A., … Spreafico, R. (2013). International consensus classification of hippocampal sclerosis in temporal lobe epilepsy: A Task Force report from the ILAE Commission on Diagnostic Methods. *Epilepsia*, *54*(7), 1315–1329. http://doi.org/10.1111/epi.12220

Blümcke, I., Thom, M., Aronica, E., Armstrong, D. D., Vinters, H. V., Palmini, A., … Spreafico, R. (2011). The clinicopathologic spectrum of focal cortical dysplasias: A consensus classification proposed by an ad hoc Task Force of the ILAE Diagnostic Methods Commission. *Epilepsia*, *52*(1), 158–174. http://doi.org/10.1111/j.1528-1167.2010.02777.x

Bromfield, E., Cavazos, J., & Sirven, J. (2006). Neuropharmacology of Antiepileptic Drugs. *An Introduction to Epilepsy*.

Burn, J., Dennis, M., Bamford, J., Sandercock, P., Wade, D., & Warlow, C. (1997). Epileptic seizures after a first stroke: the Oxfordshire Community Stroke Project. *BMJ (Clinical Research Ed.)*, *315*(7122), 1582–7. http://doi.org/10.1161/01.STR.25.2.333

Cascino, G. D. (2008). When drugs and surgery don't work. *Epilepsia*, *49*(SUPPL. 9), 79–84. http://doi.org/10.1111/j.1528-1167.2008.01930.x

Centeno, M., & Carmichael, D. W. (2014). Network connectivity in epilepsy: Resting state fMRI and EEG-fMRI contributions. *Frontiers in Neurology*, *5 JUL*(July). http://doi.org/10.3389/fneur.2014.00093

Chaudhary, U. J., Carmichael, D. W., Rodionov, R., Thornton, R. C., Bartlett, P., Vulliemoz, S., … Lemieux, L. (2012). Mapping preictal and ictal haemodynamic networks using video- electroencephalography and functional imaging. *Brain*, *135*(12), 3645–3663. http://doi.org/10.1093/brain/aws302

Colliot, O., Bernasconi, N., Khalili, N., Antel, S. B., Naessens, V., & Bernasconi, A. (2006). Individual voxel-based analysis of gray matter in focal cortical dysplasia. *NeuroImage*, *29*(1), 162–71. http://doi.org/10.1016/j.neuroimage.2005.07.021

Cross, J. H., Jayakar, P., Nordli, D., Delalande, O., Duchowny, M., Wieser, H. G., … Mathern, G. W. (2006). Proposed criteria for referral and evaluation of children for epilepsy surgery: Recommendations of the subcommission for pediatric epilepsy surgery. *Epilepsia*, *47*(6), 952–959. http://doi.org/10.1111/j.1528-1167.2006.00569.x

Da Silva, F. L. (2010). EEG: Origin and measurement. In *EEG - fMRI: Physiological Basis, Technique, and Applications* (pp. 19–38). http://doi.org/10.1007/978-3-540-87919-0_2

De Ciantis, A., Barba, C., Tassi, L., Cosottini, M., Tosetti, M., Costagli, M., … Guerrini, R. (2016). 7T MRI in focal epilepsy with unrevealing conventional field strength imaging. *Epilepsia*, n/a–n/a. http://doi.org/10.1111/epi.13313

Drake, C. T., & Iadecola, C. (2007). The role of neuronal signaling in controlling cerebral blood flow. *Brain and Language*, *102*(2), 141–152. http://doi.org/10.1016/j.bandl.2006.08.002

Duncan, J. S., Winston, G. P., Koepp, M. J., & Ourselin, S. (2016). Brain imaging in the assessment for epilepsy surgery. *The Lancet Neurology*, *15*(4), 420–433. http://doi.org/10.1016/S1474-4422(15)00383-X

Eklund, A., Nichols, T. E., & Knutsson, H. (2016). Cluster failure: Why fMRI inferences for spatial extent have inflated false-positive rates. *Proceedings of the National Academy of Sciences*, 201602413. http://doi.org/10.1073/pnas.1602413113

El Azami, M., Hammers, A., Jung, J., Costes, N., Bouet, R., & Lartizien, C. (2016). Detection of Lesions Underlying Intractable Epilepsy on T1-Weighted MRI as an Outlier Detection Problem. *Plos One*, *11*(9), e0161498. http://doi.org/10.1371/journal.pone.0161498

Fahoum, F., Lopes, R., Pittau, F., Dubeau, F., & Gotman, J. (2012). Widespread epileptic networks in focal epilepsies: EEG-fMRI study. *Epilepsia*, *53*(9), 1618–1627. http://doi.org/10.1111/j.1528-1167.2012.03533.x

Fisher, R. (2016). Operational Classification of Seizure Types by the International League Against Epilepsy. *Journal of Chemical Information and Modeling*, *53*(9), 1689–1699. http://doi.org/10.1017/CBO9781107415324.004

Fisher, R. S. (2014). Commentary: Operational definition of epilepsy survey. *Epilepsia*, *55*(11), 1688. http://doi.org/10.1111/epi.12829

Flandin, G., & Friston, K. J. (2016). Analysis of family-wise error rates in statistical parametric mapping using random field theory. *Arxiv*, 1–4. http://doi.org/10.1073/pnas.1602413113

Friston, K. J., Williams, S., Howard, R., Frackowiak, R. S., & Turner, R. (1996). Movement-related effects in fMRI time-series. *Magnetic Resonance in Medicine*, *35*(3), 346–55.

Gotman, J., & Pittau, F. (2011). Combining EEG and fMRI in the study of epileptic discharges. *Epilepsia*, *52*(SUPPL. 4), 38–42. http://doi.org/10.1111/j.1528-1167.2011.03151.x

Hales, P. W., Kawadler, J. M., Aylett, S. E., Kirkham, F. J., & Clark, C. A. (2014). Arterial spin labeling characterization of cerebral perfusion during normal maturation from late childhood into adulthood: normal "reference range" values and their use in clinical studies. *Journal of Cerebral Blood Flow and Metabolism : Official Journal of the International Society of Cerebral Blood Flow and Metabolism*, *34*(5), 776–84. http://doi.org/10.1038/jcbfm.2014.17

Hales, P. W., Kirkham, F. J., & Clark, C. A. (2015). A general model to calculate the spin-lattice (T1) relaxation time of blood, accounting for haematocrit, oxygen saturation and magnetic field strength. *Journal of Cerebral Blood Flow & Metabolism*, *36*, 370–374. http://doi.org/10.1177/0271678X15605856

Ibrahim, G. M., Cassel, D., Morgan, B. R., Smith, M. Lou, Otsubo, H., Ochi, A., … Doesburg, S. (2014). Resilience of developing brain networks to interictal epileptiform discharges is associated with cognitive outcome. *Brain : A Journal of Neurology*, *137*(Pt 10), 2690–2702. http://doi.org/10.1093/brain/awu214

Ibrahim, G. M., Morgan, B. R., Lee, W., Smith, M. Lou, Donner, E. J., Wang, F., … Carter Snead, O. (2014). Impaired development of intrinsic connectivity networks in children with medically intractable localization-related epilepsy. *Human Brain Mapping*, *35*(11), 5686–5700. http://doi.org/10.1002/hbm.22580

Janecek, J. K., Swanson, S. J., Sabsevitz, D. S., Hammeke, T. a., Raghavan, M., E. Rozman, M., & Binder, J. R. (2013). Language lateralization by fMRI and Wada testing in 229 patients with epilepsy: Rates and predictors of discordance. *Epilepsia*, *54*(2), 314–322. http://doi.org/10.1111/epi.12068

Jones, C., & Reilly, C. (2016). Parental anxiety in childhood epilepsy: A systematic review. *Epilepsia*, *57*(4), n/a–n/a. http://doi.org/10.1111/epi.13326

Kasteleijn-Nolst Trenité, D. G., & Vermeiren, R. (2005). The impact of subclinical epileptiform discharges on complex tasks and cognition: Relevance for aircrew and air traffic controllers. *Epilepsy and Behavior*, *6*(1), 31–34. http://doi.org/10.1016/j.yebeh.2004.10.005

Lemieux, L., Salek-Haddadi, A., Lund, T. E., Laufs, H., & Carmichael, D. (2007). Modelling large motion events in fMRI studies of patients with epilepsy. *Magnetic Resonance Imaging*, *25*(6), 894–901. http://doi.org/10.1016/j.mri.2007.03.009

Maccotta, L., Moseley, E. D., Benzinger, T. L., & Hogan, R. E. (2015). Beyond the CA1 subfield: Local hippocampal shape changes in MRI-negative temporal lobe epilepsy. *Epilepsia*, *56*(5), 780–788. http://doi.org/10.1111/epi.12955

Mellerio, C., Labeyrie, M. A., Chassoux, F., Roca, P., Alami, O., Plat, M., … Oppenheim, C. (2014). 3T MRI improves the detection of transmantle sign in type 2 focal cortical dysplasia. *Epilepsia*, *55*(1), 117–122. http://doi.org/10.1111/epi.12464

Mouthaan, B. E., Rados, M., Barsi, P., Boon, P., Carmichael, D. W., Carrette, E., … Braun, K. P. J. (2016). Current use of imaging and electromagnetic source localization procedures in epilepsy surgery centers across Europe. *Epilepsia*, n/a–n/a. http://doi.org/10.1111/epi.13347

Ngugi, A. K., Bottomley, C., Kleinschmidt, I., Sander, J. W., & Newton, C. R. (2010). Estimation of the burden of active and life-time epilepsy: A meta-analytic approach. *Epilepsia*, *51*(5), 883–890. http://doi.org/10.1111/j.1528-1167.2009.02481.x

Okubo, Y., Matsuura, M., Asai, T., Asai, K., Kato, M., Kojima, T., & Toru, M. (1994). Epileptiform EEG Discharges in Healthy-Children: Prevalence, Emotional and Behavioral-Correlates, and Genetic Influences. *Epilepsia*, *35*(4), 832–841. http://doi.org/10.1111/j.1528-1157.1994.tb02520.x

Olsen, T. S. (2001). Post-stroke epilepsy. *Current Atherosclerosis Reports*, *3*(4), 340–344. http://doi.org/10.2217/1745509X.2.4.599

Panayiotopoulos, C. (2010). *A clinical guide to epileptic syndromes and their treatment* (2nd ed.). Springer healthcare.

Papanicolaou, A. C., Rezaie, R., Narayana, S., Choudhri, A. F., Wheless, J. W., Castillo, E. M., … Boop, F. A. (2014). Is it time to replace the Wada test and put awake craniotomy to sleep? *Epilepsia*, *55*(5), 629–632. http://doi.org/10.1111/epi.12569

Pittau, F., Dubeau, F., & Gotman, J. (2012). Contribution of EEG/fMRI to the definition of the epileptic focus. *Neurology*, *78*(19), 1479–1487. http://doi.org/10.1212/WNL.0b013e3182553bf7

Riney, C. J., Chong, W. K., Clark, C. A., & Cross, J. H. (2012). Voxel based morphometry of FLAIR MRI in children with intractable focal epilepsy: implications for surgical intervention. *European Journal of Radiology*, *81*(6), 1299–305. http://doi.org/10.1016/j.ejrad.2010.12.043

Rosenkranz, K., & Lemieux, L. (2010). Present and future of simultaneous EEG-fMRI. *Magnetic Resonance Materials in Physics, Biology and Medicine*. http://doi.org/10.1007/s10334-009-0196-9

Salek-Haddadi, A., Diehl, B., Hamandi, K., Merschhemke, M., Liston, A., Friston, K., … Lemieux, L. (2006). Hemodynamic correlates of epileptiform discharges: an EfMRI study of 63 patients with focal epilepsy. *Brain Res*, *1088*(1), 148–166. http://doi.org/10.1016/j.brainres.2006.02.098

Sanchez Fernandez, I., Loddenkemper, T., Galanopoulou, A. S., & Moshe, S. L. (2015). Should epileptiform discharges be treated? *Epilepsia*, *56*(10), 1492–1504. http://doi.org/10.1111/epi.13108

Sander, J. W. A. S., & Shorvon, S. D. (1996). Epidemiology of the epilepsies Methodological issues. *Journal of Neurology, Neurosurgery & Psychiatry*, *61*(5), 433–443.

Shamshiri, E. A., Tierney, T. M., Centeno, M., St Pier, K., Pressler, R. M., Sharp, D. J., … Carmichael, D. W. (2016). Interictal activity is an important contributor to abnormal intrinsic network connectivity in paediatric focal epilepsy. *Human Brain Mapping*, *00*(August), 1–16. http://doi.org/10.1002/hbm.23356

Skirrow, C., Cross, J. H., Harrison, S., Cormack, F., Harkness, W., Coleman, R., … Baldeweg, T. (2015). Temporal lobe surgery in childhood and neuroanatomical predictors of long-term declarative memory outcome. *Brain*, *138*(1), 80–93. http://doi.org/10.1093/brain/awu313

Thornton, R., Laufs, H., Rodionov, R., Cannadathu, S., Carmichael, D. W., Vulliemoz, S., … Duncan, J. S. (2010). EEG correlated functional MRI and postoperative outcome in focal epilepsy. *Journal of Neurology, Neurosurgery, and Psychiatry*, *81*(8), 922–927. http://doi.org/10.1136/jnnp.2009.196253

Toda, N., Ayajiki, K., & Okamura, T. (2009). Cerebral blood flow regulation by nitric oxide: recent advances. *Pharmacological Reviews*, *61*(1), 62–97. http://doi.org/10.1124/pr.108.000547

Toda, N., & Okamura, T. (2003). The pharmacology of nitric oxide in the peripheral nervous system of blood vessels. *Pharmacological Reviews*, *55*(2), 271–324. http://doi.org/10.1124/pr.55.2.3

Wang, D. D., Knox, R., Rolston, J. D., Englot, D. J., Barkovich, A. J., Tihan, T., … Chang, E. F. (2015). Surgical management of medically refractory epilepsy in patients with polymicrogyria. *Epilepsia*, 151–161. http://doi.org/10.1111/epi.13264

Wilke, M. (2012). An alternative approach towards assessing and accounting for individual motion in fMRI timeseries. *Neuroimage*, *59*(3), 2062–2072. http://doi.org/10.1016/j.neuroimage.2011.10.043

Wilner, A. N., Sharma, B. K., Thompson, A., Soucy, A., & Krueger, A. (2014). Diagnoses, procedures, drug utilization, comorbidities, and cost of health care for people with epilepsy in 2012. *Epilepsy and Behavior*, *41*, 83–90. http://doi.org/10.1016/j.yebeh.2014.08.131

Wylie, G. R., Genova, H., DeLuca, J., Chiaravalloti, N., & Sumowski, J. F. (2014). Functional magnetic resonance imaging movers and shakers: does subject-movement cause sampling bias? *Human Brain Mapping*, *35*(1), 1–13. http://doi.org/10.1002/hbm.22150

Yerys, B. E., Jankowski, K. F., Shook, D., Rosenberger, L. R., Barnes, K. A., Berl, M. M., … Gaillard, W. D. (2009). The fMRI success rate of children and adolescents: Typical development, epilepsy, attention deficit/hyperactivity disorder, and autism spectrum disorders. *Human Brain Mapping*, *30*(10), 3426–3435. http://doi.org/10.1002/hbm.20767

3. FIACH: A biophysical model for automatic retrospective noise control in fMRI

In this chapter we address two common confounds in the application of fMRI to paediatric populations: Motion and Physiological Noise.

Abstract

Different noise sources in fMRI acquisition can lead to spurious false positives and reduced sensitivity. We have developed a biophysically-based model (named FIACH: Functional Image Artefact Correction Heuristic) which extends current retrospective noise control methods in fMRI. FIACH can be applied to both General Linear Model (GLM) and resting state functional connectivity MRI (rs-fcMRI) studies. FIACH is a two-step procedure involving the identification and correction of non-physiological large amplitude temporal signal changes and spatial regions of high temporal instability. We have demonstrated its efficacy in a sample of 42 healthy children while performing language tasks that include overt speech with known activations. We demonstrate large improvements in sensitivity when FIACH is compared with current methods of retrospective correction. FIACH reduces the confounding effects of noise and increases the study's power by explaining significant variance that is not contained within the commonly used motion parameters. The method is particularly useful in detecting activations in inferior temporal regions which have proven problematic for fMRI. We have shown greater reproducibility and robustness of fMRI responses using FIACH in the context of task induced motion. In a clinical setting this will translate to increasing the reliability and sensitivity of fMRI used for the identification of language lateralisation and eloquent cortex. FIACH can benefit studies of cognitive development in young children, patient populations and older adults.

Declaration of Contribution: The model presented in this chapter was developed by Tim Tierney. However, the data used to validate this method was collected by Dr. Louise Weiss-Croft.

3.1 Introduction

3.1.1 The Problem of Noise in fMRI

The question of how to separate signal from noise in fMRI is one of crucial importance. This is primarily due to the fact fMRI signals are weak in magnitude (a few percent) and are therefore easily concealed by increased noise levels. Whether the noise is due to subject motion, physiological processes or scanner hardware it all can lead to spurious results (Murphy, Birn, & Bandettini, 2013). Specifically with regards to subject motion error variance is increased resulting in reduced sensitivity (Friston, Williams, Howard, Frackowiak, & Turner, 1996) and false positives (see Figure 4). In rs-fcMRI it has been demonstrated that noise due to head motion can result in a spurious increase in local connectivity (Van Dijk, Sabuncu, & Buckner, 2011) and that many of these issues are not remedied fully by regression of the realignment parameters (RPs) from the signal (Power, Barnes, Snyder, Schlaggar, & Petersen, 2012).

3.1.2 Motion

To account for the effects of motion induced noise a variety of retrospective methods have been proposed. Many motion-focused correction methods rely on modelling some transformation of the parameters attained from volumetric spatial realignment or from some measure of signal intensity across the whole brain such as DVARS (Derivative of VARiation) or mean global signal (Desjardins, Kiehl, & Liddle, 2001; Friston et al., 1996; Lemieux, Salek-Haddadi, Lund, Laufs, & Carmichael, 2007; Wilke, 2012).

The use of methods incorporating global signal have been debated in the literature ever since it was demonstrated that regressing out global signal can result in spurious negative correlations (Murphy, Birn, Handwerker, Jones, & Bandettini, 2009). Furthermore, if an artefact's structure is spatially specific (as is the case in Figure 4) it will only be partially reflected in the global signal. This will result in less efficient control of the artefact when it comes to the regression stage of the analysis.

It has been demonstrated that global signal is a poor reflection of motion related signal changes at each voxel (Beall & Lowe, 2014). It was concluded that it is not justifiable as a method of motion control. However,

there is conflicting opinion on this matter (Power, Schlaggar, & Petersen, 2014).

3.1.3 Localized Large Amplitude Signal Changes

While correction methods that are based on the volumetric RPs are useful (Lund, Nørgaard, Rostrup, Rowe, & Paulson, 2005) they can have limitations when used as subject exclusion criteria or metrics of data quality. This is because they do not model motion, but net displacement relative to a reference sampled every TR. This is particularly problematic in paediatric or patient populations where head motion may be faster than the volumetric sampling rate (TR). We present an illustrative example of this point where the volumetric RP is a poor reflection of subject motion in a 2D gradient echo sequence with axial acquisition (Figure 4).

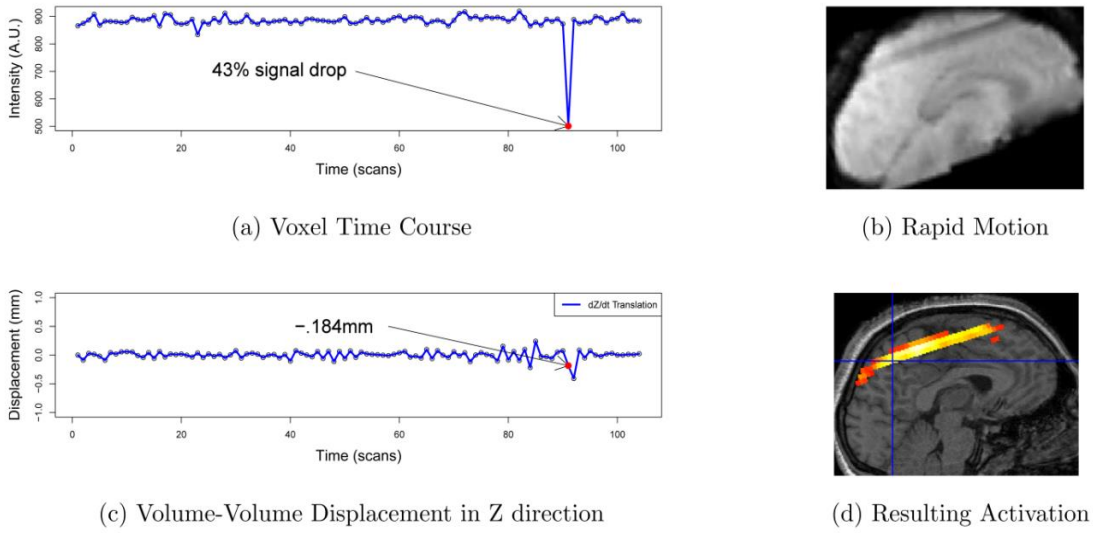

(a) Voxel Time Course

(b) Rapid Motion

(c) Volume-Volume Displacement in Z direction

(d) Resulting Activation

Figure 4. The effect of through-plane motion. Through-plane motion produces a spurious observation in the time series (a). This artefact presents spatially with a slice-specific profile (b). The effect on the time series is not reflected in the through plane derivative of the realignment parameter despite the fact that the effect of the motion is predominantly in this direction. The red sphere shows the time point where the motion occurred (c). The resulting statistical map shares the same spatial location as the artefact (d) due to motion-task correlation. The contrast is an F-contrast across the canonical haemodynamic response and its derivatives thresholded at FWE ($p<.05$).

By not fully modelling the noise effects in the data, a false positive has been obtained in Figure 4d. This false positive was obtained even after using scan nulling and the autoregressive polynomial expansion of the RPs (Friston et al., 1996; Lemieux et al., 2007).

Recent work would suggest that this is an unsurprising finding(Beall & Lowe, 2014) as the frequently used volumetric measures of motion were described as not being able to "robustly identify motion corrupted events, especially in the most realistic scenario of sudden head movement". Furthermore this type of signal change (Figure 4b) is not uncommon and has been described as the "predominant effect of motion" in a sample ranging from 8-23 year olds (Satterthwaite et al., 2012).

Large amplitude signal changes can also be observed due to k-space spikes and are localized to specific slices. Volumetric realignment parameters do not necessarily detect this type of noise. In recognition of potential artefacts from electronic noise as well as from rapid motion, software has been developed to address them such as the ArtRepair toolbox for SPM (http://cibsr.stanford.edu/tools/human-brain-project/artrepair-software.html) and 3dDespike by AFNI (http://afni.nimh.nih.gov/afni/).

3.1.4 Physiological Noise

Methods that control for physiological noise have been developed. These include utilizing external monitors of physiological processes, modelling mean white matter and CSF signals, modelling principal components from white matter, grey matter and temporally unstable areas (Behzadi, Restom, Liau, & Liu, 2007; Birn, Diamond, Smith, & Bandettini, 2006; Glover, Li, & Ress, 2000; Satterthwaite et al., 2013).

However, the efficacy of these techniques is debated. The utility of using PCA to create nuisance regressors from white matter and CSF signals has been described as not producing encouraging results (Power et al., 2014). Whereas, in contrast, other groups (Muschelli et al., 2014) have described utilizing the aCompCor approach (Behzadi et al., 2007) as just as effective as full frame-censoring approach (Siegel, Power, & Dubis, 2014). The efficacy of external monitors is also debated as it has been suggested that data-driven techniques such as tCompCor, aCompCor and multi-echo ICA denoising provide comparable or more efficient noise reduction without

external monitoring (Behzadi et al., 2007; Kundu, Inati, Evans, Luh, & Bandettini, 2012).

It must be noted that some of these techniques do not purely model physiological noise. For instance modelling signals from white matter, grey matter and temporally unstable areas may also contain information concerning motion. Furthermore techniques such as ICA denoising and Robust Weighted Least Squares (RWLS) may model both physiological noise and motion artefacts (Beckmann & Smith, 2004; Diedrichsen & Shadmehr, 2005; Griffanti et al., 2014).

There are also practical limitations to these methods as well. For instance, external monitoring and multi-echo EPI are acquisition-dependent and while promising cannot be applied retrospectively. As for ICA denoising the process is not easily automated as it requires a training dataset that may be difficult to create. The focus of this paper is both automatic and retrospective techniques and these methods shall not be discussed further.

3.1.5 Methodological Aims and Hypothesis

Considering there is wide agreement that modelling volumetric RPs is useful (Lund et al., 2005; Power et al., 2014; Satterthwaite et al., 2013) the question becomes how to extend this approach to address the issue of physiological noise and localized large amplitude signal changes (where there is less agreement). We propose to develop a biophysical framework that can be used for identifying and addressing both of these issues. This model will be applicable regardless of sequence, hardware, field strength and subject population. It is hypothesized that a method developed to these specifications will provide improvements in correction of data over existing available methods.

3.2 Theory

3.2.1 Identifying Large Amplitude Signal Changes

We define non-physiological large amplitude signal changes as those that display signal changes larger than the possible BOLD response. To estimate the signal we simulate gradient echo signal decay as follows:

$$S = S_{max} e^{-TE\ R2^*} \quad (54)$$

Where S = Signal, S = 100 (to describe signal changes in % change), TE = echo time and

$$R2^{*} = R2 + R2' \quad (55)$$

Where R2 = transverse relaxation rate of grey matter and R2' is the contribution to the relaxation rate from the local magnetic field inhomogeneities. R2 is estimated using empirical results (Uludağ, Müller-Bierl, & Uğurbil, 2009):

$$R2 = 1.74B0 + 7.77 \quad (56)$$

B0 is the magnetic field strength in Tesla (T). The following theoretical model is adopted for estimating R2' (Yablonskiy & Haacke, 1994)

$$R2' = \varsigma\delta\omega \quad (57)$$

Where ς = blood volume fraction and $\delta\omega$ isthe characteristic frequency of the object causing the magnetic field inhomogeneities. ς can be estimated using the following empirical equation (Grubb, Raichle, Eichling, & Ter-Pogossian, 1974):

$$\varsigma = .8\, CBF^{.38}/100 \quad (58)$$

Where CBF = Cerebral Blood Flow (ml $100g^{-1}$). We can estimate $\delta\omega$ according to (Yablonskiy & Haacke, 1994)by assuming the static dephasing regime and a random distribution of vessel orientation as:

$$\delta\omega = \gamma\, B0\, \Delta\chi\, Hct\, 4\pi/3\, (1 - Y) \quad (59)$$

Where γ = gyromagnetic ratio of the proton, $\Delta\chi$ = the volume susceptibility difference between oxygenated and deoxygenated blood, Hct = Hematocrit, Y= fraction of oxygenated blood. To simulate activation we solve the following equation:

$$S = S_{max}e^{-TE\ R2^{*}_{Activation}} - S_{max}e^{-TE\ R2^{*}_{Baseline}} \quad (60)$$

The difference between $R2^{*}_{Activation}$ and $R2^{*}_{baseline}$is that we allow both Y and ς to vary. To calculate the expected response magnitude we allow Y to vary from .6 - .9. The baseline of .6 is assumed so as to be similar to other studies employing this model (Buxton, Miller, Wong, & Frank, 1998; Mildner, Norris, Schwarzbauer, & Wiggins, 2001; Winawer, Horiguchi, & Sayres,

2010; Yablonskiy & Haacke, 1994). The second value of Y determines the threshold for the detection of non-physiological signal changes. We assume a value of .9 for the second value of Y as the typical range from rest to strong activation is .6 - .8 (Obata et al., 2004). This was chosen to make the threshold robust in children and in clinical populations where there may be greater variation in response magnitudes and to be conservative in terms of how much data is corrected.

For calculating ς we assume 100% change in CBF from a baseline of 55 ml $100g^{-1}$ min^{-1}. The resulting values estimated for ς (3.667-4.77%) are in good agreement with empirical values of vascular density which have been measured as having a mean value of ~3.5% and a maximum of ~4.5% (Lauwers, Cassot, Lauwers-Cances, Puwanarajah, & Duvernoy, 2008). The remaining parameters assumed to calculate $\delta\omega$ are as follows: $\Delta\chi = 4\pi$ x 1.8 x 10^{-7} (Weisskoff & Kiihne, 1992), γ = 42:57 MHz, Hct = .4. Solving Eq 60) for a 1.5 T scanner acquiring data with a TE of 30 ms produces the following threshold of 4.9 %. The following figure illustrates this process.

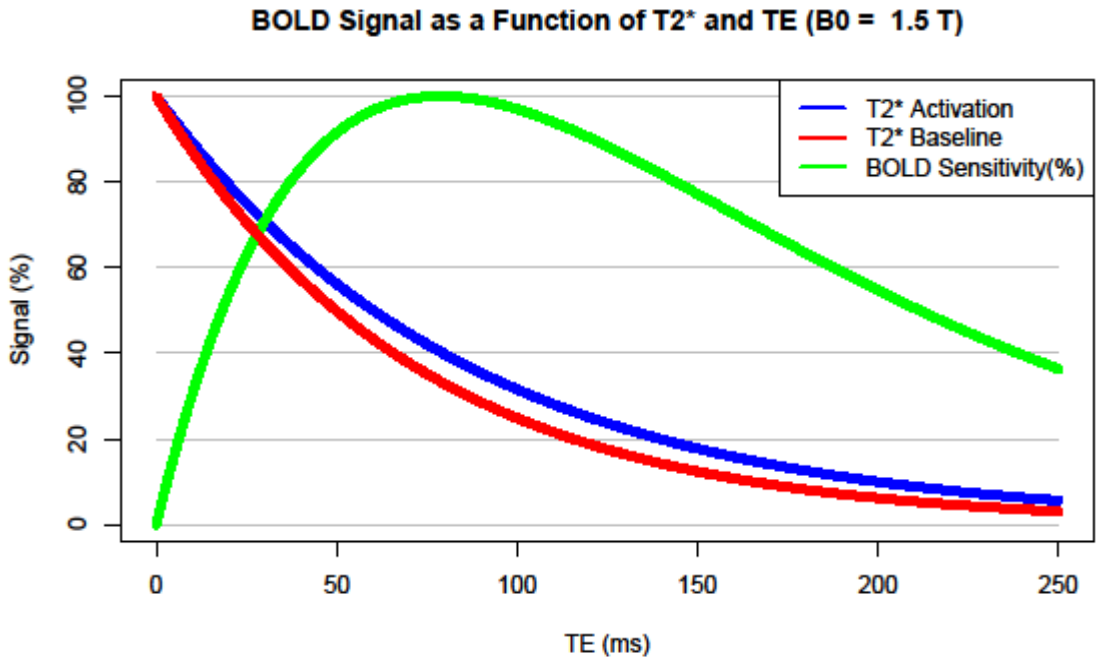

Figure 5. BOLD Contrast. The blue line represents the signal decay of the voxel during activation while the red line represents decay at rest. The green line shows one's sensitivity to the BOLD contrast. The BOLD sensitivity is given in percentage of the maximum value.

3.2.2 Identifying Physiological Noise

The model to identify large amplitude signal changes assumes a low blood volume fraction (typically < 5%). This assumption is violated in brain regions with large vascular density and is therefore not applicable in these areas. However, by using the same framework as was used to identify spurious signal changes we can identify these brain regions and model their effects. If we assume that $\delta\omega$ stochastically fluctuates with time we can describe the variable by a distribution (D) characterised by a centrality ($\mathcal{C}_{\mathrm{D}}$) and variability (V_{D}) parameter as follows:

$$\delta\omega(t) \sim \mathrm{D}(\mathcal{C}_{\mathrm{D}}, \mathrm{V}_{\mathrm{D}}) \tag{61}$$

As R2' $\propto$ blood volume (ς) then R2'(t) will be time varying with a distribution $\mathcal{R}$ that is a scaled version of D:

$$R2'(t) \sim \mathcal{R}(\mathcal{C}_{\mathcal{R}}, \mathrm{V}_{\mathcal{R}}) \tag{62}$$

Where $\mathcal{C}_{\mathcal{R}} = \varsigma\ \mathcal{C}_{\mathrm{D}}$ and $\mathrm{V}_{\mathcal{R}} = \varsigma \mathrm{V}_{\mathrm{D}}$. Rewriting Eq (54) in terms of R2'(t) we find that:

$$S(t) = S_{max} e^{-TE\ R2 - TE\ R2'(t)} \tag{63}$$

To investigate the effect of R2'(t) on S(t) we take the partial derivative of Eq (63) with respect to R2'. We assume R2 to be constant.

$$\frac{\partial S(t)}{\partial R2'(t)} = -TE\ S_{max} e^{-TE\ R2^*} \tag{64}$$

The partial derivative implies that for positive values of R2' S(t) will be decreasing. Therefore the resulting voxel time-series will be characterised by a centrality parameter ($\mathcal{C}_S$)that decreases and a variability parameter (V_S) that increases as R2' increases. Therefore, an area of higher blood volume could be characterised by signal with lower centrality and higher variability compared to areas with lower blood volume. By taking the ratio of these parameters $\mathcal{C}_S$ / V_S we create a parameter that is sensitive to blood volume and temporal stability.

3.2.3 Theory implementation

3.2.3.1 Step 1: Physiological Noise Control

Physiological noise is identified automatically using the Expectation-Maximization (EM) algorithm to fit a mixture of Gaussians on a measure of robust Temporal Signal to Noise Ratio (rTSNR). We define rTSNR as the Median/Median Absolute Deviation of the realigned images (i.e. the $\mathcal{C}_S$ / V_S parameter) which have slow drifts removed by a high pass filter. The high pass filter consists of a basis set of cosines defaulting to remove frequencies with a period greater than 128s. However this filter cut-off can be altered to better suit one's study design. Once the mixture model is estimated a mask is created from the voxels that have a $\mathcal{C}_S$ / V_S parameter less than the .05 quantile of the larger distribution. The first six principal components (PCs) are then extracted from within the mask. These components can then be included in the first level analysis as a parsimonious noise model. Figure 6illustrates this process. This step is similar to temporal Component based noise Correction (tCompCor) developed by (Behzadi et al., 2007). However, both the image used to identify the physiological noise and methods of segmentation differ.

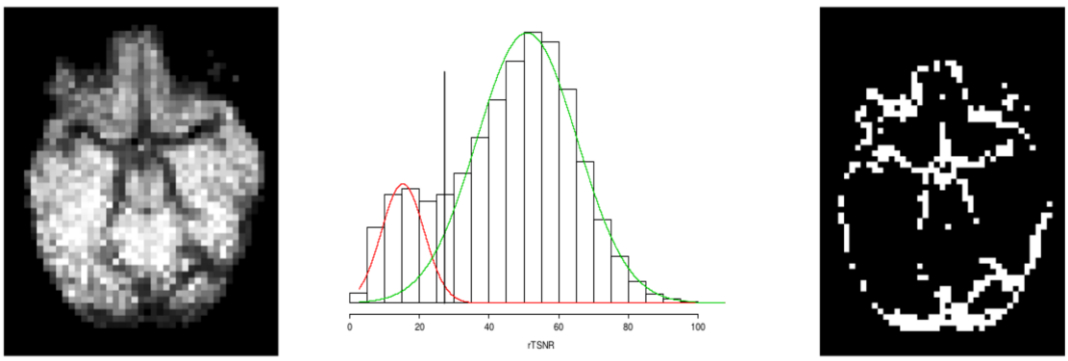

(a) The rTSNR (b) The mixture model (c) The segmentation

Figure 6. Segmentation of high noise areas. The rTSNR of a lower axial slice (a) is fitted with two Gaussians (b) and the high noise areas are segmented(c). The arteries, venous sinuses and the periphery of the brain are typically identified. The black line in (b) is the .05 quantile of the larger distribution where the masks are binarized.

3.2.3.2 Step 2: Large Amplitude Signal Change Correction

To identify a time point in a voxel as artefactual we add a measure of noise (2 x Median Absolute Deviation) to the theoretically derived threshold for a biologically plausible signal change in the presence of noise. Signal changes relative to the previously calculated median exceeding this threshold are then interpolated using a natural cubic spline with the two time points on either side. If consecutive time points of the same voxel are corrupted the spurious change is replaced with the median to avoid interpolation errors. This method is implemented using the R statistical programming language (R Core team, 2015), The following packages were used: Rcpp, RcppArmadillo and oro.nifti, (D Eddelbuettel & Francois, 2011; Dirk Eddelbuettel & Sanderson, 2014; Whitcher, Schmid, & Thornton, 2011).This method can be applied to both GLM style analysis and rs-fcMRI. Figure 7graphically explains the analysis pipeline. The only requirement is that the images are realigned prior to usage. Subsequently any fMRI analysis method can be applied with the addition of the derived regressors.

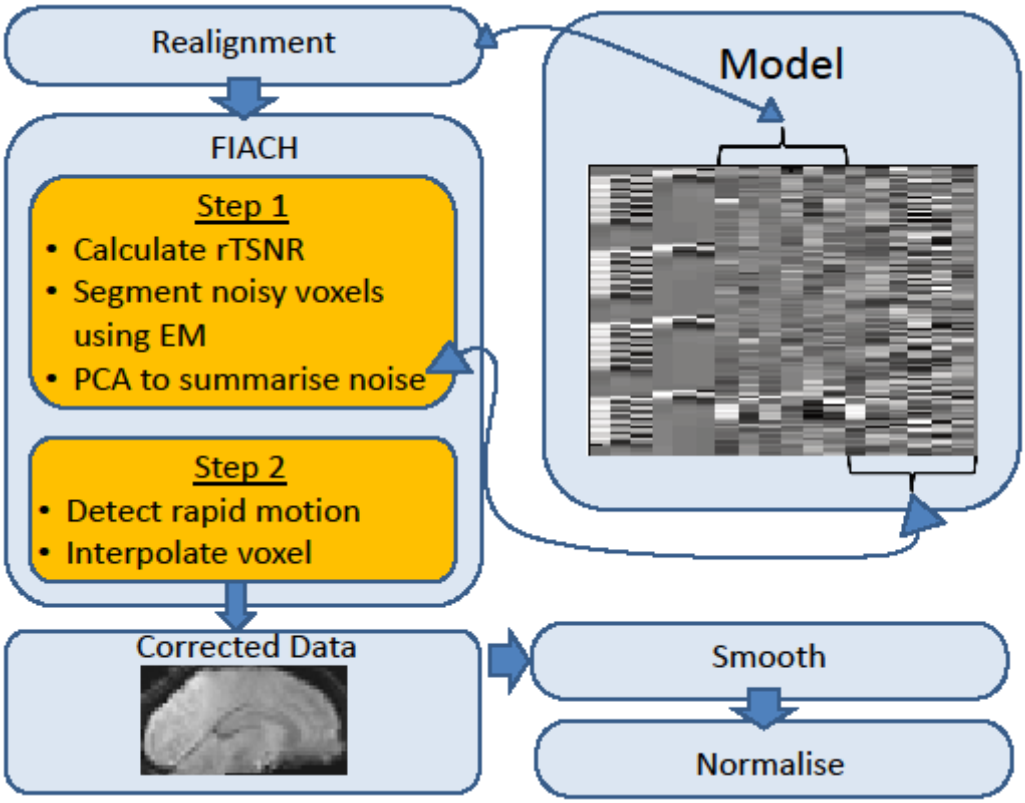

Figure 7. Flowchart for an Analysis Pipeline using FIACH. The GLM design matrix includes the task, six realignment parameters and the PCA components.

3.2.4 Theory Summary

The theory proposed for artefact identification can be broken down into two sub-models: One that identifies instances of abrupt temporal instability and one that identifies consistent temporal instability. These models form a two-step procedure for retrospective artefact correction in fMRI. We will refer to this model from now as the Functional Image Artefact Correction Heuristic (FIACH: The Irish verb to hunt).

3.3 Method

3.3.1 Participants

Forty two children with no history of psychological, neurological or sensory impairment (21 males) aged 5-16 years (mean = 11, SD = 4) were recruited from local schools via poster advertisement.

3.3.2 Task and Stimuli

The two tasks reported here were performed as part of a larger fMRI task battery investigating the development of language. In each task, twenty four stimuli were presented in a blocked event related design. The four task blocks were separated by 16 seconds of rest (with fixation to cross hairs). In each task block six stimuli were presented every six seconds, with total task block duration of 36 seconds. Each task lasted three minutes and 49 seconds.

3.3.2.1 Sentence Comprehension and Naming Task

This comprehension task was designed to induce complex auditory processing, sentence level semantic and syntactic processing from phonological input, word retrieval and articulation. Participants were asked to listen to sentence level auditory descriptions of objects and animals and then name the object or animal.

3.3.2.2 Sentence Generation

This sentence generation task was designed to induce visual processing, syntactic processing from visual input, and articulation. Participants were asked to describe what was happening in a picture, using

one simple sentence with a subject-verb-object (S-V-O) structure. Each 350 x 350 pixel colour picture showed a subject and an object, with the subject involved in one of four actions: eating, drinking, jumping or falling.

3.3.3 Data Acquisition

Functional data were acquired using a 1.5 Tesla Siemens Avanto System (Erlangen, Germany), equipped with a 12 channel head coil. Signal changes were measured using a 2D gradient echo sequence (TR = 2160 ms, TE = 30 ms, flip angle = 75 degrees, FoV = 210 mm, 3mm slice and 1mm inter-slice gap, slices = 30 (axial acquisition in ascending order), voxel size = 3.3 x 3.3 x 4 mm). The first two volumes were discarded as dummy scans resulting in 104 volumes per task. Stimuli were presented using Cogent 2000 software; Cogent 2000 team at the Welcome Trust Centre for Neuroimaging (WTCN) and the UCL Institute of Cognitive Neuroscience (www.vislab.ucl.ac.uk). Auditory stimuli were transmitted through MR compatible headphones equipped with an active noise cancellation system and speech responses were transmitted using a sensitive head-mounted microphone (http://www.mrconfon.de/en/technology.html) . Visual stimuli were presented via an MR-compatible wall-mounted screen behind the scanner, and were viewed through a mirror fixed to the head coil.

3.3.4 FIACH Validation

In order to validate FIACH we analysed data obtained from healthy children while performing two different language tasks. This population was chosen for three reasons; 1) Paediatric populations typically present with large amounts of motion. 2) There is considerable evidence in the literature as to what constitutes valid activations with regards language tasks (Price, 2010). 3) Both tasks induced task correlated motion as the children engaged in overt speech. This approach is similar to the one employed by Lund et al (2005) for assessing the impact of motion on fMRI data.

To compare the different methods we identified regions of interest (ROI), a priori, which were likely to be active in the Sentence Comprehension and Naming task (Price, 2010, 2012). These expected regions consisted of the following: left inferior frontal gyrus, bilateral superior temporal gyrus, bilateral middle temporal gyrus, bilateral primary motor, bilateral

somatosensory, bilateral cerebellum, bilateral temporal pole, left hippocampus and supplementary motor area. With regards to the Sentence Generation task the regions were as follows: bilateral cerebellum, bilateral fusiform gyrus, bilateral middle occipital gyrus, bilateral inferior occipital gyrus, bilateral inferior temporal gyrus, bilateral middle temporal gyrus, supplementary motor area, bilateral primary motor, bilateral somatosensory, bilateral lingual gyrus, bilateral hippocampus, bilateral parahippocampal gyrus, bilateral superior occipital gyrus. The AAL atlas (Tzourio-Mazoyer et al., 2002) was used to assist in anatomical localisation.

Binomial tests and Wilcoxon signed-rank tests were used to assess whether FIACH produced greater t-values and cluster extents than the other methods in the a priori defined regions of interest. All hypothesis tests, unless stated otherwise, are corrected for multiple comparisons using methods Hochberg's correction for multiple comparisons (Hochberg, 1988)at p=.05. All statistical maps, unless stated otherwise, are thresholded at FWE ($p<.05$) with a cluster extent threshold = 0.

3.3.5 Data Analysis Pipelines

All images are realigned, normalised to 2x2x2mm template using SPM and smoothed with an 8mm FWHM Gaussian kernel. The specifics of each method are given below.

Five other methods of automatic retrospective noise control were also investigated to compare the performance of FIACH. The first method was spatial realignment followed by the regression of the RPs (we will refer to this as the SPM method). We also analysed the autoregressive polynomial expansion of the RPs and scan nulling (Friston et al., 1996; Lemieux et al., 2007). The threshold for scan nulling (Also termed frame censoring) was set at 1mm volume-volume displacement measured using the volumetric realignment parameters. We will refer to this method as Realignment Parameter Expansion (RPE).

At this point we also calculated the percentage of volumes that were censored for comparison with the percentage of data that the FIACH Step 2 (the filter and the 6 RPs, no physiological noise regression) altered. The fraction of data changed was calculated as follows.

$$No.\ of\ imputations/(No.of\ voxels\ in\ mask \times No.of\ volumes) \quad (65)$$

The no. of imputations is simply the number of data points altered by the method. The third method was Motion Fingerprint (MFP). This method contrasts with RPE as it reduces the motion model complexity. It also accounts for the varying effect of motion across the brain which RPE does not (Wilke, 2012). We also compared FIACH against two methods not reliant on the RPs, RWLS (Diedrichsen & Shadmehr, 2005) and tCompCor (Behzadi et al., 2007). We did not compare against aCompCor as in the original manuscript tCompCor is described as producing better results.

3.4 Results

3.4.1 Illustrative Example

We provide examples of both steps; 1) the physiological noise correction and 2) the correction for large amplitude signal changes. First we present a subject performing the Sentence Comprehension and Naming task. This subject displayed no large amplitude signal changes. In Figure 8 bilateral motor and artefactual activations in the cerebellum can be seen (the lower most portion of the cerebellum was not acquired. This resulted in signal instability due to motion interacting with the normalization). After applying FIACH the motor cortex activations have increased statistics and additional activations in the right superior temporal gyrus and the inferior temporal lobe are revealed (Figure 8b). The cerebellar artefact is corrected due to the variance extraction in this area (Figure 8c, axial image). In Figure 8d we cap the maximum display values at F = 60 to examine the spatial distribution of the regressors effect. Maxima are now seen in the transverse sinus, inferior sagittal sinus, fourth ventricle, brain stem and the inferior temporal lobe. All these areas exhibit large and consistent variability: the sinuses due to blood volume, as predicted in section 3.2.2, the brain stem and fourth ventricle due to pulsatile motion. The inferior temporal signal instability is due susceptibility related artefacts that interact with bulk and pulsatile head motion. It is therefore suggested that the improvement is a result of modelling these effects.

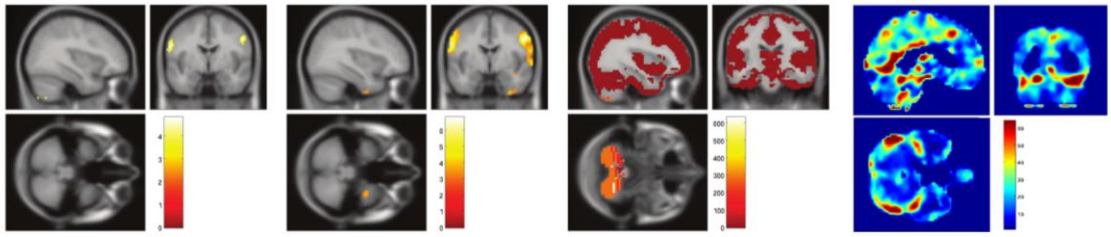

(a) Standard SPM (b) FIACH (c) FIACH PCs (d) PCs (thresholded)

Figure 8. Illustrative example of the physiological noise correction. a) Estimated t-map before correction. b) Estimated t-map after correction. c) F-contrast across the PCs. d) same as `c' but display thresholded at F=60. All statistical maps are grey matter masked and thresholded at p<.001 (k=10).

In Figure 9 we show an example of the effect of the large amplitude signal change correction on a corrupted voxel time series. The artefact seen in Figure 9a is corrected in Figure 9b. No other time points are altered and neither are spatial locations outside the affected slice (see Figure 7for corrected image and Figure 4for the corrupted image).

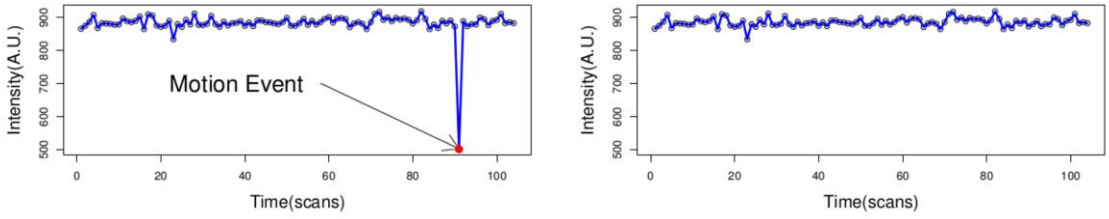

(a) Voxel Time Course Affected by Artefact (b) Corrected Time Course

Figure 9. Example of FIACH step 2. a) Corrupted voxel time course. b) Corrected voxel time course.

3.4.2 Group level Results

In the sentence comprehension and naming task FIACH produced the highest t-value in 8 out of the 16 ROIs specified. This was found to be a statistically significant effect using a binomial test (p<.05). The probability of the proposed method having the highest t-value in the ROIs = 0.5 (95% CI [0.247, 0.753]). FIACH had the maximum number of voxels in 11 out of the 16 areas specified. This was found to be a statistically significant effect using a binomial test (p<.05). The probability of the proposed method having the greatest extent in the region of interest = 0.688 (95% CI [0.413, 0.89]).

Figure 10and Table 1 summarize the results obtained for the Sentence and Naming task using all 6 approaches.

	FIACH	FIACH(Step 2)	MFP	RPE	RWLS	SPM	tCompCor
STGl	13.66(575)	11.75(494)	12.66(512)	10.92(423)	10.56(483)	10.8(470)	13.24(540)
STGr	13(327)	12.14(334)	12.52(354)	9.41(307)	11.54(314)	11.06(326)	12.31(335)
Cr	8.18(210)	5.92(60)	0(0)	0(0)	7.04(62)	6.22(53)	7.47(174)
MTGl	10.1(170)	8.62(83)	8.23(50)	6.49(37)	7.13(37)	7.38(63)	10.23(116)
Cl	8.65(167)	5.41(4)	5.99(2)	5.44(3)	6.46(15)	5.8(9)	6.08(30)
MTG	10.83(105)	10.85(97)	10.19(94)	8.26(67)	9.33(62)	9.38(80)	11.23(110)
Sr	8.35(101)	6.86(36)	7.56(61)	7.29(19)	6.46(8)	6.06(12)	7.19(55)
Sl	7.7(92)	7.04(73)	7.92(61)	7.18(20)	8.2(78)	7.02(32)	7.09(52)
IFGl	7.25(90)	5.94(9)	6.62(30)	0(0)	6.34(15)	6.26(3)	7.95(30)
SMA	8.55(86)	5.97(4)	6.72(18)	6.73(21)	6.33(5)	0(0)	0(0)
PMl	8.38(70)	7.23(25)	7.94(46)	7.06(24)	8.33(59)	7.33(26)	7.28(32)
TPl	9.21(42)	7.41(29)	9.24(83)	7.65(35)	5.74(5)	7.66(25)	8.7(38)
ITGl	6.9(38)	7.41(28)	5.54(1)	0(0)	0(0)	5.47(1)	6.12(13)
Hl	7.41(30)	6.49(53)	7.13(35)	7.14(17)	8.42(68)	6.81(57)	7.04(63)
PMr	7.88(29)	6.19(7)	7.41(26)	6.54(14)	6.84(16)	5.67(6)	6.53(11)
TPr	6.95(9)	7.51(8)	7.65(55)	6.57(14)	6.31(5)	7.59(8)	7.58(13)

Table 1 Sentence Comprehension and Naming t-values (Cluster extents) for all correction methods: STGl = left superior temporal gyrus, STGr = right superior temporal gyrus, Cr = right cerebellum, MTGl = left middle temporal gyrus, Cl = left cerebellum, MTGr = right middle temporal gyrus, Sr = right somatosensory, Sl = left somatosensory, IFGl = left inferior frontal gyrus, SMA = supplementary motor area, PMl = left primary motor, TPl = left temporal pole, ITGl = left inferior temporal gyrus, Hl = left hippocampus, PMr = right primary motor, TPr = right temporal pole. A value of 0 indicates that the area did not survive FWE ($p<.05$).

In the sentence generation task FIACH had the highest t-value in 19 out of the 25 areas specified. This was found to be a statistically significant effect using a binomial test ($p<.05$). The probability of the proposed method having the highest t-value in the regions of interest = 0.76 (95% CI [0.549, 0.906]). FIACH had the maximum number of voxels in 21 out of the 25 areas specified. This was found to be a statistically significant effect using a binomial test ($p<.05$). The probability of the proposed method having the greatest extent in the regions of interest = 0.84 (95% CI [0.639, 0.955]). Figure 10 and Table 2 summarize the results obtained for the Sentence Generation task using all 6 approaches

	FIACH	FIACH(Step 2)	MFP	RPE	RWLS	SPM	tCompcor
Cr	13.46(478)	9.46(191)	6.81(64)	7.53(76)	7.95(68)	8.46(111)	9.27(180)
FGr	14.3(392)	11.82(300)	7.94(244)	7.26(180)	8.95(197)	8.97(201)	10.72(285)
MOGr	11.48(366)	10.66(274)	10.24(279)	8.7(179)	11.53(301)	10.69(183)	7.83(120)

Cl	12.02(328)	8.73(115)	6.63(20)	6.83(41)	6.02(11)	6.28(41)	7.71(122)
FGl	12.99(320)	9.69(143)	7.85(161)	7.35(89)	8.47(116)	7.59(113)	8.37(124)
IOGl	12.15(256)	12.7(214)	7.9(127)	8.16(75)	10.52(114)	8.98(94)	8.71(183)
ITGl	12.46(217)	9.94(143)	7.38(164)	6.95(100)	9.17(120)	7.73(116)	8.61(121)
IOGr	14.03(195)	13.07(136)	7.7(95)	7.05(59)	8.39(58)	9.36(63)	9.41(112)
MOGl	11.85(170)	11.65(132)	7.98(117)	8.17(35)	11.08(120)	9.06(72)	7.33(28)
MTGl	10.55(134)	8.37(62)	7.06(37)	5.59(7)	7.64(47)	7.44(38)	8.11(21)
ITGr	13.7(116)	11.84(71)	7.75(53)	6.31(12)	9.01(37)	8.19(40)	9.28(61)
SMA	8.41(110)	0(0)	6.71(99)	0(0)	0(0)	5.39(5)	5.85(20)
PMl	7.97(69)	6.37(20)	7.32(46)	7.42(11)	7.02(11)	0(0)	5.58(7)
Sl	8.19(62)	6.3(14)	7.1(22)	6.82(7)	7.39(19)	5.1(1)	6.51(21)
MTGr	10.61(60)	8.8(17)	6.15(11)	0(0)	6.98(7)	7.07(13)	7.44(10)
Sr	7.39(32)	0(0)	6.21(11)	5.5(1)	0(0)	0(0)	0(0)
LGr	7.55(27)	5.59(2)	0(0)	0(0)	0(0)	0(0)	5.18(1)
Hl	6.56(22)	5.7(1)	6.02(4)	0(0)	7.47(14)	0(0)	0(0)
LGl	9.02(19)	7.52(5)	6.45(5)	6.36(3)	8.12(3)	6.31(4)	6.77(2)
PMr	6.7(18)	0(0)	6.47(20)	5.83(4)	0(0)	0(0)	0(0)
PHGl	6.39(8)	0(0)	6.68(12)	0(0)	5.54(1)	0(0)	0(0)
Hr	6.33(6)	6.36(14)	6.41(13)	5.82(1)	8.95(29)	5.91(3)	5.49(1)
PHGr	7.6(5)	7.35(4)	5.7(6)	0(0)	7.27(5)	6.45(4)	6.37(4)
SOGr	5.92(5)	0(0)	0(0)	0(0)	6.15(1)	0(0)	0(0)
SOGl	5.73(4)	0(0)	0(0)	0(0)	5.72(1)	0(0)	0(0)

Table 2. Sentence generation, t-values(cluster extents) for all correction methods: Cr = right cerebellum, FGr = right fusiform gyrus, MOGr = right middle occipital gyrus, Cl = left cerebellum, FGl = left fusiform gyrus, IOGl = left inferior occipital gyrus, ITGl= left inferior temporal gyrus, IOGr = right inferior occipital gyrus, MOGl = left middle occipital gyrus, MTGr = left middle temporal gyrus, ITGr = right inferior temporal gyrus, SMA = supplementary motor area, PMl = left primary motor, Sl = left somatosensory, MTGr = right middle temporal gyrus, Sr = right somatosensory, LGr = right lingual gyrus, Hl = left hippocampus, LGl = left lingual gyrus, PMr = right primary motor, PHGl = left parahippocampal gyrus, Hr = Right Hippocampus, PHGr = right parahippocampal gyrus, SOGr = right superior occipital gyrus, SOGl = left superior occipital gyrus. A value of 0 indicates that the area did not survive FWE ($p<.05$)

To compare the change in t-values and cluster extent (k) in both tasks Wilcoxon signed-rank tests were used. The hypothesis that FIACH would outperform each of the other methods was tested. We also tested the hypothesis that FIACH Step 2 (the filter and the 6 RPs, no physiological noise regression) would provide improvements relative to the SPM approach in order to demonstrate the individual contribution of this step. All these hypotheses were found to be statistically significant at $p < .05$. The summaries of these tests are provided in Table 3.

	Δ Median	Statistic(V)		ΔMedian	Statistic(V)
FIACH(t) > FIACH Step 2(t)	1.23	130***	FIACH(t) > FIACH Step 2(t)	1.89	320***
FIACH(t) > MFP(t)	0.76	124**	FIACH(t) > MFP(t)	1.42	321***

FIACH(t) > RPE(t)	1.47	136***	FIACH(t) > RPE(t)	2.13	325***
FIACH(t) > RWLS(t)	1.43	129***	FIACH(t) > RWLS(t)	2.09	300***
FIACH(t) > SPM(t)	1.45	134***	FIACH(t) > SPM(t)	2.11	325***
FIACH(t) > tCompCor(t)	0.99	116**	FIACH(t) > tCompcor(t)	1.65	325***
FIACH Step 2(t) > SPM(t)	0.22	101*	FIACH Step 2 (t) > SPM(t)	1.2	192***
FIACH(k) > FIACH Step 2 (k)	58.5	126**	FIACH(k) > FIACH Step 2(k)	52	320***
FIACH(k) > MFP(k)	43	110*	FIACH(k) > MFP(k)	47	312***
FIACH(k) > RPE(k)	71.5	135***	FIACH(k) > RPE(k)	62	325***
FIACH(k) > RWLS(k)	64.5	128***	FIACH(k) > RWLS(k)	55	293***
FIACH(k) > SPM(k)	65.5	130***	FIACH(k) > SPM(k)	64	325***
FIACH(k) > tCompCor(k)	46	120**	FIACH(k) > tCompcor(k)	49	325***
FIACH Step 2(k) > SPM(k)	7	108**	FIACH Step 2 (k) > SPM(k)	12	185***

(a) Sentence Comprehension and Naming (b) Sentence Generation

Table 3. Summary of wilcoxon signed-rank tests for both tasks. t = t-value, k = cluster extent, *** = significant at $p < .001$, ** = significant at $p < .01$,* = significant at $p < .05$. Statistic (V) = is the non-parametric equivalent of a t- value in the Wilcoxon-signed rank test

As there was a large discrepancy between the percentages of data changed using FIACH compared to the percentage of data censored using scan nulling (see Figure 11) we conducted further Wilcoxon singed-rank tests to directly compare the FIACH (Step 2) only with RPE. It was found that using the FIACH (Step 2) in combination with 6 RPs resulted in more voxels and greater t-values in the sentence comprehension and naming task compared to the RPE approach ($V = 103$, $p < .05$; $V = 116:5$, $p < .05$). The same result was found in the sentence generation task ($V = 195$, $p < .05$; $V = 224$, $p < .05$).

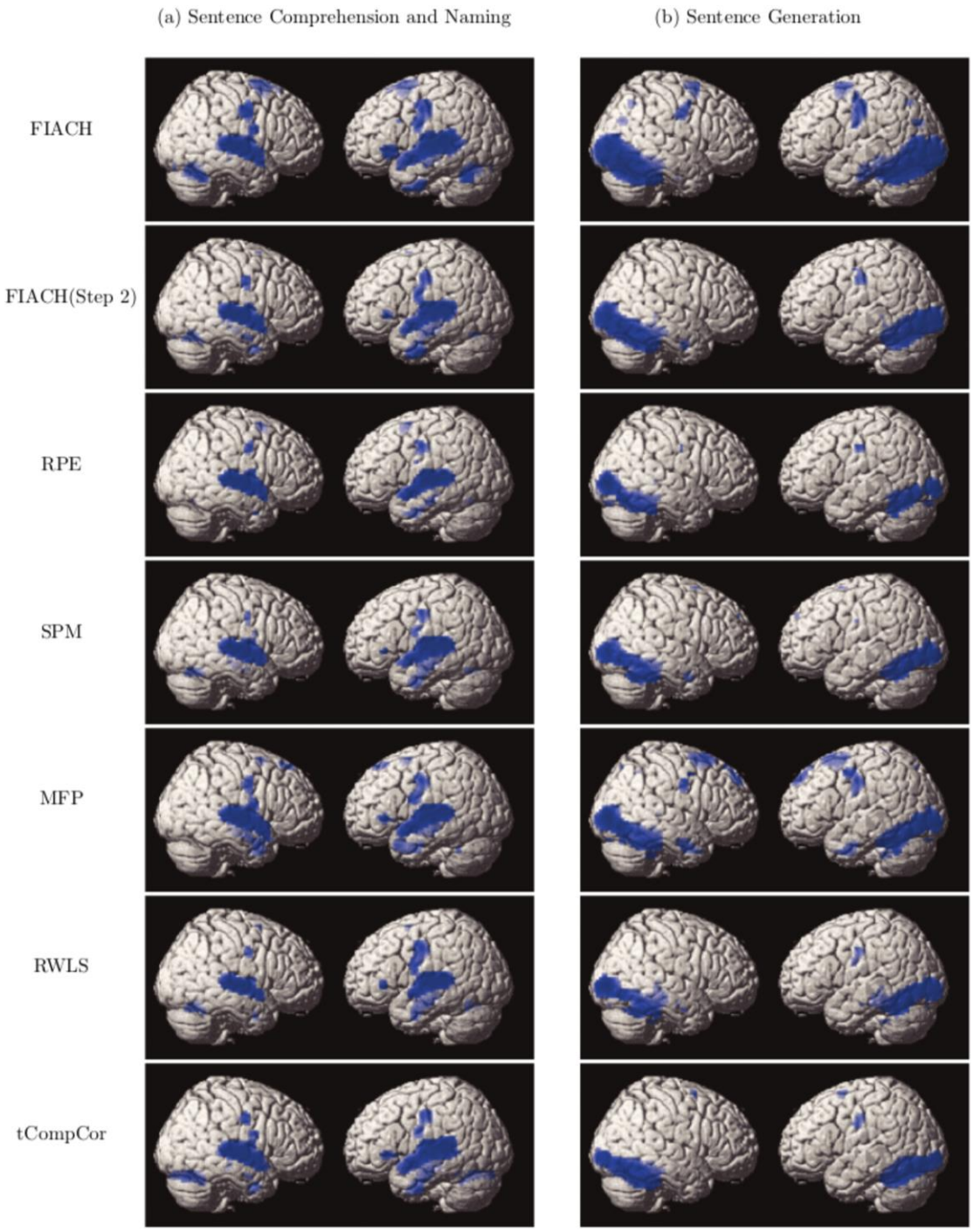

Figure 10. t-maps for both tasks (task>rest) rendered on a normalized T1, thresholded at FWE (p<.05). Intensity is proportional to the activations distance from the cortical surface. FIACH = Functional Image Artefact Correction Heuristic, RPE = Realignment Parameter Expansion, SPM = Statistical Parametric Mapping, MFP = Motion Fingerprint, RWLS = Robust Weifghted Least Squares, tCompCor= temporal Component based Correction

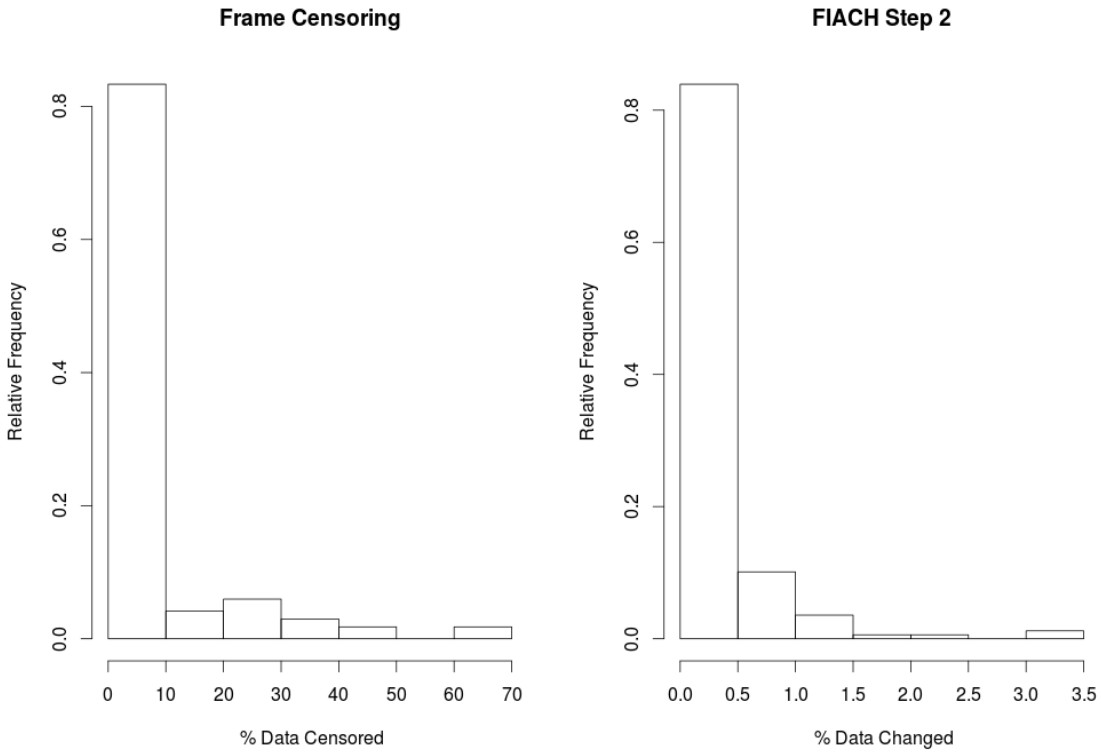

Figure 11. Comparison of FIACH (Step 2) with Frame Censoring across both tasks. The histograms demonstrate that traditional frame censoring using a 1mm threshold results in on average ~20 times more data changes than using FIACH. Mean(FIACH)= 0.25%, mean(Censored)= 6:18%, range(FIACH)= 0 - 3.41%, range (Censored) = 0 - 65.38%.

3.5 Discussion

3.5.1 Summary of Findings

We have evaluated the efficacy of 5 currently available automatic retrospective noise corrections methods in the context of paediatric fMRI where motion control is problematic. We have developed a method that performs favourably in comparison with these methodologies. FIACH produced increased t-value and cluster extent in plausible task related areas. Moreover this effect was largely consistent across brain areas. This was not the case for the other methodologies which had variable performance across brain areas (see Table 1,Table 2 and Figure 10). We will now discuss some of the key findings from each task.

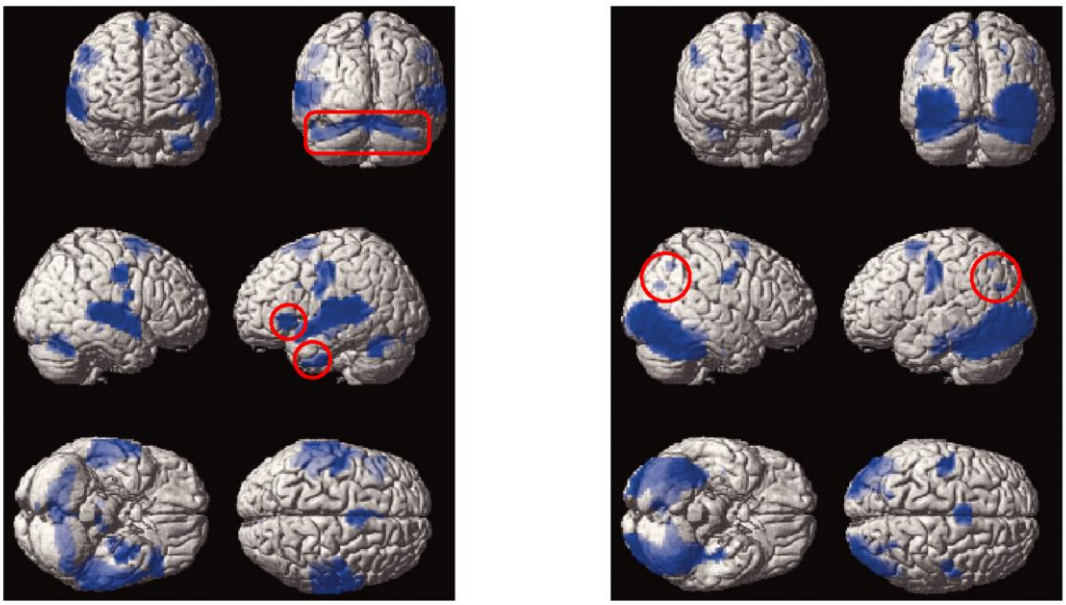

(a) Sentence Comprehension and Naming (FIACH) (b) Sentence Generation (FIACH)

Figure 12. Task t-maps (task>rest) generated by FIACH rendered on normalized T1, thresholded at FWE (p<.05). Areas where FIACH substantially improved statistical power relative to other methods are surrounded in red. Intensity is proportional to the activations distance from the cortical surface.

3.5.2 Sentence Comprehension and Naming

Of substantial interest is the varying performance of the reviewed methodologies in identifying activation in the inferior frontal gyrus. This area is of particular interest as it can be used to assess language laterality in candidates for brain surgery (Liegeois, 2002). It has also been documented that activations in this area correlate most with the results of the Wada test (Lehericy et al., 2000). A potential reason for this area's vulnerability to motion artefact is due to its position (regions further from the neck experience greater displacement when an individual rotates/nods their head). Due to its anterior position a rotation through plane is quite likely to result in the more anterior position of the slice being excited twice in rapid succession leading to magnetisation saturation and a large signal reduction. It is also possible that the FIACH PCs are modelling the signal variance effects produced by the large vessels located near the gyrus. This would explain the large difference between the improved results of FIACH in this area compared to the other methodologies.

An interesting difference was also observed between the methodologies concerning the left inferior temporal gyrus. In this area the signal is very unstable due to its position at the brain's edge and the local susceptibility induced distortions which are exacerbated by motion. By the application of Step 2 alone and a substantial activation is yielded (28 voxels, see Table 1). By applying both steps of FIACH the cluster size increases by a factor of ~3 (38 voxels) compared to the next most competitive method (see Table 1). The increased efficacy of FIACH is most likely due to the noise regressor's capabilities of representing a reasonable model of the signal instability in these areas (see Figure 8d & b, axial images). It has previously been reported that due to the high magnetic susceptibility effects in the areas next to the air-filled sinuses it would be more appropriate to use small volume corrections for observing activations in these areas (Devlin et al., 2000). Furthermore, in the same study it was shown that these activations are observable with PET and less so with fMRI. Optimised sequences have also been developed for observing activations in these areas (Weiskopf, Hutton, Josephs, & Deichmann, 2006) which produce moderate improvement in signal levels. However, we show that by directly modelling the temporal instability in these areas it is possible to recover the activations at high statistical thresholds. This suggests that it is not sufficient to recover signal in these areas but also necessary to model sources of signal instability to recover activations in these regions.

Another brain region of interest for speech/language is the cerebellum. The cerebellum has been heavily implicated in articulation and language and substantial activations would be expected in this area (Price, 2010). The large difference in activation strength between FIACH and the other methods is due to the use of the FIACH PCs. These regressors typically model information from the transverse sinuses which are adjacent to the cerebellum. The sinuses cause local disruptions to the main (B0) magnetic field and can therefore corrupt the surrounding area. This problem has been identified previously) in the context of fMRI studies of the visual system (Winawer et al., 2010).

3.5.3 Sentence Generation

This task was more corrupted by motion as the children overtly produced entire sentences. This also served to increase the correlation of the task with the motion parameters. It is unsurprising therefore that the t-values of the RPE method decrease in 19 of the 25 areas compared to the standard SPM method and that the cluster extent decrease in 21 out of the 25 areas. The overall poor performance of RPE can potentially be explained by the limitations of the RPs. In this task the head motion was task correlated and as a result it is likely that the correction methods derived from these parameters regresses true information from task related areas. MFP, although similarly derived from motion parameters, reduces model complexity and therefore is more sensitive than RPE. The reduction in model complexity is not a trivial issue as, on average, the lower bound for the amount of real signal variance removed by chance will be rank (Nuisance Regressors)/number of scans (Friston et al., 1996).

The difference between FIACH and the other methodologies is much more pronounced in this task (see Table 2). This is because the majority of expected activations (inferior temporal, fusiform, and occipital) all are next to areas of pronounced susceptibility (air filled sinuses, transverse sinus). Furthermore, the increased period of overt speech in this task leads to far more through plane movements which FIACH is optimally suited to correct. This is particularly important as the use of overt tasks has been advocated over covert tasks (Croft et al., 2013). The other methods lack the spatial specificity to substantially correct these artefacts.

An interesting and unexpected finding was FIACH's ability to identify activations in the inferior parietal regions where other methods failed to do so (see Figure 10b). The inferior parietal lobe has recently been implicated in cross-modal semantic processing (Binder, Desai, Graves, & Conant, 2009; Seghier, 2013). However, parietal activations have only been reported previously in two studies of sentence production in adults (Blank, Scott, Murphy, Warburton, & Wise, 2002; Müller et al., 1997). As such, we did not hypothesise activation in these regions. Crucially, the fact that FIACH may be able to enhance activation of these regions is encouraging, as it may enable us to better understand the neural substrates of language production.

Activation in the IFG was not hypothesised for this task as results from previous studies in adults are variable (Awad, Warren, Scott, Turkheimer, & Wise, 2007; Tremblay & Small, 2011). Further, functional neuroanatomical models of language predict tasks with a large semantic load induce activation of the IFG (Price, 2012). However, the semantic and syntactic demands of the sentence generation task were relatively low; participants were asked to construct a sentence based on images which contained animals and objects with high word frequency, using a limited set of only four common verbs.

3.5.4 Local and Global Signal Changes.

A large difference was observed between the amount of data that was changed by FIACH step 2 and by frame censoring highlighting that aggressive cleaning strategies may be sub-optimal. This may be attributed to the most damaging effects of motion being local (due to repeated excitation of the same tissue or in regions of spatially fast changing signal intensity such as at the edges of the brain) while the average signal changes across the brain are much lower in magnitude. The results shown in Figure 11 suggest that when an individual meets the threshold for a frame to be censored the image does not always exhibit widespread signal changes large enough to be discriminated from BOLD signal amplitudes.

This difference could also be attributed to the limited accuracy in using volumetric realignment parameters as models of motion. This has been previously highlighted by (Beall & Lowe, 2014) who had ground truth measures of motion which we do not have in this study.

It should also be noted that the FIACH model is very conservative in terms of data correction so a direct comparison between FIACH step 2 and RPE is difficult. Less conservative thresholds for FIACH step 2 or more conservative thresholds for censoring will result in more comparable amounts of data being changed/censored. Furthermore FIACH may correct artefacts due to electrical noise which frame censoring (based on RPs) cannot. As such this further limits the comparison. Bearing in mind these limitations the application of FIACH step 2 was still seen to increase t-values and cluster extent relative to the RPE method. This highlights that there may be diminishing returns to using expansions of the realignment parameters.

More widespread signal changes that are lower in magnitude may become more problematic in less efficient designs such as in those seen in studies of epilepsy where the method of censoring used in this paper was developed (Lemieux et al., 2007). In this context,the combination of FIACH step 2 and censoring may be beneficial in these situations. Furthermore if there are global changes still present in the data after FIACH step 2 (or censoring) a statistically elegant strategy would be to use a weighted least squares approach such as RWLS as a subsequent step to FIACH.

3.5.5 Methodological Considerations and Limitations

A primary limitation of FIACH is the single imputation of values for corrupt time points. While we do show improvements in observed activations a more statistically optimal strategy would be to use a multiple imputation framework (Rubin, 1988). A potential secondary benefit of multiple imputation would be for spectral analysis of rs-fcMRI which can potentially be affected by single imputation/scrubbing (replacing with mean/median). Future work will focus on the development of this approach in the context of fMRI.

It is also worth considering the choice of model parameters used in this study. In this work we deliberately chose to estimate the maximum possible magnitude of the BOLD response. This was done to deliberately minimise data alteration, and in the knowledge that children and patients may have responses greater than the range typically found in healthy adults. More realistic parameters could be chosen but we demonstrate that FIACH still performs favourably in comparison with other methods even with a conservative approach to data correction. We have demonstrated that applying FIACH produces superior results in both tasks compared to the other methods reviewed.

However, we have not explored the possibility of combining FIACH with other methods for an even better method. For instance one could combine the FIACH regressors with motion estimates from Motion Fingerprint and then estimate the model using RWLS. Frame-censoring/scan nulling could also be applied. This is because the results presented are not primarily intended to be comparative but highlight the potential gains from utilizing a biophysical framework for extending traditional approaches.

3.5.6 Conclusion

We have developed a biophysical framework for extending the traditional approach of using volumetric measures of motion to control for noise in fMRI. It can be integrated as a pre-processing step within current standard strategies for mass-univariate GLM based analysis and rs-fcMRI. This method is a two-step procedure involving the identification and correction of large amplitude signal changes and modelling the effects of regions of high temporal instability.

We have demonstrated its efficacy in a paediatric population during overt speech where subject motion is a severely limiting factor in both research and clinical applications of fMRI. We have shown that FIACH reveals additional brain areas involved in language at the group and individual level. It also substantially increases the statistical power in language related areas relative to other methods. Furthermore, this methodology is capable of improving results in regions of low SNR due to local field inhomogeneities (inferior temporal and high blood volume regions). These areas have proven particularly problematic for fMRI, and FIACH provides the opportunity to improve knowledge of the function within these areas.

References

Awad, M., Warren, J. E., Scott, S. K., Turkheimer, F. E., & Wise, R. J. S. (2007). A common system for the comprehension and production of narrative speech. *The Journal of Neuroscience : The Official Journal of the Society for Neuroscience*, *27*(43), 11455–64. http://doi.org/10.1523/JNEUROSCI.5257-06.2007

Beall, E. B., & Lowe, M. J. (2014). SimPACE: Generating simulated motion corrupted BOLD data with synthetic-navigated acquisition for the development and evaluation of SLOMOCO: A new, highly effective slicewise motion correction. *NeuroImage*, *101*, 21–34. http://doi.org/10.1016/j.neuroimage.2014.06.038

Beckmann, C., & Smith, S. (2004). Probabilistic independent component analysis for functional magnetic resonance imaging. *… Imaging, IEEE Transactions on*, *23*(2), 137–152.

Behzadi, Y., Restom, K., Liau, J., & Liu, T. T. (2007). A component based noise correction method (CompCor) for BOLD and perfusion based

fMRI. *NeuroImage*, *37*(1), 90–101. http://doi.org/10.1016/j.neuroimage.2007.04.042

Binder, J. R., Desai, R. H., Graves, W. W., & Conant, L. L. (2009). Where is the semantic system? A critical review and meta-analysis of 120 functional neuroimaging studies. *Cerebral Cortex (New York, N.Y. : 1991)*, *19*(12), 2767–96. http://doi.org/10.1093/cercor/bhp055

Birn, R. M., Diamond, J. B., Smith, M. A., & Bandettini, P. A. (2006). Separating respiratory-variation-related fluctuations from neuronal-activity-related fluctuations in fMRI. *NeuroImage*, *31*(4), 1536–1548. http://doi.org/10.1016/j.neuroimage.2006.02.048

Blank, S., Scott, S., Murphy, K., Warburton, E., & Wise, R. (2002). Speech production: Wernicke, Broca and beyond. *Brain*, *125*, 1829–1838.

Buxton, R. B., Miller, K. L., Wong, E. C., & Frank, L. R. (1998). of the Balloon Model to the BOLD Response to Stimuli of Different Duration, *855*, 36722.

Croft, L. J., Rankin, P. M., Liégeois, F., Banks, T., Cross, J. H., Vargha-Khadem, F., & Baldeweg, T. (2013). To speak, or not to speak? The feasibility of imaging overt speech in children with epilepsy. *Epilepsy Research*, *107*(1-2), 195–9. http://doi.org/10.1016/j.eplepsyres.2013.08.008

Desjardins, a E., Kiehl, K. A., & Liddle, P. F. (2001). Removal of confounding effects of global signal in functional MRI analyses. *NeuroImage*, *13*(4), 751–8. http://doi.org/10.1006/nimg.2000.0719

Devlin, J. T., Russell, R. P., Davis, M. H., Price, C. J., Wilson, J., Moss, H. E., … Tyler, L. K. (2000). Susceptibility-induced loss of signal: comparing PET and fMRI on a semantic task. *NeuroImage*, *11*(6 Pt 1), 589–600. http://doi.org/10.1006/nimg.2000.0595

Diedrichsen, J., & Shadmehr, R. (2005). Detecting and adjusting for artifacts in fMRI time series data. *NeuroImage*, *27*(3), 624–34. http://doi.org/10.1016/j.neuroimage.2005.04.039

Eddelbuettel, D., & Francois, R. (2011). Rcpp: Seamless R and C plus plus Integration. *Journal of Statistical Software*, *40*(8), 1–18.

Eddelbuettel, D., & Sanderson, C. (2014). RcppArmadillo: Accelerating R with high-performance C++ linear algebra. *Computational Statistics and Data Analysis*, *71*, 1054–1063. http://doi.org/10.1016/j.csda.2013.02.005

Friston, K. J., Williams, S., Howard, R., Frackowiak, R. S., & Turner, R. (1996). Movement-related effects in fMRI time-series. *Magnetic Resonance in Medicine*, *35*(3), 346–55.

Glover, G. H., Li, T. Q., & Ress, D. (2000). Image-based method for retrospective correction of physiological motion effects in fMRI: RETROICOR. *Magnetic Resonance in Medicine*, *44*(March), 162–167. http://doi.org/10.1002/1522-2594(200007)44:1<162::AID-MRM23>3.0.CO;2-E

Griffanti, L., Salimi-Khorshidi, G., Beckmann, C. F., Auerbach, E. J., Douaud, G., Sexton, C. E., … Smith, S. M. (2014). ICA-based artefact removal and accelerated fMRI acquisition for improved resting state network imaging. *NeuroImage*, *95*, 232–47. http://doi.org/10.1016/j.neuroimage.2014.03.034

Grubb, R. L., Raichle, M. E., Eichling, J. O., & Ter-Pogossian, M. M. (1974). The Effects of Changes in PaCO2 Cerebral Blood Volume, Blood Flow, and Vascular Mean Transit Time. *Stroke*, *5*(5), 630–639. http://doi.org/10.1161/01.STR.5.5.630

Hochberg, Y. (1988). A sharper bonferroni procedure for multiple tests of significance. *Biometrika*. http://doi.org/10.1093/biomet/75.4.800

Kundu, P., Inati, S. J., Evans, J. W., Luh, W.-M., & Bandettini, P. A. (2012). Differentiating BOLD and non-BOLD signals in fMRI time series using multi-echo EPI. *NeuroImage*, *60*(3), 1759–70. http://doi.org/10.1016/j.neuroimage.2011.12.028

Lauwers, F., Cassot, F., Lauwers-Cances, V., Puwanarajah, P., & Duvernoy, H. (2008). Morphometry of the human cerebral cortex microcirculation: general characteristics and space-related profiles. *NeuroImage*, *39*(3), 936–48. http://doi.org/10.1016/j.neuroimage.2007.09.024

Lehericy, S., Cohen, L., Bazin, B., Samson, S., Giacomini, E., Rougetet, R., … Baulac, M. (2000). Functional MR evaluation of temporal and frontal language dominance compared with the Wada test. *Neurology*, *54*(8), 1625–1633. http://doi.org/10.1212/WNL.54.8.1625

Lemieux, L., Salek-Haddadi, A., Lund, T. E., Laufs, H., & Carmichael, D. (2007). Modelling large motion events in fMRI studies of patients with epilepsy. *Magnetic Resonance Imaging*, *25*(6), 894–901. http://doi.org/10.1016/j.mri.2007.03.009

Liegeois, F. (2002). A Direct Test for Lateralization of Language Activation using fMRI: Comparison with Invasive Assessments in Children with Epilepsy. *NeuroImage*, *17*(4), 1861–1867. http://doi.org/10.1006/nimg.2002.1327

Lund, T. E., Nørgaard, M. D., Rostrup, E., Rowe, J. B., & Paulson, O. B. (2005). Motion or activity: their role in intra- and inter-subject variation in fMRI. *NeuroImage*, *26*(3), 960–4. http://doi.org/10.1016/j.neuroimage.2005.02.021

Mildner, T., Norris, D. G., Schwarzbauer, C., & Wiggins, C. J. (2001). A qualitative test of the balloon model for BOLD-based MR signal changes at 3T. *Magnetic Resonance in Medicine : Official Journal of the Society of Magnetic Resonance in Medicine / Society of Magnetic Resonance in Medicine*, *46*(5), 891–9.

Müller, R.-A., Rothermel, R. D., Behen, M. E., Muzik, O., Mangner, T. J., & Chugani, H. T. (1997). Receptive and expressive language activations for sentences. *NeuroReport*, *8*(17), 3767–3770. http://doi.org/10.1097/00001756-199712010-00022

Murphy, K., Birn, R. M., & Bandettini, P. A. (2013). Resting-state fMRI confounds and cleanup. *NeuroImage*, *80*, 349–359. http://doi.org/10.1016/j.neuroimage.2013.04.001

Murphy, K., Birn, R. M., Handwerker, D. A., Jones, T. B., & Bandettini, P. A. (2009). The impact of global signal regression on resting state correlations: are anti-correlated networks introduced? *NeuroImage*, *44*(3), 893–905. http://doi.org/10.1016/j.neuroimage.2008.09.036

Muschelli, J., Nebel, M. B., Caffo, B. S., Barber, A. D., Pekar, J. J., & Mostofsky, S. H. (2014). Reduction of motion-related artifacts in resting state fMRI using aCompCor. *NeuroImage*, *96*, 22–35. http://doi.org/10.1016/j.neuroimage.2014.03.028

Obata, T., Liu, T. T., Miller, K. L., Luh, W.-M., Wong, E. C., Frank, L. R., & Buxton, R. B. (2004). Discrepancies between BOLD and flow dynamics in primary and supplementary motor areas: application of the balloon model to the interpretation of BOLD transients. *NeuroImage*, *21*(1), 144–153. http://doi.org/10.1016/j.neuroimage.2003.08.040

Power, J. D., Barnes, K. A., Snyder, A. Z., Schlaggar, B. L., & Petersen, S. E. (2012). Spurious but systematic correlations in functional connectivity MRI networks arise from subject motion. *NeuroImage*, *59*(3), 2142–54. http://doi.org/10.1016/j.neuroimage.2011.10.018

Power, J. D., Schlaggar, B. L., & Petersen, S. E. (2014). Recent progress and outstanding issues in motion correction in resting state fMRI. *NeuroImage*, 1–16. http://doi.org/10.1016/j.neuroimage.2014.10.044

Price, C. J. (2010). The anatomy of language: a review of 100 fMRI studies published in 2009. *Annals of the New York Academy of Sciences*, *1191*, 62–88. http://doi.org/10.1111/j.1749-6632.2010.05444.x

Price, C. J. (2012). A review and synthesis of the first 20 years of PET and fMRI studies of heard speech, spoken language and reading. *NeuroImage*, *62*(2), 816–47. http://doi.org/10.1016/j.neuroimage.2012.04.062

R Core team. (2015). R Core Team. *R: A Language and Environment for Statistical Computing. R Foundation for Statistical Computing , Vienna, Austria. ISBN 3-900051-07-0, URL http://www.R-Project.org/.*

Rubin, D. B. (1988). An Overview of Multiple Imputation. *Proceedings of the Survey Research Methods Section of the American Statistical Association*, 79–84.

Satterthwaite, T. D., Elliott, M. A., Gerraty, R. T., Ruparel, K., Loughead, J., Calkins, M. E., … Wolf, D. H. (2013). An improved framework for confound regression and filtering for control of motion artifact in the preprocessing of resting-state functional connectivity data. *NeuroImage*, *64*, 240–256. http://doi.org/10.1016/j.neuroimage.2012.08.052

Satterthwaite, T. D., Wolf, D. H., Loughead, J., Ruparel, K., Elliott, M. A., Hakonarson, H., … Gur, R. E. (2012). Impact of in-scanner head motion on multiple measures of functional connectivity: relevance for studies of neurodevelopment in youth. *NeuroImage*, *60*(1), 623–32. http://doi.org/10.1016/j.neuroimage.2011.12.063

Seghier, M. L. (2013). The angular gyrus: multiple functions and multiple subdivisions. *The Neuroscientist : A Review Journal Bringing Neurobiology, Neurology and Psychiatry*, *19*(1), 43–61. http://doi.org/10.1177/1073858412440596

Siegel, J., Power, J., & Dubis, J. (2014). Statistical improvements in functional magnetic resonance imaging analyses produced by censoring high-motion data points. *Human Brain Mapping*, *35*(5), 1981–1996. http://doi.org/10.1002/hbm.22307.Statistical

Tremblay, P., & Small, S. L. (2011). Motor response selection in overt sentence production: a functional MRI study. *Frontiers in Psychology*, *2*(September), 253. http://doi.org/10.3389/fpsyg.2011.00253

Tzourio-Mazoyer, N., Landeau, B., Papathanassiou, D., Crivello, F., Etard, O., Delcroix, N., … Joliot, M. (2002). Automated anatomical labeling of activations in SPM using a macroscopic anatomical parcellation of the MNI MRI single-subject brain. *NeuroImage*, *15*(1), 273–89. http://doi.org/10.1006/nimg.2001.0978

Uludağ, K., Müller-Bierl, B., & Uğurbil, K. (2009). An integrative model for neuronal activity-induced signal changes for gradient and spin echo functional imaging. *NeuroImage*, *48*(1), 150–65. http://doi.org/10.1016/j.neuroimage.2009.05.051

Van Dijk, K. R. A., Sabuncu, M. R., & Buckner, R. L. (2011). The influence of head motion on intrinsic functional connectivity MRI. *NeuroImage*, *59*(1), 431–8. http://doi.org/10.1016/j.neuroimage.2011.07.044

Weiskopf, N., Hutton, C., Josephs, O., & Deichmann, R. (2006). Optimal EPI parameters for reduction of susceptibility-induced BOLD sensitivity

losses: a whole-brain analysis at 3 T and 1.5 T. *NeuroImage*, *33*(2), 493–504. http://doi.org/10.1016/j.neuroimage.2006.07.029

Weisskoff, R., & Kiihne, S. (1992). MRI susceptometry: Image-based measurement of absolute susceptibility of MR contrast agents and human blood. *Magnetic Resonance in Medicine*, *383*, 375–383.

Whitcher, B., Schmid, V. J., & Thornton, A. (2011). Working with the DICOM and NIfTI Data Standards in R. *Journal Of Statistical Software*, *44*(6), 1–29. http://doi.org/10.1093/rpd/ncr352

Wilke, M. (2012). An alternative approach towards assessing and accounting for individual motion in fMRI timeseries. *Neuroimage*, *59*(3), 2062–2072. http://doi.org/10.1016/j.neuroimage.2011.10.043

Winawer, J., Horiguchi, H., & Sayres, R. (2010). Mapping hV4 and ventral occipital cortex: the venous eclipse. *Journal of Vision*, *10*, 1–22. http://doi.org/10.1167/10.5.1.Introduction

Yablonskiy, D., & Haacke, E. (1994). Theory of NMR signal behavior in magnetically inhomogeneous tissues: the static dephasing regime. *Magnetic Resonance in Medicine*, (32), 749–763.

4. Optimising EEG-fMRI for application in paediatric focal epilepsy

In this chapter I discuss the benefits of implementing a natural stimulus during simultaneous EEG-fMRI and evaluate the clinical utility of 3 metrics used for quality assurance.

Abstract

The application of EEG-fMRI in paediatric populations is limited by one's ability to ensure the quality of the data is sufficient for clinical inference to be made. One issue is subject compliance; the other is assessment of data quality. Both these topics will be addressed in this chapter. To increase subject compliance a natural stimulus was played (a cartoon) while 46 focal epilepsy patients were scanned using simultaneous EEG-fMRI. It was found that the implementation of the natural stimulus did not have an adverse effect on the rate of occurrence of Interictal Epileptiform Discharges (IEDs). This means that the stimulus can be implemented without the risk of losing statistical power due to suppression of IEDs. It was also noted that the natural stimulus reduced subject motion if played within the first twenty minutes of scanning. Lastly commonly used metrics of data quality such as temporal Signal to Noise Ratio (tSNR) and Mean Framewise Displacement (MFD) were not capable of predicting clinical utility of EEG-fMRI in the current sample. However, design efficiency was predictive of clinical utility and it is recommended this metric be reported when conducting EEG-fMRI experiments on patients with focal epilepsy.

Declaration of Work: Dr Maria Centeno recruited the subjects who participated in this study. Maria Centeno created the EEG-fMRI maps. David Carmichael and Maria Centeno created the definition of concordance used in this study. Tim Tierney performed all subsequent analyses and interpretation presented in this chapter.

4.1 Introduction

A primary limitation of fMRI in the paediatric population is subject compliance. Most previous EEG-fMRI studies in children have used sedation to ensure compliance (Jacobs et al., 2007; Moeller et al., 2013). This is problematic as it is poorly understood how sedation may affect epileptic activity and haemodynamics. Sedation also confounds group studies as the degree of sedation may vary between patients and is extremely unlikely to be performed in control groups. The current study examines the feasibility of EEG-fMRI in a paediatric population of focal epilepsy population and explores ways in which the process can be optimised. This is of key importance as paediatric populations are the most likely group to benefit from surgery (Skirrow et al., 2015).

Natural stimulation has been proposed as a non-invasive approach to increase compliance in paediatric populations (Kana et al., 2011). Natural stimulation essentially involves the presentation of low level (usually audio-visual) stimulation (such as a video). The impact of natural stimuli on the occurrence of epileptic activity is unknown although some research suggests that stimulation may suppress epileptic activity (Aarts, Binnie, Smit, & Wilkins, 1984). If this is the case then the efficacy of EEG-fMRI would be reduced as fewer epileptic events would reduce the statistical power of the experiment by reducing the design efficiency (Dale, 1999).

Furthermore the issue of how to assess data quality in EEG-fMRI (without looking at the resulting statistical map) is unknown. In the previous chapter we demonstrated that some typical measures of data quality such as framewise displacement may overestimate the rate of data corruption due to movement (Figure 11). It is therefore of interest to assess what measures can be calculated before analysis is performed to predict clinical utility of EEG-fMRI. The metrics we intend to look at are design efficiency, a metric proportional to the BOLD signal induced by the epileptic events (Dale, 1999), Mean Framewise Displacement (MFD: a metric describing subject motion derived from the realignment parameters) and temporal Signal to Noise Ratio (tSNR: defined in this study as the median of the signal divided by the median absolute deviation in time). Of special note is how design efficiency

differs from rate of IEDs. Usually the number of IEDs per minute is reported for each patient. However two patients with the same IED rate (e.g. 10 per minute) may have different design efficiencies. This is because the IED rate is not stationary over time. The design efficiency captures this non stationarity mathematically and is therefore a better representation of epileptic activity. The three primary research questions associated with this study were as follows.

a) What is the effect of the natural stimulation on in-scanner movement
b) What is the effect of the natural stimulation on the occurrence of Interictal Epileptiform Discharges (IED)
c) Can design efficiency, tSNR and framewise displacement predict clinical utility of EEG-fMRI

4.2 Method

4.2.1 Subjects

Forty-six children (25 female) with drug resistant were recruited. Patient's ages ranged from 7 to 18 with a mean age of 13.7 years. A control group of 20 healthy volunteers (11 female) with an age range (6.61-16.73 years) and mean age of 11.64 were also recruited. Localization of the epileptogenic region was agreed for every patient by consensus between a group of expert epileptologists after reviewing a panel of diagnostic tests. The tests included T1 weighted MRI, T2 weighted MRI, FLAIR, PET, SPECT, EEG, MEG and electro-clinical information derived from video-EEG telemetry by a neurologist (MC). The relevant clinical information is presented in Table 4

ID	Age (Gender)	Localisation	MRI diagnosis	Scalp EEG IED	EEG-FMRI Concordance
# 1	8(F)	L Temporal	TS	L temporal	D
# 2	14(F)	L Frontal pole	N/A	No IED	N/A
# 3	11(M)	Hypothalamus	Hypothalamic hamartoma	Left temporal	D
# 4	15(M)	L Fronto-Temporal	N/A	No IED	N/A
# 5	11(F)	R Fronto-Temporal	N/A	R Fronto-Temporal	D
# 6	17(M)	R Parietal	FCD	R Temporal	C
# 7	15(M)	R Frontal-central	N/A	No IED	N/A
# 8	15(M)	L Temporal/R Frontal	FCD	R Frontal	C
# 9	11(F)	L Frontal-central	Unspecific cortical atrophy	L central	C
# 10	14(F)	R Temporal	FCD 2B	R Temporal	C
# 11	11(F)	R Frontal pole	FCD	R Fronto-Temporal	C

# 12	11(F)	R Fronto-temporal	N/A	R Fronto-polar	C
# 13	12(M)	R central	R hemispheric atrophy	R central	D
# 14	17(F)	R Frontal	N/A	R Frontal	C
# 15	16(F)	L Frontal	N/A	spike-wave runs	C
# 16	11(F)	L Frontal	N/A	L Frontal lateral	D
# 17	14(M)	L fronto-temporal	Autoimmune	L Temporal	C
# 18	16(F)	L posterior insula	FCD	L central	D
# 19	18(M)	R precuneus	FCD 2A	R Parietal	D
# 20	11(M)	R Frontal	N/A	R Frontal	C
# 21	16(F)	L frontal	Polymicrogyria	L posterior quadrant	C
# 22	15(M)	Temporo-Occipital	HS	L posterior quadrant	C
# 23	17(F)	L Unknown	N/A	No IED	N/A
# 24	17(F)	L Frontal	N/A	No IED	N/A
# 25	8(F)	L Frontal	MCA stroke	spike-wave runs	C
# 26	16(M)	R Frontal	N/A	R Frontal	D
# 27	11(M)	L posterior quadrant	Choroid plexus papilloma	L posterior quadrant	D
# 28	13(M)	L Frontal	FCD	L Frontal	D
# 29	10(F)	L Frontal	N/A	L Frontal	D
# 30	11(M)	R Temporo-Parietal	N/A	R Parietal	C
# 31	14(M)	L Occipital	PCA stroke	L Occipital	C
# 32	17(M)	L Frontal	N/A	No IED	N/A
# 33	17(M)	R Occipital	Posterior territory stroke	L Occipital	C
# 34	13(M)	L Occipital	Unspecific cortical atrophy	L posterior quadrant	C
# 35	18(F)	R Frontal	FCD	No IED	N/A
# 36	17(F)	R Fronto-temporal	Polymicrogyria	R Temporal	C
# 37	18(F)	R Fronto-Parietal	FCD	No IED	N/A
# 38	11(F)	R Parietal	N/A	R central	D
# 39	18(M)	R Parietal	DNET	R Parietal	D
# 40	11(F)	R Parietal	FCD	R Parietal	C
# 41	13(F)	R medial Temporal	DNET	R anterior Temporal	C
# 42	12(M)	R Perisylvian	Polymicrogyria	R Fronto-Parietal	D
# 43	17(F)	L Frontal	N/A	L Frontal-vertex	C
# 44	13(F)	L Frontal	FCD	L Frontal lateral	C
# 45	15(F)	R posterior cingulate	DNET	R Frontal	D
# 46	7(M)	L Frontal	N/A	L Frontal vertex	C

Table 4. Clinical information pertaining to subjects. In the age and gender column M indicates Male and F indicates Female. The localisation columns describe the localisation defined by clinical consensus. In MRI diagnosis the following acronyms are used: TS = Tuber sclerosis, FCD = Focal Cortical Dysplasia, MCA = Middle Cerebral Artery, DNET = Dysembryonic Neuroepithelical Tumour. In the Scalp EEG IED column the location of the observed IED spike field is described. In the concordance column the letter C indicates concordance while D indicates Discordant. If the patient did not

have an IED no localisation was obtained and therefore a value of N/A was ascribed.

4.2.2 Data Acquisition

We acquired simultaneous EEG-fMRI in a 1.5T Siemens Avanto scanner (Erlangen, Germany) at the Great Ormond Street Hospital MRI Department with a 12 channel receive coil. Subjects were fitted with a vacuum cushion during scanning to reduce head movement, and given headphones to dampen the noise from the MRI. Subjects were videoed inside the scanner with an MRI compatible camera (Nordic NeuroLabs, Bergen, Norway) interfaced with Brain Products recording software. Scalp EEG was recorded with a 64-channel MR compatible cap (BrainAmp MR plus, Brain Products, Gilching, Germany). EEG data were band-pass filtered at 0.016 Hz–1 kHz, 16-bit digitalization (0.05 mV resolution) and the sampling rate was 5 kHz. MR gradient and pulse-related artefacts were removed from the EEG using template artefact subtraction(Allen, Josephs, & Turner, 2000; Allen, Polizzi, Krakow, Fish, & Lemieux, 1998) implemented in a commercial EEG processing package (Brain Analyzer; Brain Products). Subjects underwent four sessions of echo-planar imaging (EPI). The parameters of the experiment were as follows: a 3.3x3.3x4 mm effective resolution with a field of view FOV =210 mm, TR = 2,160 ms, TE = 30 ms, flip angle = 75 degrees, number of slices = 30, slice thickness=3 mm, slice gap = 1 mm, ascending order 300 volumes (4 sessions of 300).

4.2.3 Natural Stimulus Paradigm

During 2/4 fMRI sessions subjects were asked to rest with eyes closed and for the remaining two, to watch a video. Sessions of rest (eyes closed) and video were alternated with the first session randomly assigned to be a rest or video session. The video sessions were divided into two conditions “cartoon” and “please wait”. A schematic depicts the task structure (see Figure 13)

Figure 13. Schematic depicting structure of video session.

Participants were either instructed to close their eyes and rest or asked to watch the video via the in-scanner headphones. Verbal responses and in-scanner video monitoring were used to verify that the subjects were following these instructions.

4.2.4 EEG-fMRI analysis

Patient's fMRI time series were analysed using a general linear model to determine the presence of regional IED-related BOLD changes in SPM8 (spm.fil.ac.uk). IEDs were modelled as delta function convolved with the canonical hemodynamic response function (HRF) and its temporal and dispersion derivatives.

fMRI pre-processing consisted of volume-volume realignment using SPM8 followed by pre-processing with FIACH (Tierney et al., 2016) which removes non-physiological signal changes and creates a model of physiological noise. The six realignment parameters and six FIACH noise regressors were entered as regressors of no interest in the GLM. An additional regressor with the paradigm waveform convolved with the HRF was entered for the video sessions to account for the main effect of the task. Images were also smoothed using a Gaussian smoothing kernel with FWHM = 8mm.

An F-contrast was constructed across the canonical Haemodynamic Response Function (HRF) and its derivatives. Changes in BOLD signal were considered statistically significant above a threshold of $p<0.001$ and a minimum cluster size of five contiguous voxels on a single subject. While this threshold is not corrected for multiple comparisons it was defined

heuristically by Dr. Centeno to achieve a balance between sensitivity and specificity. Issues surrounding sensitivity while using multiple comparisons corrections are highlighted in the next chapter of this thesis.

4.2.5 Defining Concordance

EEG-fMRI maps were classified as concordant if a cluster of significant BOLD signal change was found within the presumed epileptogenic zone or discordant if not. For those patients with multiple types of IED, maps were considered concordant if a cluster of significant BOLD signal changes was present within the presumed epileptogenic zone for at least one of the IED types(Pittau, Dubeau, & Gotman, 2012; Salek-Haddadi et al., 2006). The localisation of the epileptogenic zone was based on clinical consensus. Consensus was derived from an assimilation of a variety of imaging procedures (T1 weighted MRI, T2 weighted MRI, FLAIR, PET, SPECT, EEG, MEG) and electro-clinical information derived from video-EEG telemetry by a neurologist (MC)

4.2.6 Analysis

The effect of natural stimulation on subject movement was estimated using a regression model. The dependant variable was movement inside the scanner which was quantified by mean frame-wise displacement (MFD); and the independent variables were the session type (video/rest sessions), time (session order, 1 to 4) and subject age. The interaction between session type and time was also explored. The MFD was transformed using the natural logarithm to normalize the distribution of the residuals.

The model parameters were estimated using a mixed effects model using the R statistical programming language (R Core team, 2015). This model was chosen to accurately estimate the variance associated with the time variable as each individual's ability to tolerate longer scan times varied greatly. The autoregressive component of the model was described by an AR(1) process.

To compare the rate of IED during the video and the rest sessions across all the patients we divided video sessions into the different blocks of the paradigm (cartoon and "please wait" blocks) to account for potential differences in IED rate during the stimulus periods with the cartoon or

“please wait” screen. To establish whether design efficiency, framewise displacement or temporal signal to noise ratio could predict clinical utility, a logistic regression was performed. The dependent variable was the binary classification of concordant/not concordant. The independent variables were design efficiency, tSNR and MFD.

4.3 Results

The movement inside the scanner was greater for sessions 2-3-4 relative to session 1, $t(176) = 2.54, 2.72, 4.34$ respectively ($p<0.05$ for all). The main effect of time on motion is displayed in Figure 14. Older subjects moved less than younger subjects as there was an effect of age, $t(64) = -2.49$, $p <0.05$. There was a non-significant main effect of video across all sessions. However the video significantly reduced movement when played in the first two sessions, as evidenced by the significant video-time interaction: $t(176) = -2.495$, $p <0.05$. In these sessions this amounted to, on average, an approximately 40% reduction in movement as measured by MFD.

For those patients that had IEDs, the mean rate of IED was not significantly different between rest sessions, video and “please wait” screen blocks (Figure 15). Mean rate of IEDS in these three conditions across all patients was 11.160009 IEDs/minute (SE 1.01), 9.69 (SE 1.0) and 9.92 (SE 1.0) respectively. Using an ANOVA There was no statistically significant effect of condition observed on IED rate ($F(2,226)=0.273, p>.05$).

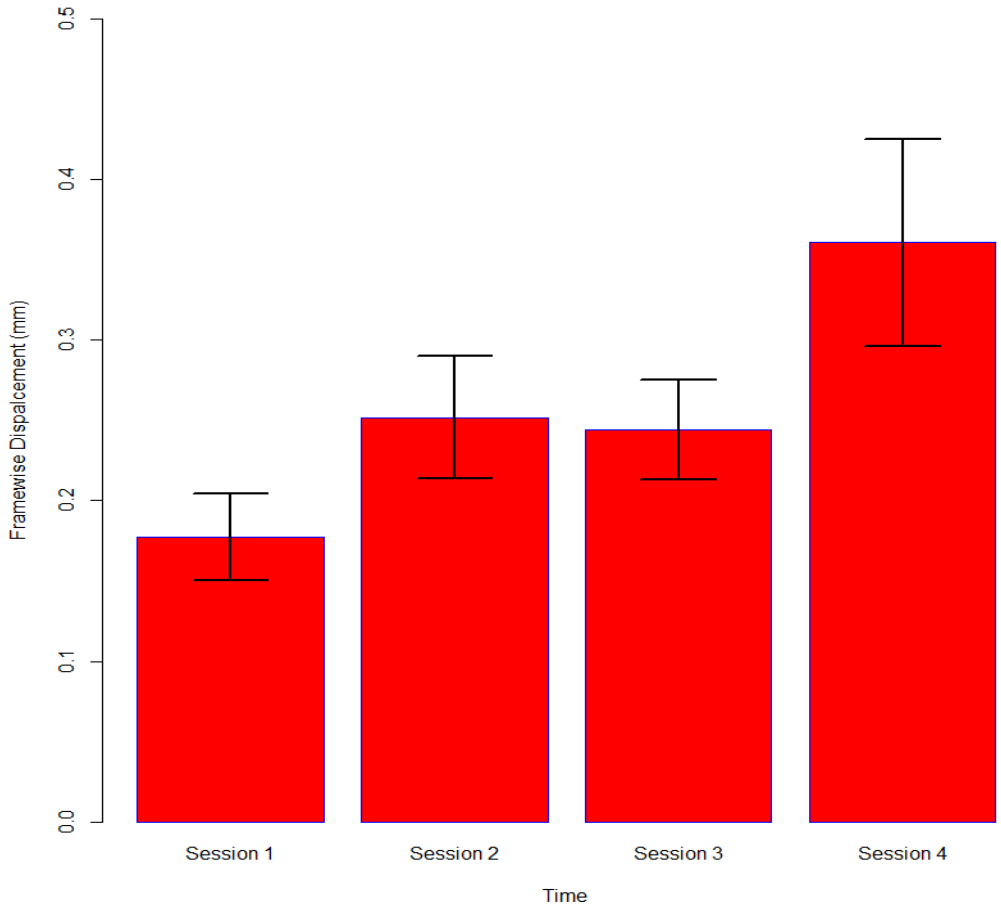

Figure 14. The effect of time (x-axis) on framewise displacement (y-axis). Bars represent mean framewise displacement for each session. The standard error is used to reflect uncertainty in the estimate.

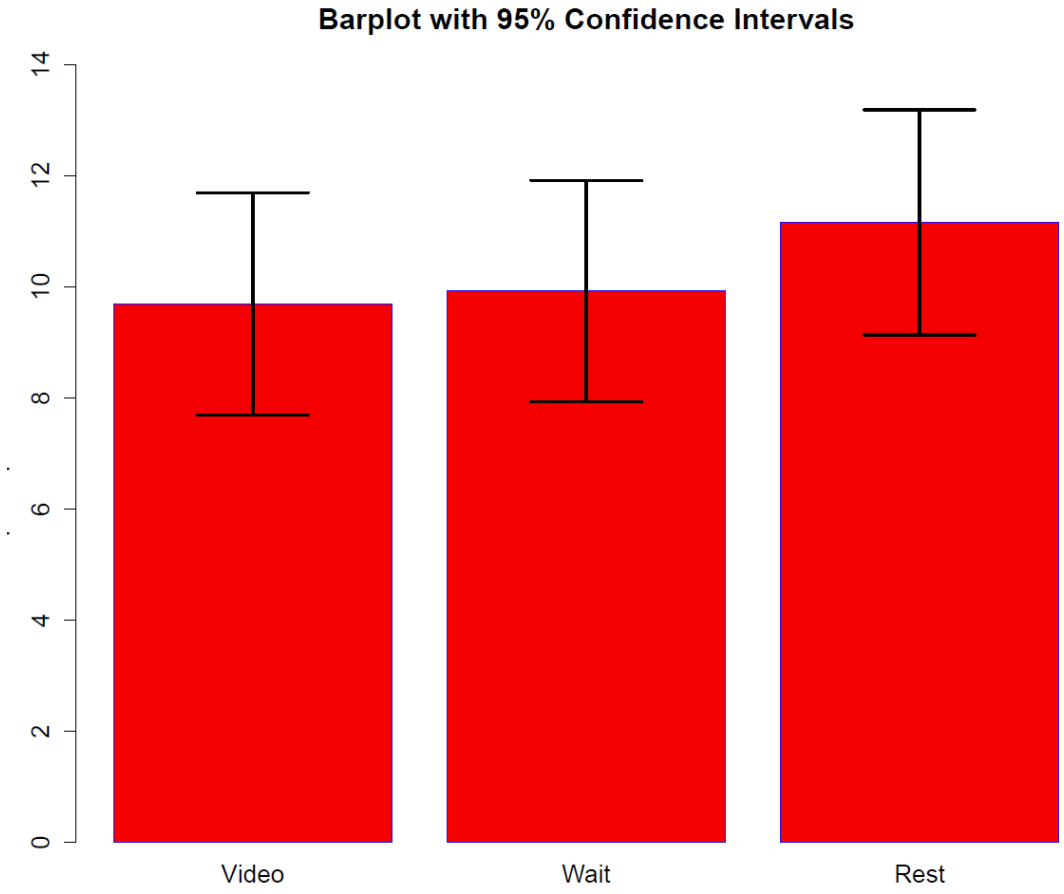

Figure 15. Rate of Interictal Epileptiform discharges (IED). Bars represent mean number of IEDs per minute during the resting state sessions and during the two conditions of the video session (video clip and “please wait” screen). The standard error is used to reflect uncertainty in the estimate.

The classification accuracy of the logistic regression of design efficiency on EEG-fMRI concordance was 65%. This was found to be a statistically significant effect ($Z = 2.925$, $p<0.05$). The effect of motion on concordance as measured by mean framewise displacement, was found not to be statistically significant ($Z = -1.43$, $p>.05$). TSNR was did not predict concordance either ($Z = -.453$, $p>.05$).

4.4 Discussion

4.4.1 Exploring the impact of the natural stimulus.

Interestingly there was no effect of stimulation reported on the rate of occurrence of IEDs despite this being suggested in previous literature (Aarts

et al., 1984). This is encouraging as the implementation of the natural stimulus decreased subject motion, albeit only within the first twenty minutes. It seemed there was duration of scanning beyond which the children in this study were not going to keep still. This decrease in motion is important for a number of reasons. The first is data quality. Less motion means less reliance on post processing techniques (that may fail) to remove the effects of motion. The second is patient comfort. If patients are not comfortable in the scanner they may leave earlier (in a research setting) or require general anaesthetic (in a clinical context) which is costly and not without risks.

4.4.2 A priori metrics of data quality

Perhaps surprisingly MFD was not capable of predicting concordance. As the definition of concordance used in this study (see section 4.2.5) measured the sensitivity of EEG-fMRI one might expect the sensitivity of the method to be altered due to biased parameter estimation (due to motion). While it is true that some motion events bias parameter estimation (see Chapter 3. Figure 4.) this is made substantially less likely by utilising FIACH. After the application of FIACH all signal changes are roughly constrained to be in the range of what is physiologically possible. As such each data point will contribute more or less equally to the regression making biased parameter estimation unlikely.

That does not mean there are no motion related signal changes in the time-series. However these changes will simply serve to increase residual variance and thus contribute to decreasing sensitivity. This however was not the case as our metric of concordance explicitly tests sensitivity which MFD was not capable of predicting. Instead it is more likely that MFD is simply not appropriate for use in paediatric populations as it is a global measure of motion. Often the children we scan move so quickly the effects on the image are often local and thus not reflected in the MFD or the maximum FD or the FD at the point in time that motion occurred (See Chapter 3 Figure 4; Chapter 3 Figure 11).

It was also found that tSNR was not predictive of concordance. However, upon closer inspection an analytical conclusion can be drawn. A schematic is provided to assist interpretation (see Figure 16). The mean

tSNR in our sample was 61 while the 5th percentile was 47 which demonstrates that the tSNR varied very little in our sample. If we assume that the beta is estimated in an unbiased way then only the standard error of the beta is affected by the drop in tSNR. According to the variations in tSNR observed in our sample we would expect at most an increase of 30% in the standard error and thus a 30% drop in the magnitude of the t-value. However when we consider design efficiency this parameter varies as much as 3 orders of magnitude between individuals (.075- 75, units are arbitrary). This has a very large effect on the standard error of the beta as it will cause standard error to vary by approximately a factor of 30 (sqrt(1000)). Once this fact is noted, it is entirely expected that design efficiency is a better predictor of concordance than MFD and tSNR. This makes it so much more important that individuals performing EEG-fMRI report their design efficiencies when assessing the clinical utility of their technique (which has never been done before).

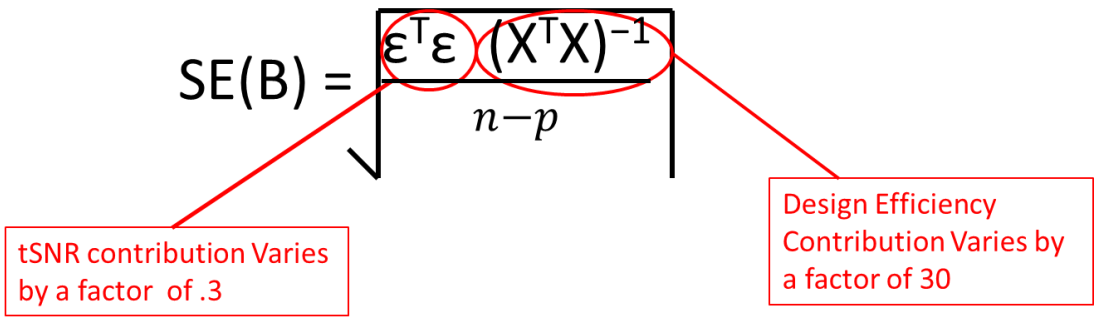

Figure 16. Standard Error of Regression Coefficient (B)

4.4.3 Limitations

There are two primary limitations associated with this study. The first is the definition of concordance between the EEG-fMRI map and the localisation of the epileptogenic zone which was based on clinical consensus. Consensus was derived from an assimilation of a variety of imaging procedures (T1 weighted MRI, T2 weighted MRI, FLAIR, PET, SPECT, EEG, MEG) and electro-clinical information derived from video-EEG telemetry by a neurologist (MC). A greater confidence in the localisation

would be determined typically by post-surgical follow up. However this severely limits the population and may itself be biased (e.g. patients with greater seizure frequency are more likely to be operated). Furthermore concordance is defined if a blob occurs in the presumed epileptogenic zone. This strictly speaking only captures the sensitivity of the method. No correction is made for the fact that many other blobs may co-occur with the concordant one.

The second limitation is one of statistical inference. We have used a heuristic threshold that is not corrected for multiple comparisons to define the threshold at which concordance is assessed ($p<.001$, $k>5$). Using a threshold such as this is typically not advised (Eklund, Nichols, & Knutsson, 2016). However the use of this threshold was clinically defined by Dr. Centeno as striking a balance between sensitivity and specificity. This contrast between clinical definition and statistical best practices motivated further investigation. Upon inspection it was found that in nearly every case a Bonferroni correction offered more sensitivity than utilising Random Field Theory within SPM for multiple comparisons correction. This indicated that the use of FWE correction was indeed overly conservative and motivated the work found in the following chapter to explore this issue in greater detail

4.5 Conclusions

In this study we have demonstrated the feasibility and benefits of employing a natural stimulus when performing EEG-fMRI. Subject motion is reduced while the rates of IED occurrence are not affected. We also identify design efficiency as increasing the likelihood of getting a concordant localisation making it an important factor when using EEG-fMRI in a clinical context. It is recommended that studies performing EEG-fMRI should report this metric.

4.6 References

Aarts, J. H. P., Binnie, C. D., Smit, A. M., & Wilkins, A. J. (1984). Selective cognitive impairment during focal and generalized epileptiform eeg activity. *Brain*, *107*(1), 293–308. http://doi.org/10.1093/brain/107.1.293

Allen, P. J., Josephs, O., & Turner, R. (2000). A method for removing imaging artifact from continuous EEG recorded during functional MRI. *NeuroImage*, *12*(2), 230–9. http://doi.org/10.1006/nimg.2000.0599

Allen, P. J., Polizzi, G., Krakow, K., Fish, D. R., & Lemieux, L. (1998). Identification of EEG events in the MR scanner: the problem of pulse artifact and a method for its subtraction. *NeuroImage*, *8*(3), 229–239. http://doi.org/10.1006/nimg.1998.0361

Dale, a M. (1999). Optimal experimental design for event-related fMRI. *Human Brain Mapping*, *8*(2-3), 109–14. http://doi.org/10.1002/(SICI)1097-0193(1999)8:2/3<109::AID-HBM7>3.0.CO;2-W

Eklund, A., Nichols, T. E., & Knutsson, H. (2016). Cluster failure: Why fMRI inferences for spatial extent have inflated false-positive rates. *Proceedings of the National Academy of Sciences*, 201602413. http://doi.org/10.1073/pnas.1602413113

Jacobs, J., Kobayashi, E., Boor, R., Muhle, H., Stephan, W., Hawco, C., … Siniatchkin, M. (2007). Hemodynamic responses to interictal epileptiform discharges in children with symptomatic epilepsy. *Epilepsia*, *48*(11), 2068–2078. http://doi.org/10.1111/j.1528-1167.2007.01192.x

Kana, R. K., Murdaugh, D. L., Libero, L. E., Pennick, M. R., Wadsworth, H. M., Deshpande, R., & Hu, C. P. (2011). Probing the Brain in Autism Using fMRI and Diffusion Tensor Imaging. *Journal of Visualized Experiments*, *55*(September), 1–6. http://doi.org/10.3791/3178

Moeller, F., Moehring, J., Ick, I., Steinmann, E., Wolff, S., Jansen, O., … Siniatchkin, M. (2013). EEG-fMRI in atypical benign partial epilepsy. *Epilepsia*, *54*(8), 103–108. http://doi.org/10.1111/epi.12243

Pittau, F., Dubeau, F., & Gotman, J. (2012). Contribution of EEG/fMRI to the definition of the epileptic focus. *Neurology*, *78*(19), 1479–1487. http://doi.org/10.1212/WNL.0b013e3182553bf7

R Core team. (2015). R Core Team. *R: A Language and Environment for Statistical Computing. R Foundation for Statistical Computing , Vienna, Austria. ISBN 3-900051-07-0, URL http://www.R-Project.org/.*

Salek-Haddadi, A., Diehl, B., Hamandi, K., Merschhemke, M., Liston, A., Friston, K., … Lemieux, L. (2006). Hemodynamic correlates of epileptiform discharges: an EfMRI study of 63 patients with focal epilepsy. *Brain Res*, *1088*(1), 148–166. http://doi.org/10.1016/j.brainres.2006.02.098

Skirrow, C., Cross, J. H., Harrison, S., Cormack, F., Harkness, W., Coleman, R., … Baldeweg, T. (2015). Temporal lobe surgery in childhood and neuroanatomical predictors of long-term declarative memory outcome. *Brain*, *138*(1), 80–93. http://doi.org/10.1093/brain/awu313

Tierney, T. M., Weiss-Croft, L. J., Centeno, M., Shamshiri, E. a., Perani, S., Baldeweg, T., … Carmichael, D. W. (2016). FIACH: A biophysical model for automatic retrospective noise control in fMRI. *NeuroImage*, *124*, 1009–1020. http://doi.org/10.1016/j.neuroimage.2015.09.034

5. Is Bonferroni correction more sensitive than random field theory for most fMRI studies?

In the previous chapter we made the observation that the many of the EEG-fMRI studies performed would have had greater sensitivity using a Bonferroni correction for multiple comparisons than corrections using Random Field Theory. In this chapter we therefore discuss the implications of the inappropriate use of Random Field Theory as a method of multiple comparisons correction with reference to a review of parameters derived from recently published studies.

Abstract

Random Field Theory has been used extensively in the fMRI literature to address the multiple comparisons problem. The method provides an analytical solution for the computation of precise p-values when its assumptions are met. When its assumptions are not met the thresholds generated by Random Field Theory can be more conservative than Bonferroni corrections, which are arguably too stringent for use in fMRI. As this has been well documented theoretically it is surprising that a majority of current studies (~80%) would not meet the assumptions of Random Field Theory and therefore would have reduced sensitivity. Specifically most data is not smooth enough to meet the good lattice assumption. Current studies smooth data on average by twice the voxel size which is rarely sufficient to meet the good lattice assumption. We provide simulations that identify the critical smoothness at which the application of RFT becomes appropriate. For some applications such as presurgical mapping or, imaging of small structures, probing the laminar/columnar structure of the cortex these smoothness requirements may be too great to preserve spatial structure. As such, this study suggests developments are needed in Random Field Theory to fully exploit the resolution of modern neuroimaging.

Declaration of work: The review presented and simulations performed were conducted by Tim Tierney.

5.1 Introduction

The question of how to address the issue of multiple comparisons in fMRI has received a lot of attention during recent years. It has been suggested that a large number of studies were using thresholds uncorrected for multiple comparisons (Bennett, Wolford, & Miller, 2009). Furthermore, the inadequacy of uncorrected thresholds have been highlighted when it was demonstrated that post-mortem images of a salmon could display "activation" when multiple comparisons were not controlled for (Bennett, Baird, Miller, & Wolford, 2011).

The key difference between the multiple comparisons issue in traditional statistics and imaging is the presence of spatial correlation. Spatial correlation makes methods such as Bonferroni correction inappropriate for the control of statistical error rates in imaging as they are too conservative. Topological inference was introduced to address this issue using the theory of stochastic processes (Friston, Frith, Liddle, & Frackowiak, 1991) and the Euler characteristic (Worsley, Evans, Marrett, & Neelin, 1992), which is often referred to as Random Field Theory (RFT: Worsley et al., 1996). The advantage of RFT is that it recognises that data is sampled from a continuous field. This means that researchers can make inference on topological features (and not voxels) at arbitrary resolution.

This method is computationally inexpensive and accurate when its assumptions are met. Unfortunately the mathematical complexity of the method means that it is difficult to precisely test the assumptions necessary for its application. However, a reviews of the assumptions are available (Petersson, Nichols, Poline, & Holmes, 1999). This lack of clarity surrounding the assumptions concerning RFT is evident from the fact that few studies (in the fMRI literature) have explicitly tested and reported whether or not they have met all the assumptions of RFT before utilising the method. Therefore in each case the validity of RFT is implicitly assumed.

This can potentially explain the large number of studies that have reported that RFT can be conservative (Durnez, Moerkerke, & Nichols, 2014; Eklund, Nichols, & Knutsson, 2016; Hayasaka & Nichols, 2003; Hayasaka, Phan, Liberzon, Worsley, & Nichols, 2004; Li et al., 2014; Li, Nickerson,

Zhao, Nichols, & Gao, 2015; Pantazis, Nichols, Baillet, & Leahy, 2005; Roels, Bossier, Loeys, & Moerkerke, 2015; Worsley, 2003; Worsley, 2005). The conservative nature of RFT in these scenarios is most likely due to situations where the good lattice assumption is not met as these studies largely report results are smoothness dependent. The good lattice assumption has been stated by as the following (Flandin & Friston, 2015):

"The component (error) fields conform to a reasonable lattice approximation of an underlying random field with a multivariate Gaussian distribution."

This statement can be broken down into two sub-statements. The first is that the component (error) fields have a multivariate Gaussian distribution. This is a testable assumption using Mardia's test for multivariate normality (Barnes, Ridgway, Flandin, Woolrich, & Friston, 2013). We will not consider further how departures from multivariate normality may hinder inferences using RFT.

However, the second statement that the components (error) fields conform to a reasonable lattice approximation to an underlying random field is not as easily testable. This statement can be intuitively understood as meaning the data needs to be sampled sufficiently to represent the topological features of interest. This can be facilitated by smoothing the data so the topological features (the "blobs") become large relative to the voxel size and therefore well sampled. The question remains as to how smooth the data needs to be to meet this assumption.

The literature is quite variable concerning advice on this matter. Smoothing is recommended to be between 3-5 times the native space voxel size for RFT to be accurate (Barnes et al., 2013; Petersson et al., 1999; Worsley, 2003; K. J. Worsley, 2005). This ambiguity in the literature means that it is difficult for a researcher to assess if their dataset has met this assumption. This is problematic because if this assumption is not met then the thresholds produced by RFT will be more conservative than a Bonferroni correction (Worsley, 2005). This study therefore poses the following question.

1. Do current data analysis and acquisition strategies produce thresholds more stringent than Bonferroni?

To answer this question, we performed simulations using parameters derived from a survey of recent fMRI studies.

5.2 Theory

It is possible to argue that RFT and Bonferroni should not be compared as RFT is designed to work in continuous space and Bonferroni in discrete space. This fundamental difference means that RFT theory derived thresholds do not change by image resampling whereas a bonferroni will as it is based on the number of voxels.

However, one can use the Bonferroni correction to establish the lower bound on smoothness above which RFT provides accurate p-values. In other words, by decreasing the spatial resolution of images, (or increasing voxel size for a fixed smoothness) there will be a point at which the RFT correction becomes more conservative than the Bonferroni correction. For the purposes of this study we use this point as our definition of when the good lattice assumption is violated. This definition is chosen for practical reasons as it defines regimes of smoothness (or voxel size) in which it is and is not appropriate to apply RFT and is therefore of practical relevance to the imaging community.

5.3 Methods

5.3.1 Analysis

5.3.1.1 fMRI Survey Descriptive Statistics

Brain volume data is taken from a meta-analysis of brain volume (Borzage, Bluml, & Seri, 2014). Voxel size and smoothness are taken from fMRI studies published in *NeuroImage and NeuroImage:Clinical* between January 1st and February 25th 2016. This included articles in press. For the survey we assume that papers published in *NeuroImage* are a representative sample of the data analysis and acquisition practices of imaging researchers and therefore allow us to make an appropriate generalisation of current practice.

Using Science Direct 198 studies included the word fMRI. Only 137 were included in the analysis due to the following reasons: 1) not all studies reported smoothness and voxel size, 2) they were simulations, 3) they were introducing software/repositories, 4) they were animal studies, 5) they were not fMRI studies but mentioned fMRI (fNIRS, optogenetics), 6) they were reviews/meta analyses.

The 137 studies used a variety of different error control methods. These were corrected parametric (68/137 = 49.6%), uncorrected parametric (24/137 = 17.5%), simulation-based corrections (17/137 =12.4%, machine learning (8/137=5.8%) FDR (6/137 = 4.4%), threshold free cluster enhancement (3/137 =2.2%), non-parametric permutation (1/137 = 0.73%), mixture modelling (1/137 = 0.73%), Bonferroni (1/137 = 0.73%), not reported (8/137 = 5.8%). One might expect that as only the corrected parametric approaches (RFT) make assumptions concerning the image smoothness the smoothness may be different between studies that use RFT and those that do not. This was not found to be the case (using Welch's two sample t-test). Studies that use RFT on average smooth their data by 2.05 times voxels size where as those that do not use RFT smooth by 1.94 times voxel size(t (133.85) = 1.0225, p = .3084, effect size: r = .088). As such, using values of smoothing obtained from all of these studies is justified when trying to infer the appropriateness of RFT for current image acquisition and analysis strategies.

As no study reported the estimated residual smoothness from their analysis, which is crucial to determining the appropriateness of RFT, we only documented the applied smoothing kernel width. This is an underestimate of the smoothness of the component error fields as images are already slightly smooth due to the point spread function of the image, T2* blurring and post processing techniques such as interpolation which also increase smoothness. We account for this in our analysis by using empirical data to describe the relationship between estimated residual smoothness and applied smoothing kernel width.

This empirical data is drawn from 47 EEG-fMRI studies of focal epilepsy patients (for the purpose of localising the epileptic focus) conducted

in the data's native space (Chapter 4). The fact that these studies were conducted in native space is important because the process of normalisation/nonlinear warping alters smoothness in an algorithm specific fashion which we do not intend to investigate here. Having calculated the ratio of estimated residual smoothness to applied smoothing kernel width we use the 5th, 50th and 95th quantiles to quantify the uncertainty in this relationship.

5.3.1.2 Simulation of RFT thresholds and Bonferroni Thresholds

In order to simulate RFT thresholds smoothness was defined relative to native voxel size (e.g. if voxel size is 3mm and FWHM = 9 the smoothness was 3) and was varied between 1 and 6. The degrees of freedom (df) were varied between 10 and 100. This was repeated for 1mm, 2mm and 3mm isotropic voxels. This simulation was performed using t-fields designed to achieve FWE correction at p<0.05. We make the following simplification for calculating the Resel Count (R) from the image volume (V) and smoothness ($FWHM$).

$$R = \frac{V}{FWHM_x FWHM_y FWHM_z} \qquad 66$$

While this is not strictly true it is a reasonable approximation for large unmasked volumes (Worsley et al., 1996). Furthermore, if all the components that constitute R were to be included in the analysis RFT thresholds would be even more conservative (Worsley et al., 1996). It is also worth noting that the volume can be in mm^3 or cubic voxels as long as the FWHM is measured in the same unit. The Bonferroni correction was calculated based on the number of voxels, for a given resolution, that would fit in a whole brain volume of 1.4 litres. The expectation of the Euler characteristic ($E\{\chi(R)\}$: asymptotically the p-value) was then calculated as follows with t the t-statistic and df being the degrees of freedom:

$$E\{\chi(R)\} = R\,\frac{(4log_e 2)^{\frac{3}{2}}}{(2\pi)^2}\left(1+\frac{t^2}{df}\right)^{-\frac{1}{2}(df-1)}\left(\frac{df-1}{df}\,t^2-1\right) \qquad 67$$

5.3.1.3 Comparison of Theory and Practice

Having established when RFT would produce overly conservative thresholds (from the simulation described in Section 5.3.1.2) and given the typical values of smoothness and voxel sizes found in the literature (found in the survey described in Section 5.3.1.1) we can now assess how likely a given study is to meet the assumptions of RFT. By taking the ratio of the smoothing kernel width to the voxel size (both found from the survey) we create a new distribution. This new variable (the ratio of smoothness to voxel size) can be compared to the simulation described in section 5.3.1.1 to see how many studies reach the critical smoothness required for the successful application of RFT.

To account for the limitation of unknown residual smoothness we assume a multiplicative relationship between residual smoothness and smoothing kernel width. We use the empirical quantiles described in section 5.3.1.1to get more realistic estimates of residual smoothness. As we will show that the distribution of applied smoothing kernel width relative to voxel sizes is normal the adjusted distribution, obtained using the empirical quantiles, has an analytical form that is obtained by simply multiplying the mean and the standard deviation of the original distribution by the quantiles described in section 5.3.1.1 to calculate a an upper bound, measure of central tendency and lower bound on the number of studies likely to meet the good lattice assumption.

5.3.2 Software

All probabilities are computed using the R programming language (R Core team, 2015). The normal distribution of the ratio of smoothness to voxel size was fit using the fitdistrplus package (Delignette-muller & Dutang, 2015). The RFT thresholds are computed using SPM12 (www.fil.ion.ucl.ac.uk).

5.4 Results

5.4.1 Descriptive Statistics

Of the 137 studies reviewed the average voxel size in the x and y direction is 3.01 mm (SD = 0.62 mm). In the slice direction the average slice thickness was found to have a mean of 3.53 mm (SD= .080 mm). The

average FWHM of smoothing kernels used was 6.12 mm (SD =2.11 mm). The histograms describing these variables are presented in Figure 17.

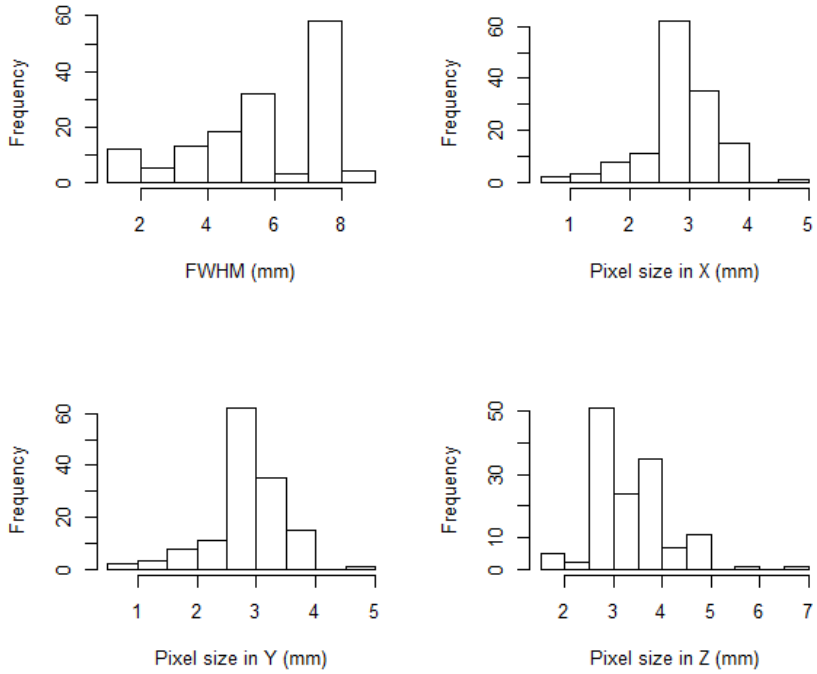

Figure 17. Histograms of smoothing kernel widths and voxel sizes and.

From Figure 17 it is clear that the observed distributions are complex and do not obviously conform to easily describable probability distributions. In particular the histogram of smoothing kernel width is interesting as it shows a clear peak at 8mm which corresponds to the SPM default smoothing kernel width (89/137 studies used SPM).

The ratio of estimated smoothness to applied smoothing kernel width from Chapter 4 had a .05 quantile = 1.26, median (.5 quantile) = 1.36 and .95 quantile = 1.77. The distribution is graphically represented in Figure 18.

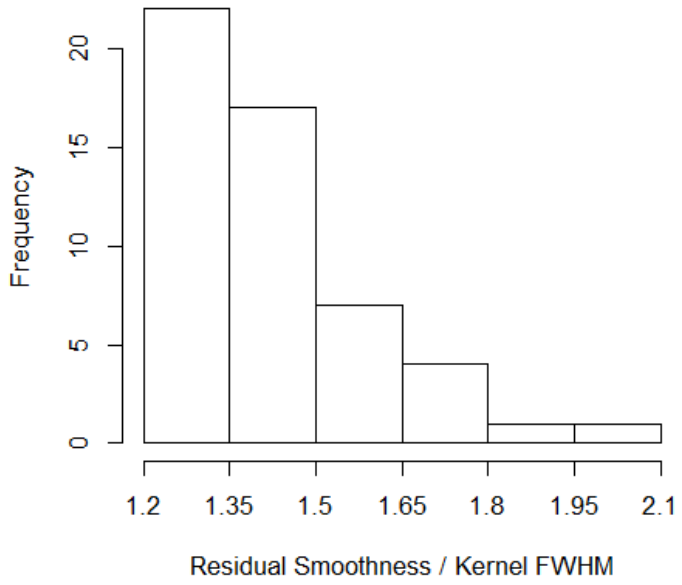

Figure 18. Histogram of estimated residual smoothness (i.e. the smoothness of residual fields – as opposed to signal) relative to applied smoothing kernel width in a sample of N=46 subjects taken from chapter 4.

5.4.2 When does RFT produce less conservative thresholds than Bonferroni?

To address this question we compare RFT theory thresholds to the Bonferroni threshold for different degrees of smoothness and degrees of freedom using a t-field. The results are represented graphically in Figure 19. The black lines in Figure 19 indicate the location of the critical smoothness threshold at which RFT becomes more conservative than Bonferroni. As expected there is strong dependence of the critical threshold on the degrees of freedom but there is a more surprising dependence on resolution as well. High resolution data needs to be smoothed relatively more in order to meet the good lattice assumption: the black lines are shifted to the right indicating larger relative smoothness is required. These results show that there is no rule of thumb that is valid for all experimental designs. The smoothness requirements to meet the good lattice assumption are study specific.

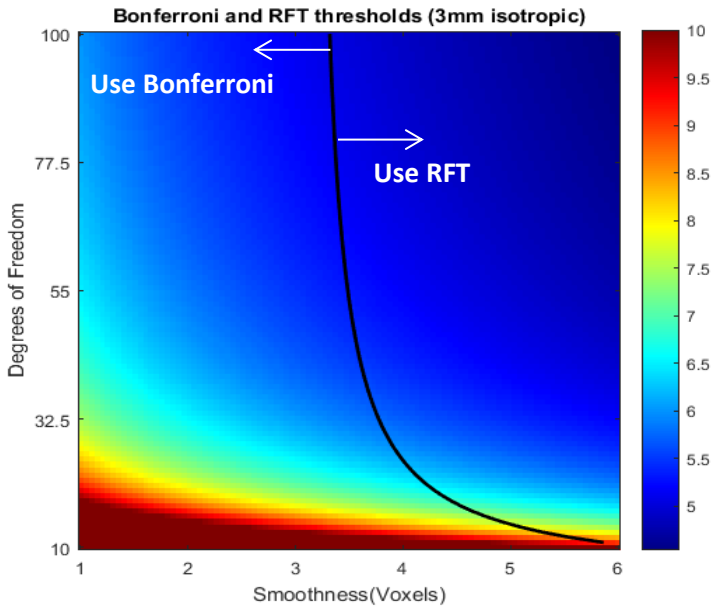
Bonferroni and RFT thresholds (3mm isotropic)
Use Bonferroni
Use RFT
Degrees of Freedom
Smoothness(Voxels)
100
77.5
55
32.5
10
1
2
3
4
5
6
10
9.5
9
8.5
8
7.5
7
6.5
6
5.5
5

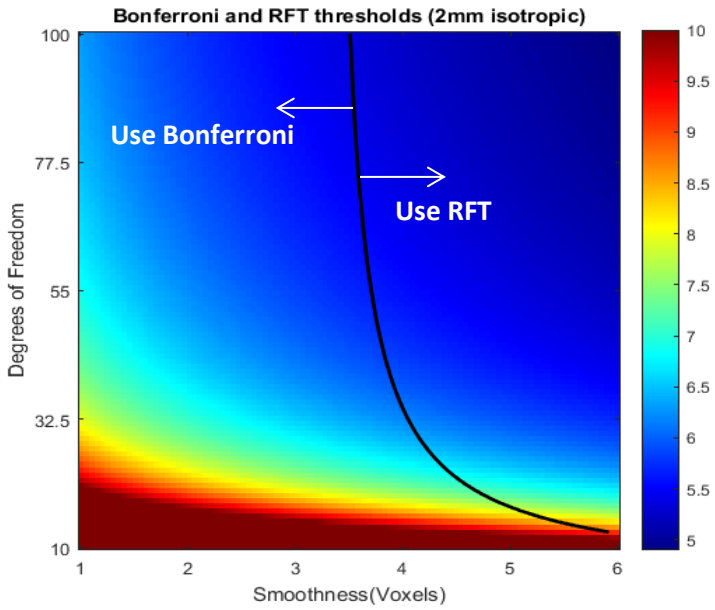
Bonferroni and RFT thresholds (2mm isotropic)
Use Bonferroni
Use RFT
Degrees of Freedom
Smoothness(Voxels)
100
77.5
55
32.5
10
1
2
3
4
5
6
10
9.5
9
8.5
8
7.5
7
6.5
6
5.5
5

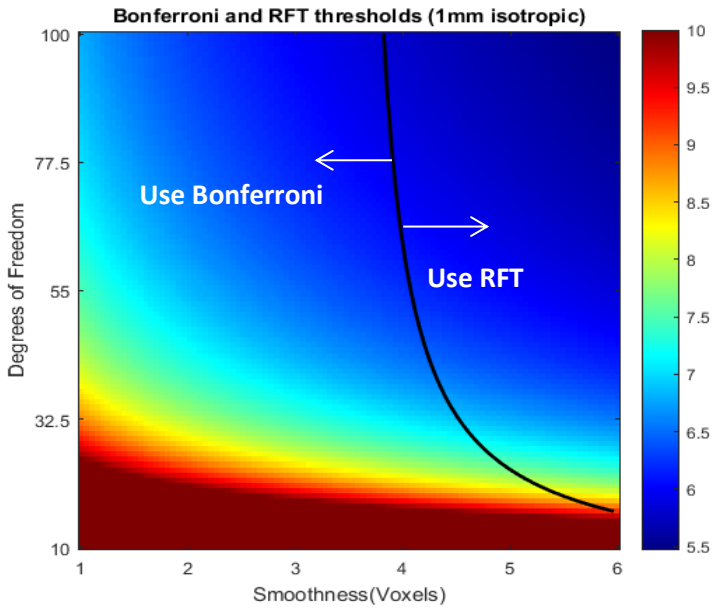
Bonferroni and RFT thresholds (1mm isotropic)
Use Bonferroni
Use RFT
Degrees of Freedom
Smoothness(Voxels)
100
77.5
55
32.5
10
1
2
3
4
5
6
10
9.5
9
8.5
8
7.5
7
6.5
6
5.5

Figure 19. Sensitivity of RFT to degrees of freedom and smoothness. The x axis represents the smoothness relative to the voxel size. The y axis displays the degrees of freedom. The colour bar encodes the height of the t-statistic required to achieve FWE p<.05 using RFT on a brain that is 1.4 litres in volume. The black line shows where the RFT threshold is equal to the Bonferroni threshold (where RFT starts producing accurate thresholds). To the right of the black line RFT is less conservative than Bonferroni and to the left of the black line RFT is more conservative than Bonferroni. This simulation is repeated for 3mm, 2mm and 1mm voxels. For display purposes colour bars have been capped at t=10.

5.4.3 Do current data analysis strategies meet the assumptions of RFT?

The histogram of the applied smoothing kernel width relative to voxel size is displayed in Figure 20. Empirical and theoretical quantiles, probabilities and a cumulative density function accompany this histogram to illustrate the reasonably close fit of this variable to a normal distribution (The closer the points are to the lines the more appropriate the assumption of normality is). The mean of this distribution = 1.99 voxels (SD =.64 voxels).

Using this distribution we can predict the probability of a study having smoothness greater than 3.5 (the point in Figure 19 where the degrees of freedom dependence begins to vanish in the lowest resolution condition) times the voxel size – therefore satisfying the RFT assumptions. The probability is .009 corresponding to a less than 1% chance of a study fulfilling RFT assumptions and obtaining a threshold less conservative than Bonferroni.

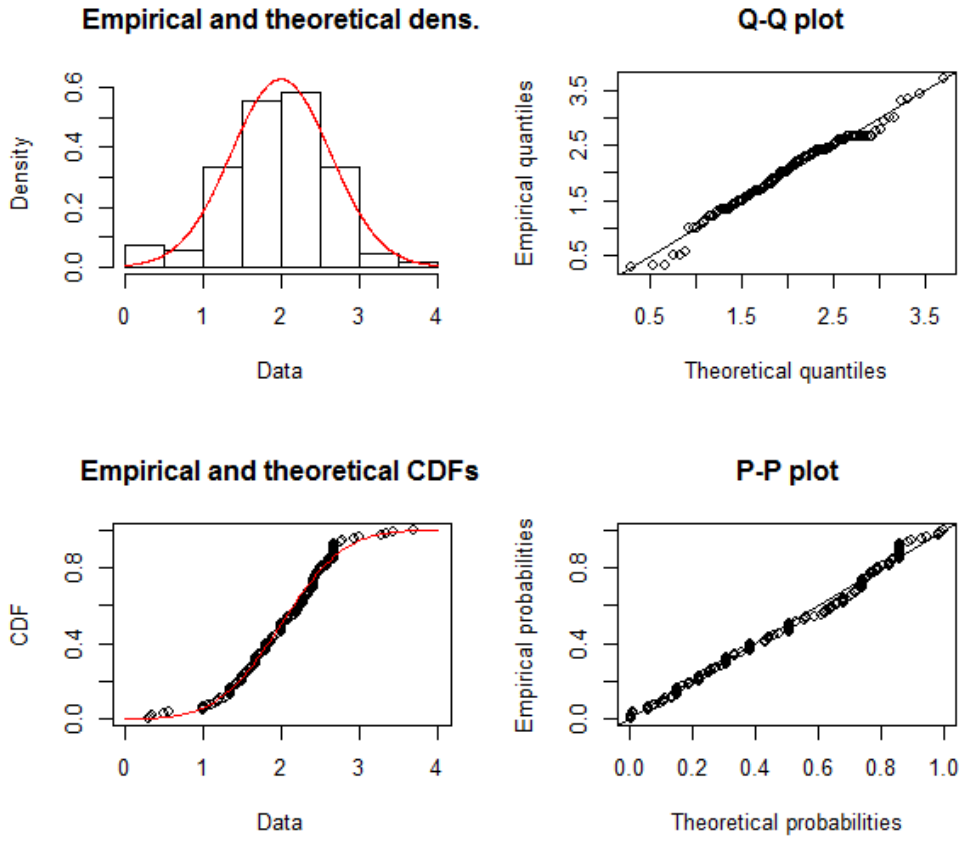

Figure 20. Normality of FWHM / voxel size. The empirical values for FWHM/voxel size are compared with theoretical values for a normal distribution of mean = 1.99 voxels, SD =.64 voxels. As the empirical, quantiles, probabilities and cumulative density function are a good fit to their theoretically predicted values the assumption of normality of FWHM/voxel size is reasonable.

This is an overestimate of the numbers of studies that do not meet the assumptions of RFT – as it is based on smoothing kernel width and not the residual smoothness. However, using the empirical bounds described in Section 5.3.1.1we can adjust the distribution in Figure 20 and recompute the probabilities. This produces a more realistic probability of a study being sufficiently smooth enough to meet the assumptions of RFT.

Adjusting by the multiplicative factors in Section 5.4.1 the median prediction of the percentage of studies likely to not meet the assumptions of RFT is 82%. The upper and lower bounds for the prediction derived using the .95 and .05 quantile described in Section 5.3.1.3 and computed in Section

5.4.1 are 49% and 89% (obtained by multiplying mean and standard deviation by 0.95 and 0.05 quantiles respectively). Therefore the majority of studies are unlikely to meet the assumptions of RFT. This is graphically represented in Figure 21.

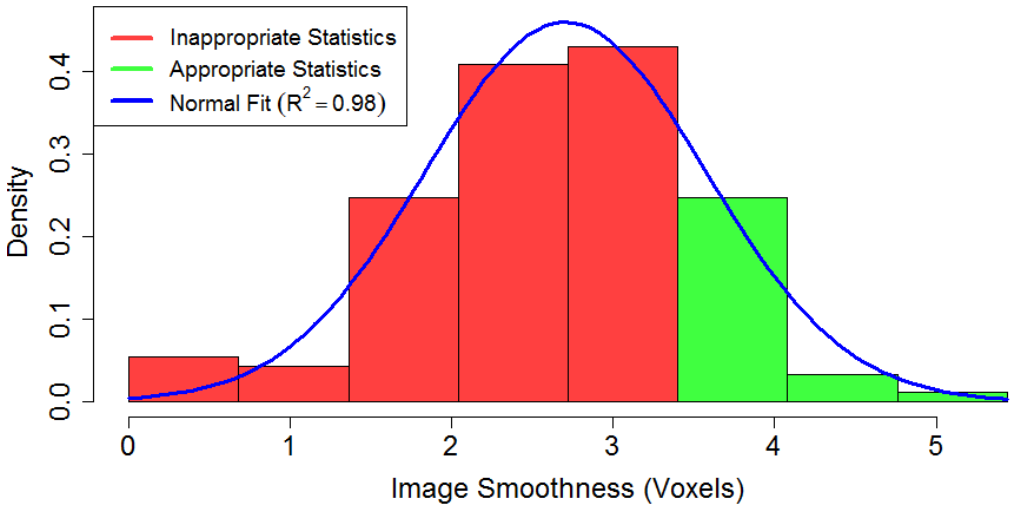

Figure 21. Estimate of residual smoothness in current studies. In this figure the distribution of smoothness to voxel size is re-estimated accounting for relationship between residual smoothness and applied smoothing kernel width. The figure demonstrates that ~80% of studies are unlikely to meet the good lattice assumption in the most lenient case of low resolution data (3mm isotropic) where the criteria for meeting the good lattice assumption is that smoothness be ~3.5 times voxel size.

5.5 Discussion

5.5.1 Summary

We have demonstrated that there is no rule of thumb regarding how smooth one's data should be that can account for the variability in study designs found in the literature. However researchers can use Figure 19 to identify the critical smoothness necessary to apply RFT in a meaningful way. Although it should be noted this is a lower bound on the smoothness that should be applied to the data and the threshold will still be conservative just less so than a Bonferroni correction. In reality, to achieve optimal control of FWE the data may need to be smoothed even further. The simulations

presented in this chapter (Figure 19) build upon previous simulations (Worsley, 2005) by examining a greater range in degrees of freedom and image resolution. These figures are important to interpret the empirical data we have reviewed. We have presented empirical data that shows that – on average – researchers smooth by twice their voxel size and very few are likely to reach the minimal smoothness required to meet the assumptions of RFT. In short for the majority (~80%) of current fMRI studies Bonferroni corrections are more sensitive than RFT.

5.5.2 Alternate Solutions

If researchers do not wish to smooth their data sufficiently to meet the assumptions of RFT (which was found to be the case in this study) a number of other options exist. An initial framework for addressing these issues has been developed (Worsley, 2005) but requires numerical integration, is inaccurate for t and F fields with low degrees of freedom and requires that the autocorrelation function of the field be Gaussian. Furthermore, the results were often conservative for some values of smoothness.

Different error rates could be controlled such as the False Discovery Rate (FDR : Genovese, Lazar, & Nichols, 2002) as described by While this is a reasonable form of error control the continuity inherent in brain imaging data means there are a number of situations where the direct application of FDR (although it does not make any assumptions on image smoothness) is limited. There have been attempts to address these issues (Chumbley & Friston, 2009) but they rely on the use of theoretical results from RFT, which require smooth data.

Alternate approaches to control for FWE include non-parametric permutation tests. These methods make minimal assumptions about the data and are suitable for group-level studies regardless of smoothness, voxel size and degrees of freedom (unlike RFT). The cost incurred is one of computational burden and difficulties in construction of models with covariates and nuisance variables (Winkler, Ridgway, Webster, Smith, & Nichols, 2014). Furthermore the application of permutation tests to the analysis of individual subjects (important in clinical applications) is difficult as the assumption of exchangeability is often violated due to autocorrelation in

the data. This is not a trivial issue as modern fMRI sequences can reach repetition times of 100ms in clinical applications (Jacobs et al., 2014). Some work has been done to address this issue but requires knowledge of the autocorrelation function (Adolf et al., 2014).

In practice some software such as SPM simply chooses the minimum of the Bonferroni correction and the RFT correction. While this is a perfectly reasonable approach to prevent the use of needlessly strict thresholds it should be noted that the Bonferroni correction itself is an overly stringent threshold and inappropriate for smooth data (Worsley, 2005).

5.5.3 Implications

In theory the use of RFT for topological inference seems a reasonable choice for controlling FWE in any spatial dataset as it allows for inference that is independent of the native resolution, has an analytical solution for many different statistical fields, can be computed quickly and is highly accurate for smooth fields of arbitrary dimensionality and geometry.

However, in spite of these benefits our simulations and empirical data presented seem to suggest that very few current studies would benefit from the use of RFT; indeed the thresholds generated are more conservative than a Bonferroni correction. This is because the RFT derived p-values are valid only for continuous fields. Measured data is always discrete but can approximate continuous data if smoothed sufficiently. In short, the reviewed data is not smoothed sufficiently.

As the majority of studies in the fMRI literature are group-level studies the situation becomes slightly more complex as one cannot assume the degrees of freedom are large. In fact when degrees of freedom are less than 30 (see Figure 19) the smoothness requirements begin to increase rapidly. It is therefore difficult to know how much inference is hampered at the group level due to varying sample sizes and nonlinear warping methods (which will influence smoothness in an algorithm specific fashion). As such it is crucial that residual smoothness values are reported and smoothing kernels are chosen carefully with respect to these factors if RFT is used. In these

situations, if the assumptions are not met non-parametric inference may be a reasonable alternative so as to ensure validity (Winkler, Ridgway, Webster, Smith, & Nichols, 2014).

There are a number of situations where it is not feasible to perform group analyses. In these cases there are very few alternatives to RFT for the control of FWE rates. These include clinical applications such as the presurgical mapping of epilepsy patients (Duncan, Winston, Koepp, & Ourselin, 2016) or basic science applications involving small structures. In particular researchers are now interested in probing the layered/columnar structure of the cortex using high resolution fMRI which must be done in the single subject space (Heinzle, Koopmans, den Ouden, Raman, & Stephan, 2016; Yacoub, Harel, & Ugurbil, 2008).

The increased capability to image at high resolution brought about by the availability of MRI scanners with increased magnetic field strength and high density receive array coils means that there is a much greater need for methods that can control for multiple comparisons in this context. It is therefore necessary for developments in RFT to explicitly incorporate the sampling of the continuous field (the brain) in situations where image smoothness needs to be kept at a minimum.

RFT would then be bounded by Bonferroni (so that RFT thresholds are never higher than Bonferroni thresholds) and make them appropriate with less stringent requirements for smoothing (which is crucial for imaging at higher resolution). This would allow for the application in single subject analysis and high resolution imaging. Some work has been done to address this issue using simulations (Li et al., 2014, 2015) but it is not an analytical solution and as such it is difficult to treat theoretically or extend the results to other statistical fields.

5.5.4 Limitations

The results presented suggest that 80% of current studies do not meet the assumptions of RFT at an individual level. However, we had to approximate residual smoothness as it is seldom reported and therefore could not be incorporated into our analysis. We finessed this limitation by

assuming a multiplicative relationship between estimated smoothness and applied smoothing kernel and created bounds on this relationship with empirical data at the individual level. While this is not optimal, it is likely to be a reasonable approximation.

The implications for cluster based inference are also not considered here but are considered elsewhere (Eklund et al., 2016; Guillaume Flandin & Friston, 2016). This is because the purpose of this study was not to provide a complete validation of RFT but to highlight this issue of reduced sensitivity researchers may face when trying to interpret their data at an individual level. That being said the number of studies using parametric peak level statistics (29/137, peak level corrected and 24/137 peak level uncorrected) outweighed the number of studies using parametric cluster level corrected (39/137) further highlighting the need for the simulations presented to achieve optimal peak level statistics.

5.6 Conclusions

We have argued that the Bonferroni correction provides a crucial point of reference that identifies a critical bound on smoothness (or voxel size), which permits the use – or not – of RFT. We have further shown that it is impossible to generate a rule of thumb that could guide researchers on how much smoothing should be applied to their data considering the variability in study designs. They must instead carefully choose the kernel to account for their voxel size, degrees of freedom (at the single subject level and group level) and registration routines (although for the “average” study with 3mm resolution and more than 20 subjects a FWHM = 4 times voxel size may suffice). While the effects of smoothing have been previously documented we extend these results over a greater range of degrees of freedom and image resolutions. We also present evidence suggesting most published studies in 2016 (80%) do not meet the assumptions of RFT. However this inference is limited by the lack of reported estimated smoothness values in the literature. This information is crucial to understanding the validity of statistical thresholds and should always be reported. Future work is required in RFT to explicitly incorporate the sampling of continuous fields in order to fully exploit the ever increasing spatial precision of fMRI data.

5.7 References

Adolf, D., Weston, S., Baecke, S., Luchtmann, M., Bernarding, J., & Kropf, S. (2014). Increasing the reliability of data analysis of functional magnetic resonance imaging by applying a new blockwise permutation method. *Frontiers in Neuroinformatics*, *8*(August), 1–9. http://doi.org/10.3389/fninf.2014.00072

Barnes, G. R., Ridgway, G. R., Flandin, G., Woolrich, M., & Friston, K. (2013). Set-level threshold-free tests on the intrinsic volumes of SPMs. *NeuroImage*, *68*, 133–140. http://doi.org/10.1016/j.neuroimage.2012.11.046

Bennett, C. M., Baird, A. a, Miller, M. B., & Wolford, G. L. (2011). Neural Correlates of Interspecies Perspective Taking in the Post-Mortem Atlantic Salmon: An Argument For Proper Multiple Comparisons Correction. *Journal of Serendipitous and Unexpected Results*, *1*, 1–5. http://doi.org/10.1016/S1053-8119(09)71202-9

Bennett, C. M., Wolford, G. L., & Miller, M. B. (2009). The principled control of false positives in neuroimaging. *Social Cognitive and Affective Neuroscience*, *4*(4), 417–422. http://doi.org/10.1093/scan/nsp053

Borzage, M., Bluml, S., & Seri, I. (2014). Equations to describe brain size across the continuum of human lifespan. *Brain Structure and Function*, *219*(1), 141–150. http://doi.org/10.1007/s00429-012-0490-6

Chumbley, J., & Friston, K. (2009). False discovery rate revisited: FDR and topological inference using Gaussian random fields. *NeuroImage*, *44*(1), 62–70. http://doi.org/10.1016/j.neuroimage.2008.05.021

Delignette-muller, M. L., & Dutang, C. (2015). fitdistrplus : An R Package for Fitting Distributions. *Journal of Statistical Software*, *64*(4), 1–34. http://doi.org/10.18637/jss.v064.i04

Duncan, J. S., Winston, G. P., Koepp, M. J., & Ourselin, S. (2016). Brain imaging in the assessment for epilepsy surgery. *The Lancet Neurology*. http://doi.org/10.1016/S1474-4422(15)00383-X

Durnez, J., Moerkerke, B., & Nichols, T. E. (2014). Post-hoc power estimation for topological inference in fMRI. *NeuroImage*, *84*, 45–64. http://doi.org/10.1016/j.neuroimage.2013.07.072

Eklund, A., Nichols, T. E., & Knutsson, H. (2016). Cluster failure: Why fMRI inferences for spatial extent have inflated false-positive rates. *Proceedings of the National Academy of Sciences*, 201602413. http://doi.org/10.1073/pnas.1602413113

Flandin, G., & Friston, K. J. (2015). *Topological Inference*. *Introduction to methods and modelling*. Elsevier Inc. http://doi.org/10.1016/B978-0-12-397025-1.00322-5

Flandin, G., & Friston, K. J. (2016). Analysis of family-wise error rates in statistical parametric mapping using random field theory. *Arxiv*, 1–4. http://doi.org/10.1073/pnas.1602413113

Friston, K. J., Frith, C. D., Liddle, P. F., & Frackowiak, R. S. J. (1991). Comparing functional (PET) images: the assessment of significant change. *Journal of Cerebral Blood Flow and Metabolism : Official Journal of the International Society of Cerebral Blood Flow and Metabolism*, *11*(4), 690–699. http://doi.org/10.1038/jcbfm.1991.122

Genovese, C. R., Lazar, N. a, & Nichols, T. (2002). Thresholding of statistical maps in functional neuroimaging using the false discovery rate. *NeuroImage*, *15*(4), 870–8. http://doi.org/10.1006/nimg.2001.1037

Hayasaka, S., & Nichols, T. E. (2003). Validating cluster size inference: Random field and permutation methods. *NeuroImage*, *20*(4), 2343–2356. http://doi.org/10.1016/j.neuroimage.2003.08.003

Hayasaka, S., Phan, K. L., Liberzon, I., Worsley, K. J., & Nichols, T. E. (2004). Nonstationary cluster-size inference with random field and permutation methods. *NeuroImage*, *22*(2), 676–687. http://doi.org/10.1016/j.neuroimage.2004.01.041

Heinzle, J., Koopmans, P. J., den Ouden, H. E. M., Raman, S., & Stephan, K. E. (2016). A hemodynamic model for layered BOLD signals. *NeuroImage*, *125*, 556–570. http://doi.org/10.1016/j.neuroimage.2015.10.025

Jacobs, J., Stich, J., Zahneisen, B., Assländer, J., Ramantani, G., Schulze-Bonhage, A., … LeVan, P. (2014). Fast fMRI provides high statistical power in the analysis of epileptic networks. *NeuroImage*, *88*, 282–294. http://doi.org/10.1016/j.neuroimage.2013.10.018

Li, H., Nickerson, L. D., Xiong, J., Zou, Q., Fan, Y., Ma, Y., … Gao, J. H. (2014). A high performance 3D cluster-based test of unsmoothed fMRI data. *NeuroImage*, *98*, 537–546. http://doi.org/10.1016/j.neuroimage.2014.05.015

Li, H., Nickerson, L. D., Zhao, X., Nichols, T. E., & Gao, J. H. (2015). A voxelation-corrected non-stationary 3D cluster-size test based on random field theory. *NeuroImage*, *118*, 676–682. http://doi.org/10.1016/j.neuroimage.2015.05.094

Pantazis, D., Nichols, T. E., Baillet, S., & Leahy, R. M. (2005). A comparison of random field theory and permutation methods for the statistical analysis of MEG data. *NeuroImage*, *25*(2), 383–394. http://doi.org/10.1016/j.neuroimage.2004.09.040

Petersson, K. M., Nichols, T. E., Poline, J. B., & Holmes, a P. (1999). Statistical limitations in functional neuroimaging. II. Signal detection and statistical inference. *Philosophical Transactions of the Royal Society of*

London. Series B, Biological Sciences, *354*(1387), 1261–81. http://doi.org/10.1098/rstb.1999.0478

R Core team. (2015). R Core Team. *R: A Language and Environment for Statistical Computing. R Foundation for Statistical Computing , Vienna, Austria. ISBN 3-900051-07-0, URL http://www.R-Project.org/.*

Roels, S. P., Bossier, H., Loeys, T., & Moerkerke, B. (2015). Data-analytical stability of cluster-wise and peak-wise inference in fMRI data analysis. *Journal of Neuroscience Methods*, *240*, 37–47. http://doi.org/10.1016/j.jneumeth.2014.10.024

Winkler, A. M., Ridgway, G. R., Webster, M. a., Smith, S. M., & Nichols, T. E. (2014). Permutation inference for the general linear model. *NeuroImage*, *92*, 381–397. http://doi.org/10.1016/j.neuroimage.2014.01.060

Worsley, K. J. (2003). Developments in Random Field Theory. *Human Brain Function*, (2), 881–886. http://doi.org/10.1016/0029-5493(82)90100-5

Worsley, K. J. (2005). An improved theoretical P value for SPMs based on discrete local maxima. *NeuroImage*, *28*(4), 1056–1062. http://doi.org/10.1016/j.neuroimage.2005.06.053

Worsley, K. J., Evans, A. C., Marrett, S., & Neelin, P. (1992). A three-dimensional statistical analysis for CBF activation studies in human brain. *Journal of Cerebral Blood Flow and Metabolism : Official Journal of the International Society of Cerebral Blood Flow and Metabolism*, *12*(6), 900–18. http://doi.org/10.1038/jcbfm.1992.127

Worsley, K. J., Marrett, S., Neelin, P., Vandal, A. C., Friston, K. J., & Evans, A. C. (1996). A unified statistical approach for determining significant signals in images of cerebral activation. *Human Brain Mapping*, *4*(1), 58–73. http://doi.org/10.1002/(SICI)1097-0193(1996)4:1<58::AID-HBM4>3.0.CO;2-O

Yacoub, E., Harel, N., & Ugurbil, K. (2008). High-field fMRI unveils orientation columns in humans. *Proceedings of the National Academy of Sciences of the United States of America*, *105*(30), 10607–12. http://doi.org/10.1073/pnas.0804110105

6. Stationary and dynamic connectivity in paediatric focal epilepsy

In this chapter, having determined optimised procedures for fMRI data acquisition and analysis we aim to characterise, using fMRI, differences in functional connectivity between individuals with focal epilepsy and healthy controls in terms of network dynamics and Interictal Epileptiform Discharges.

Abstract

It has been frequently reported that individuals with focal epilepsy have abnormal stationary Functional Connectivity (FC) measured with fMRI. However, the contribution of Interictal Epileptiform Discharges (IEDs) to this abnormal stationary FC and dynamic FC is not fully yet understood. Therefore we examined both dynamic and stationary FC in a sample of 21 healthy children and 47 paediatric focal epilepsy patients with heterogeneous aetiology and seizure onset zone. We performed a factor analysis to identify Intrinsic Connectivity Networks (ICNs) in both groups in a multivariate fashion. We then compared dynamic and stationary FC between both groups within each of the networks to determine spatial and temporal differences in FC. The factor analysis decomposed the brain into seven commonly observed ICNS: Primary Visual Network, Secondary Visual Network, Auditory Network, Motor, Default Mode, Left Fronto-Parietal and Right Fronto-Parietal. When controlling for the effects of IEDs it was found that the Default Mode Network and the Left Fronto-Parietal network had reduced stationary FC in the patient group. The dynamic connectivity (as characterised by phase synchrony metastability) did not differ between groups in any of the ICNs. Interestingly it was found that the stationary FC of the piriform cortex (a functionally defined seizure trigger zone) to the default mode network was increased by the occurrence of IEDs despite the variable location of the epileptogenic zone. This is the first demonstration of how the connectivity of the piriform cortex is associated with IEDs. This leads to the postulation of a general mechanism by which widespread changes in connectivity, epileptogenicity and IEDs may be related.

Declaration of contribution: Dr Maria Centeno recruited the subjects who participated in this study. Tim Tierney designed and performed all analysis presented in this chapter.

6.1 Introduction

The use of functional connectivity in fMRI studies has revealed that the brain can be organised into Intrinsic Connectivity Networks (ICNs). The functioning of these networks at rest has been demonstrated to explain individual variability in the brain's response to stimuli, perceptual efficiency and IQ (Tavor et al., 2016; van den Heuvel, Stam, Kahn, & Hulshoff Pol, 2009). As such there has been great interest in utilising functional connectivity in the study of patients with focal epilepsy. This is because focal epilepsy is now regarded by the International League Against Epilepsy (ILAE) as a "Network" disease where seizures arise within networks limited to one hemisphere (Berg et al., 2010).

A large number of studies have reported network abnormalities in patients with focal epilepsy (Centeno & Carmichael, 2014). However, many studies were conducted without simultaneous EEG and therefore are not able to control for the confounding effects of Interictal Epileptiform Discharges (IEDs) which have a controversial relationship to cognition and clinical treatment (Aja-Fernández & Tristán-Vega, 2013).

A number of recent studies have tried to estimate the network connectivity while controlling for the effects of IEDs (Iannotti et al., 2016; Shamshiri et al., 2016; Warren, Abbott, Vaughan, Jackson, & Archer, 2016) although their methodologies and samples differ. When studying the epileptic network itself it has been concluded that the epileptic network was very highly connected even when IED related connectivity increases were controlled for (Iannotti et al., 2016). In contrast, when investigating how IEDs affect ICNs associated with a natural stimulus (not at rest) it was found that IEDs were a strong driver of abnormal ICN connectivity observed across heterogeneous groups of paediatric focal epilepsy patients (Shamshiri et al., 2016).

These results (Shamshiri et al., 2016) suggest a common mechanism by which IEDs may interact with ICNs regardless of epilepsy syndrome. This finding will be developed upon in this study by using a multivariate framework to separate the effect of IEDs on multiple ICNs at rest from the effects of IEDs on stimulus driven ICNs (Shamshiri et al., 2016). To explore the

common effects of epilepsy on the functional organisation of the brain FC will be measured in a sample of heterogeneous focal epilepsy patients at rest. This offers the potential to relate the effects of IEDs on FC to the majority of studies examining FC in epilepsy which were also conducted at rest (Centeno & Carmichael, 2014). One could identify the ICNs using Independent Component Analysis (Warren et al., 2016) but we chose to employ a factor analysis to identify ICNs as this methodology will be sensitive to the temporal disruption IEDs cause (Shamshiri et al, 2016) due to fact that the factor analysis directly decomposes the temporal correlation matrices. Ultimately this portion of the study aims to determine the main ICNs in our data and ascertains whether they demonstrate a differing *stationary* pattern of FC.

As previously stated epilepsy is characterised as a network disease (Berg et al., 2010) where the network can periodically display hypersynchrony (due to IEDs). However, it is unclear what the impact of differences in synchrony at the timescale of fMRI is. Furthermore, it is unknown whether the stationary measures of FC are associated with dynamic changes in synchrony. Therefore, in addition to determining any stationary changes in network connectivity, we also sought to examine if there were temporal differences in the dynamics of the observed networks. We will characterise the dynamic changes in synchrony by metastability (see Chapter 1, Eq 53) which directly measures the variability in phase synchrony over time.

This style of approach also has been applied previously in cases of Major Depressive Disorder, traumatic brain injury (Demirtas et al., 2016; Hellyer, Scott, Shanahan, Sharp, & Leech, 2015) and in predicting performance in narrative comprehension (Simony et al., 2016). This multivariate dynamical framework will allow us to explore whether the differences previously reported in stationary FC in focal epilepsy (Iannotti et al., 2016; Shamshiri et al., 2016; Warren et al., 2016) are also associated with metastability in children with epilepsy which has not previously been explored. As such there were a number of research questions posed by this study

1. Are there common stationary FC differences observable at rest across ICNs in a heterogeneous sample of focal epilepsies?
2. Are these stationary differences associated with IEDs
3. Are ICN abnormalities associated with changes in metastability?

6.2 Method

6.2.1 Participants

Fifty-one children with drug-resistant focal epilepsy undergoing assessment for surgery at Great Ormond Street Hospital (GOSH), London, United Kingdom were recruited for this study. Inclusion criteria for the study were: the presence of frequent IEDs on EEG and ages between 6 and 18. Exclusion criteria were: large structural lesions that prevent successful normalisation to group template space. Forty six patients remained (see Table 4, Chapter 4). 21 volunteer controls also participated in the study age range 6–16 years old (mean 11.64). These included 11 females. Subjects were recruited through advertisements to GOSH staff webpages advertising participation. The study was approved by the UK national research ethics service (NRES 11/LO/1421). All participants/families provided informed consent and assent as appropriate.

6.2.2 Data Acquisition

We acquired simultaneous EEG-fMRI in a 1.5T Siemens Avanto scanner (Erlangen, Germany) at the Great Ormond Street Hospital MRI Department with a 12 channel receive coil. Subjects were fitted with a vacuum cushion during scanning to reduce head movement, and given headphones to dampen the noise from the MRI. Subjects were videoed inside the scanner with an MRI compatible camera (Nordic NeuroLabs, Bergen, Norway) interfaced with Brain Products recording software. Scalp EEG was recorded with a 64-channel MR compatible cap (BrainAmp MR plus, Brain Products, Gilching, Germany). EEG data were band-pass filtered at 0.016 Hz–1 kHz, 16-bit digitalization (0.05 mV resolution) and the sampling rate was 5 kHz. Subjects underwent four sessions of echo-planar imaging (EPI). The parameters of the experiment were as follows: a 3.3x3.3x4 mm effective resolution with a field of view FOV =210 mm, TR =

2,160 ms, TE = 30 ms, flip angle = 75 degrees, number of slices = 30, slice thickness=3 mm, slice gap = 1 mm, ascending order 300 volumes (4 sessions of 300).

6.2.3 Paradigm

During 2/4 fMRI sessions subjects were asked to rest with eyes closed and for the remaining two, to watch a video. Sessions of rest (eyes closed) and video were alternated with the first session randomly assigned to be a rest or video session. The first session of rest (eyes closed) was analysed in the current study. The first session was chosen as it was least likely to be contaminated by motion artefacts (see Chapter 4, Figure 14) and affected by issues such as vigilance or drowsiness. In a separate study (Shamshiri et al., 2016) the video sessions were analysed and the video paradigm is described therein. Participants were either instructed to close their eyes and rest or asked to watch the video via the in-scanner headphones. Verbal responses and in-scanner video monitoring were used to verify that the subjects were following these instructions.

6.2.4 Preprocessing

Images were realigned to the first image in the series (after excluding the first 4 to account for T1 equilibrium effects). FIACH (Tierney et al., 2016) was used to identify and correct for large amplitude signal changes (such as those due to spin history effects) and physiological noise. The subsequent images were then normalised to a T1 weighted MNI template at a resolution of 2x2x2mm3. The images were then smoothed using a Gaussian kernel of FWHM = 8mm.

The realignment, normalisation and smoothing was performed with SPM12 (www.fil.ion.ucl.ac.uk). Nuisance regression was performed to further reduce the effects of motion and physiological noise by regression of the 6 realignment parameters and the 6 physiological noise regressors produced by FIACH. The time series were then bandpass-filtered to within the range 0.1- 0.01 Hz. The nuisance regression and band pass filter were performed using the FIACH package (Tierney et al., 2016). Mean time series were then extracted from 112 cortical and subcortical regions using the AAL atlas (Tzourio-Mazoyer et al., 2002).

6.2.5 Analysis

6.2.5.1: Comparison of multivariate stationary connectivity between patient and control groups.

We constructed a correlation matrix for each individual by using all the seeds in the atlas. Each individual therefore had a 112x112 correlation matrix. We then averaged the correlation matrices within groups to create a "Control" correlation matrix and a "Patient "correlation matrix. As we were interested in documenting how regions with shared temporal dynamics differed between groups we performed a factor analysis which aimed to maximise the temporal correlation within networks and reduced temporal correlation between networks. A direct oblimin rotation was performed to assist in interpretation and to prevent brain regions heavily loading on one factor (this is because the rotation does not enforce that the resulting networks be orthogonal). The factor analysis was conducted using the Psych Package (Revelle, 2016)

The number of factors to extract was automatically determined using a parallel analysis (Glorfeld, 1995; Horn, 1965) which involves generating a null distribution of eigenvalues from randomly generated correlation matrices. Once the null data is generated any factors with eigenvalues greater than what would be expected from the null data are retained. This resulted in 14 factors being selected for both groups. We were able to reconstruct a factor time course for each factor in each individual by post multiplying the factor loadings matrix by each individual's seed matrix. We then had a total of 14 factor time courses in each individual which allowed us to perform a standard seed to voxel connectivity analysis for each of the networks (Whitfield-Gabrieli & Nieto-Castanon, 2012).

Seven networks were identified visually as corresponding to traditionally observed ICNs. These were the networks that we subsequently analysed. They consisted of the Primary Visual Network, Secondary Visual Network, Auditory Network, Motor, Default Mode, Left Fronto-Parietal and Right Fronto-Parietal.

Once each network was constructed in each individual a series of second level analyses (one for each network) were performed by performing

two sample t-tests using the fisher transformed correlation map as a summary statistic in SPM 12. Homogeneity of variance was not assumed and corrected for within the SPM framework. During the analysis a total of 18 t-contrasts were constructed. Therefore to appropriately control for multiple comparisons we divided the p-value obtained from SPM12 using RFT by 18 to achieve a global FWE of $p<.05$. We further employed an arbitrary cluster extent threshold of 20 voxels. FWHM of the residuals were all greater than 4 times the voxels size indicating an appropriate usage of Random Field Theory (see Chapter 5, Figure 19).

6.2.5.2: Comparison of stationary connectivity between patient and control groups (controlling for the effects of IEDs).

To control for the effects of IEDs we re-estimated the individual correlation maps. However, in this case we included the IEDs convolved with the canonical haemodynamic response function as well as its temporal and dispersion derivatives as confounds. This effectively amounts to calculating a partial correlation between the factor time course and the rest of the brain while partialling out the effect of IEDs.

6.2.5.3: Comparison of multivariate dynamic connectivity between patient and control groups.

To compare dynamic connectivity between groups we constructed phase synchrony time series per individual per network (Glerean, Salmi, Lahnakoski, Jääskeläinen, & Sams, 2012). In brief, to construct the phase synchrony time series we calculated the phase of the Hilbert transformed bandpass filtered data within each network. Each network mask was defined as the intersection between the control and patient networks identified in the stationary connectivity analysis. We took the intersection to maintain a constant number of voxels contributing to the synchrony measure across groups.

We then took the circular average (See Chapter 1, Eq 53) of all the time series within each network to create one time series per network reflecting the dynamic connectivity. The values of the time series ranged between 0 and 1 (with 0 representing no synchrony and 1 representing complete synchrony).

We then calculated the metastability of each network as a summary statistic to be compared between groups. This amounted to calculating the standard deviation of the phase time series. Intuitively the metastability reflects the rate of change of connectivity over time with larger values indicating greater variability in connectivity over time. We then compared the metastability between the patients and the controls using a Wilcoxon test for each network. The phase synchrony and metastability was calculated using custom scripts developed using the R programming language (R Core team, 2015).

6.3 Results

6.3.1 Stationary Connectivity

6.3.1.1 The Auditory Network.

The network was visually identified as being the Auditory Network. There were no statistically significant differences identified between patient and control groups (see Figure 22)

6.3.1.2 The Primary Visual Network

The following network was visually identified as being the Primary Visual Network. There were no statistically significant differences identified between patient and control groups (see Figure 23).

6.3.1.3 The Sensorimotor Network

The following network was visually identified as being the Sensorimotor Network. There were no statistically significant differences identified between patient and control groups (see Figure 24).

6.3.1.4 The Secondary Visual Network

The following network was visually identified as being the Secondary Visual Network. There were no statistically significant differences identified between patient and control groups (see Figure 25).

6.3.1.5 The Right Fronto-Parietal Network

The following network was visually identified as being the Right Fronto-Parietal Network. There were no statistically significant differences identified between patient and control groups (see Figure 26).

6.3.1.6 The Left Fronto-Parietal Network

The following network was visually identified as being the Left Fronto-Parietal Network (See Figure 27). In the contrast Controls>Patients there was one statistically significant difference in the right superior parietal cortex (MNI coordinate = 24,-64, 54). In the contrast Patients>Controls there were 5 statistically significant differences: left inferior parietal (MNI coordinate = -40,-60, 28), Medial Frontal (MNI coordinate = -2,-5, 26), Middle Temporal Gyrus (MNI coordinate = -65,-20, -11), Left Precuneus (MNI coordinate = -6,-54, 30) and Right Precuneus (8, -48, 24).

6.3.1.7 The Default Mode Network

The following network was visually identified as being the Default Mode Network (See Figure 28). In the contrast Controls>Patients there was 1 statistically significant differences: The Superior Medial Frontal Gyrus (MNI Coordinate = 12, -56, 46) and right Middle Occipital Gyrus (MNI Coordinate = -4, 44, 22). In the contrast Patients>Controls there were 2 statistically significant differences: Right Precuneus (MNI Coordinate = 12, -56, 46) and right Middle Occipital Gyrus (MNI Coordinate = 40,-66,34).

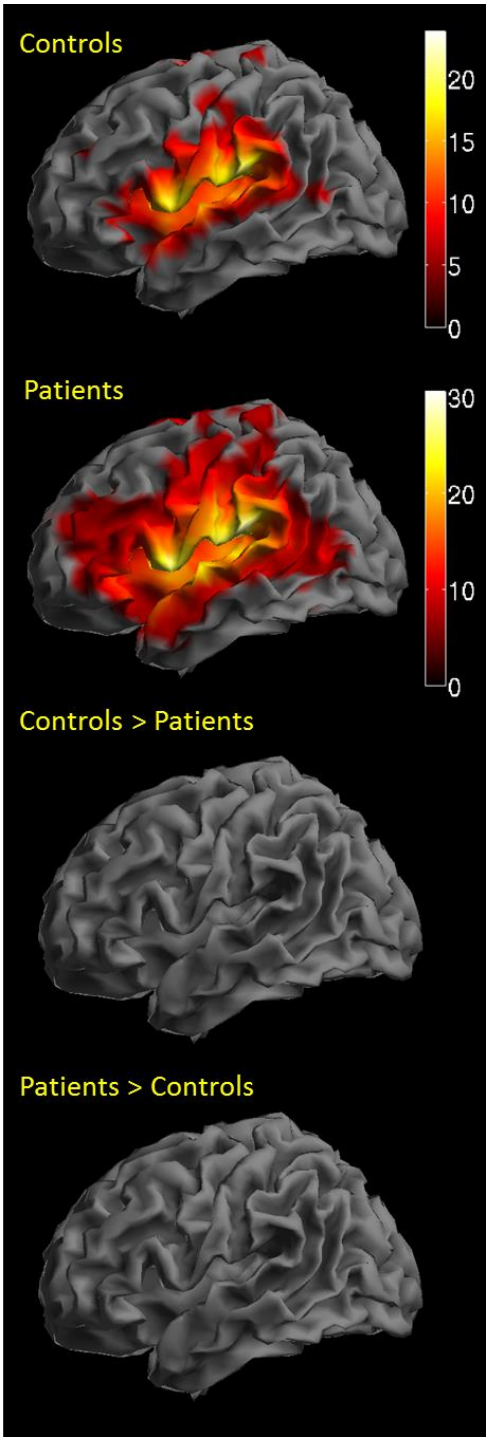

Figure 22. The Auditory Network. Images are thresholded at FWE p<.05 and rendered on a normalised surface of the brain

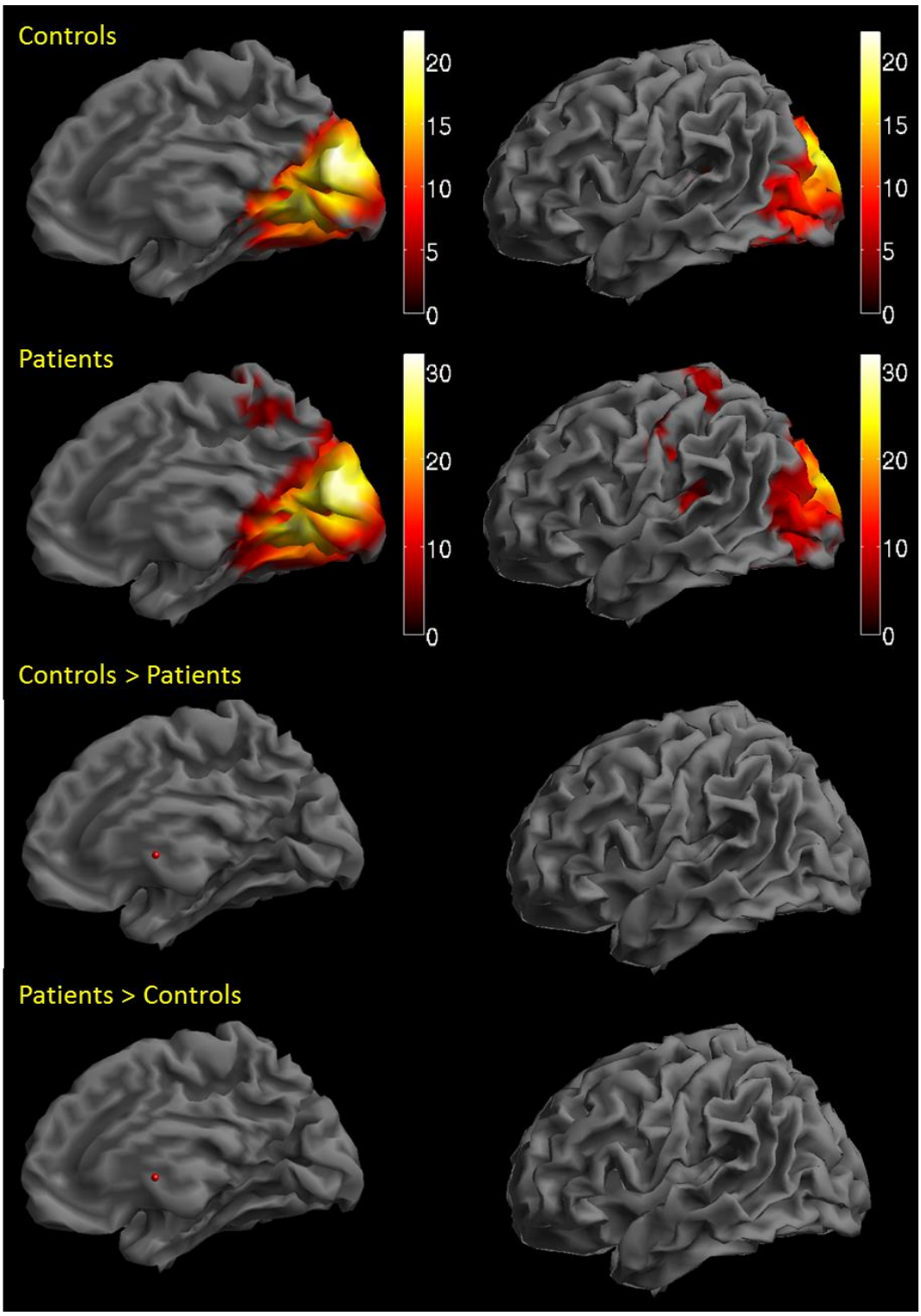

Figure 23. Primary Visual Network. Images are thresholded at FWE p<.05 and rendered on a normalised surface of the brain.

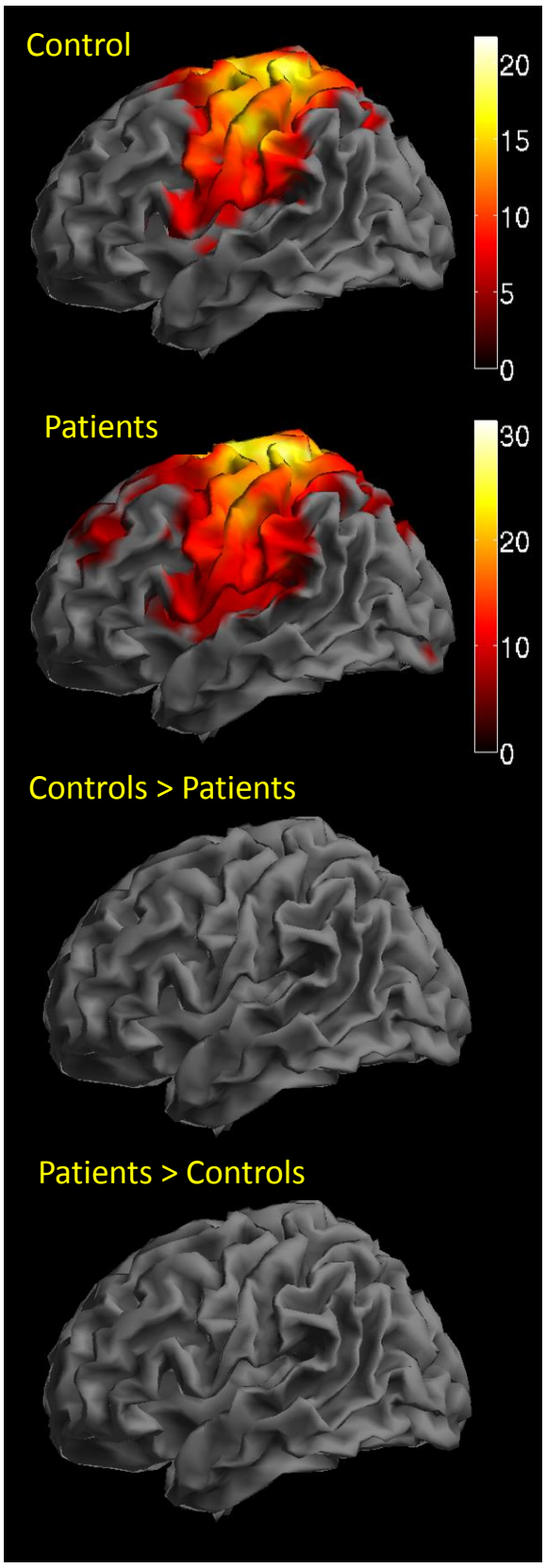

Figure 24. Sensorimotor Network. Images are thresholded at FWE p<.05 and rendered on a normalised surface of the brain.

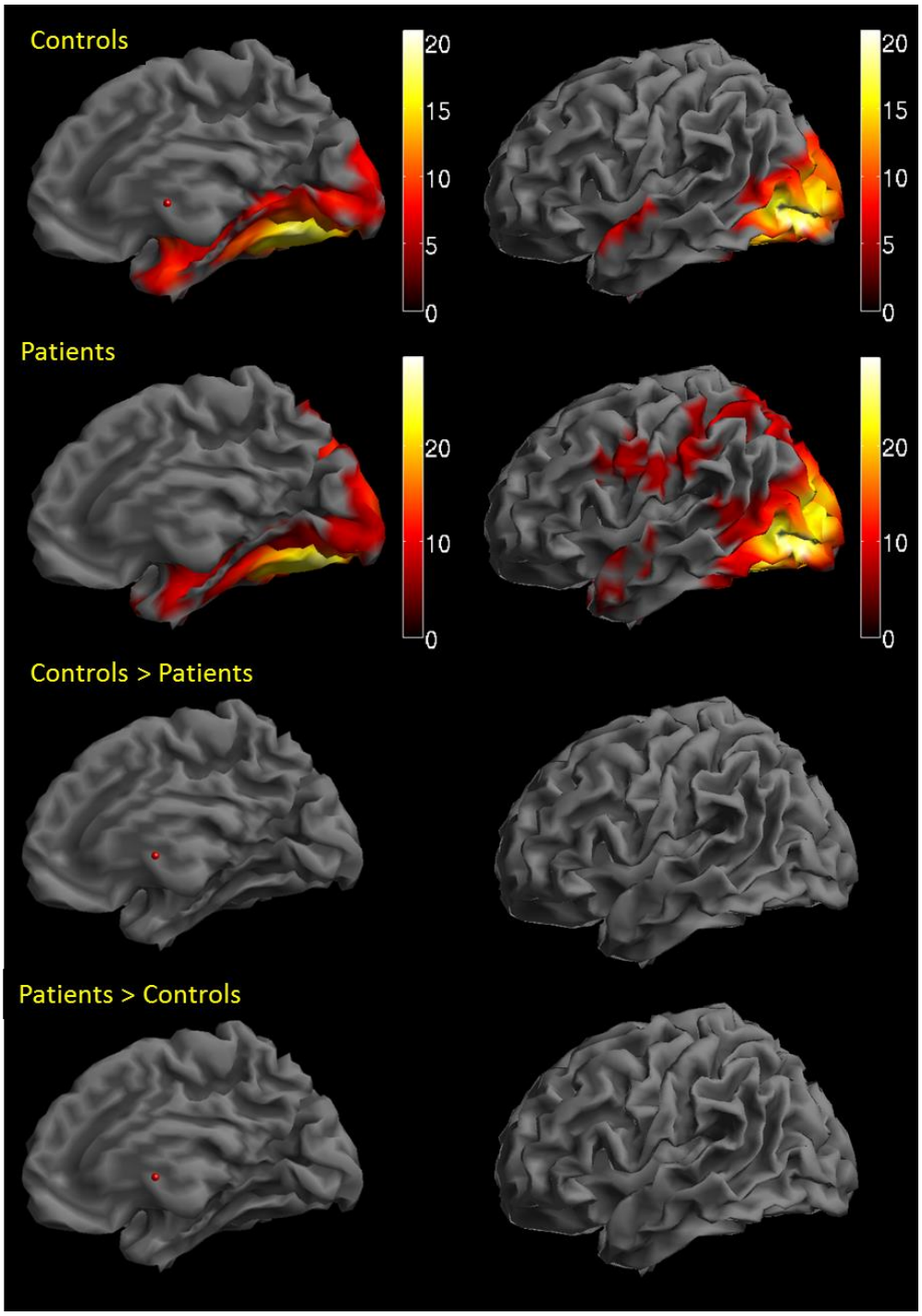

Figure 25. Secondary Visual Network. Images are thresholded at FWE p<.05 and rendered on a normalised surface of the brain.

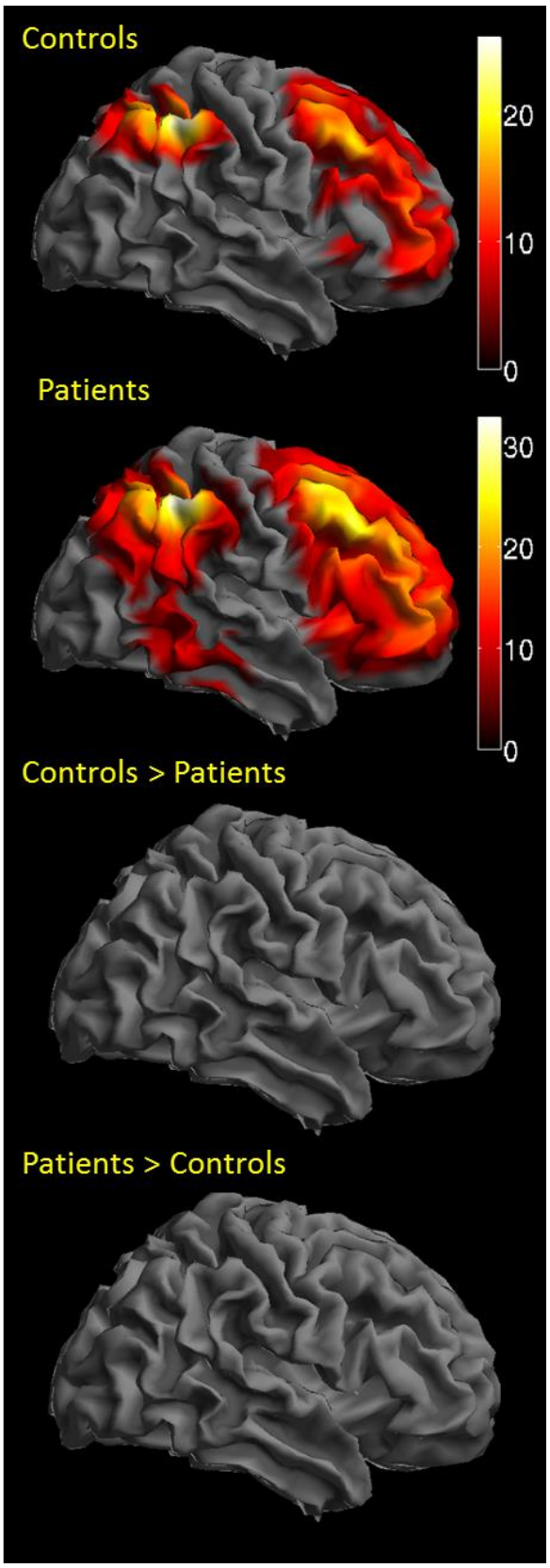

Figure 26. Right Fronto-Parietal Network. Images are thresholded at FWE p<.05 and rendered on a normalised surface of the brain.

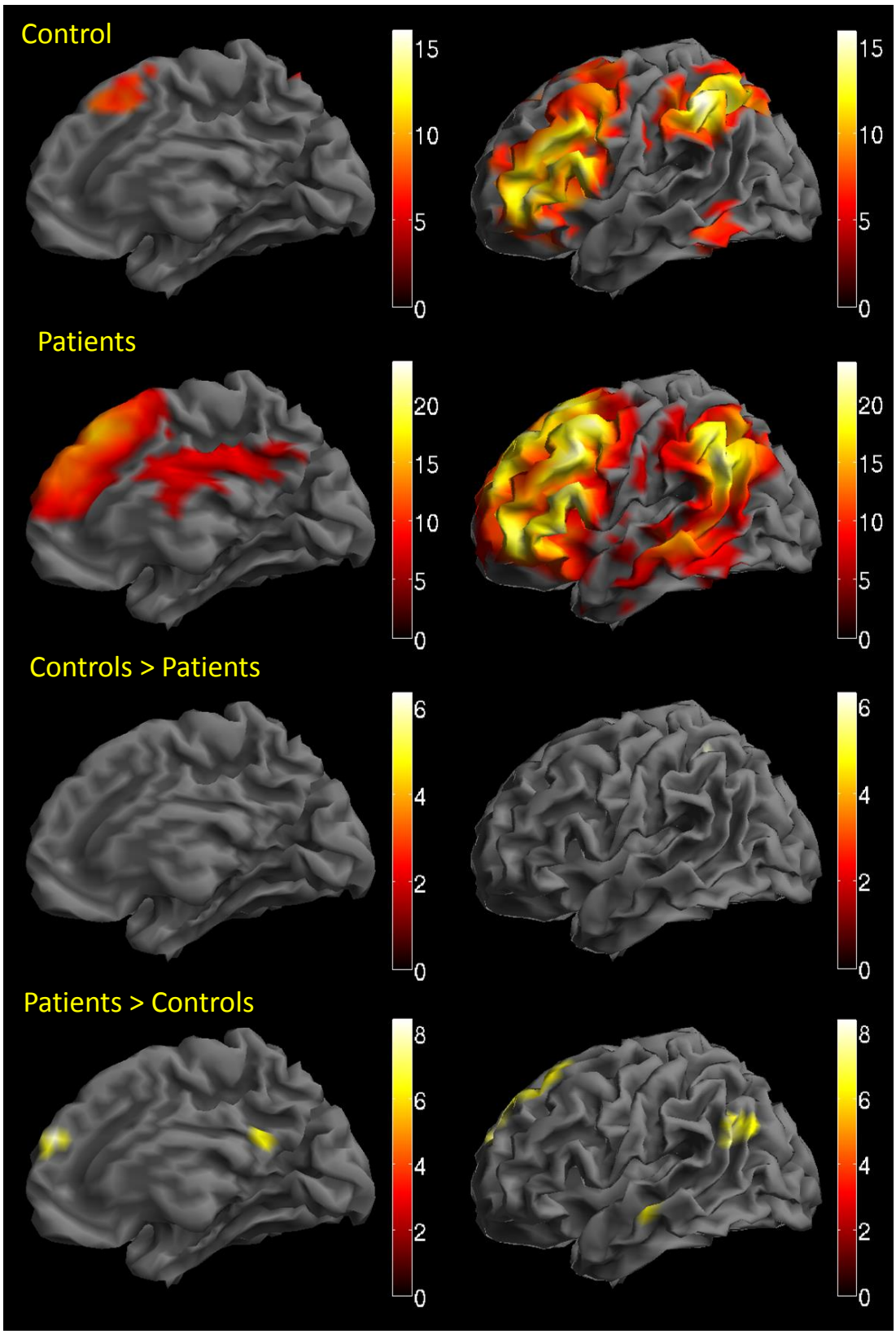

Figure 27. Left Fronto-Parietal Network. Images are thresholded at FEW p<.05 and rendered on a normalised surface of the brain.

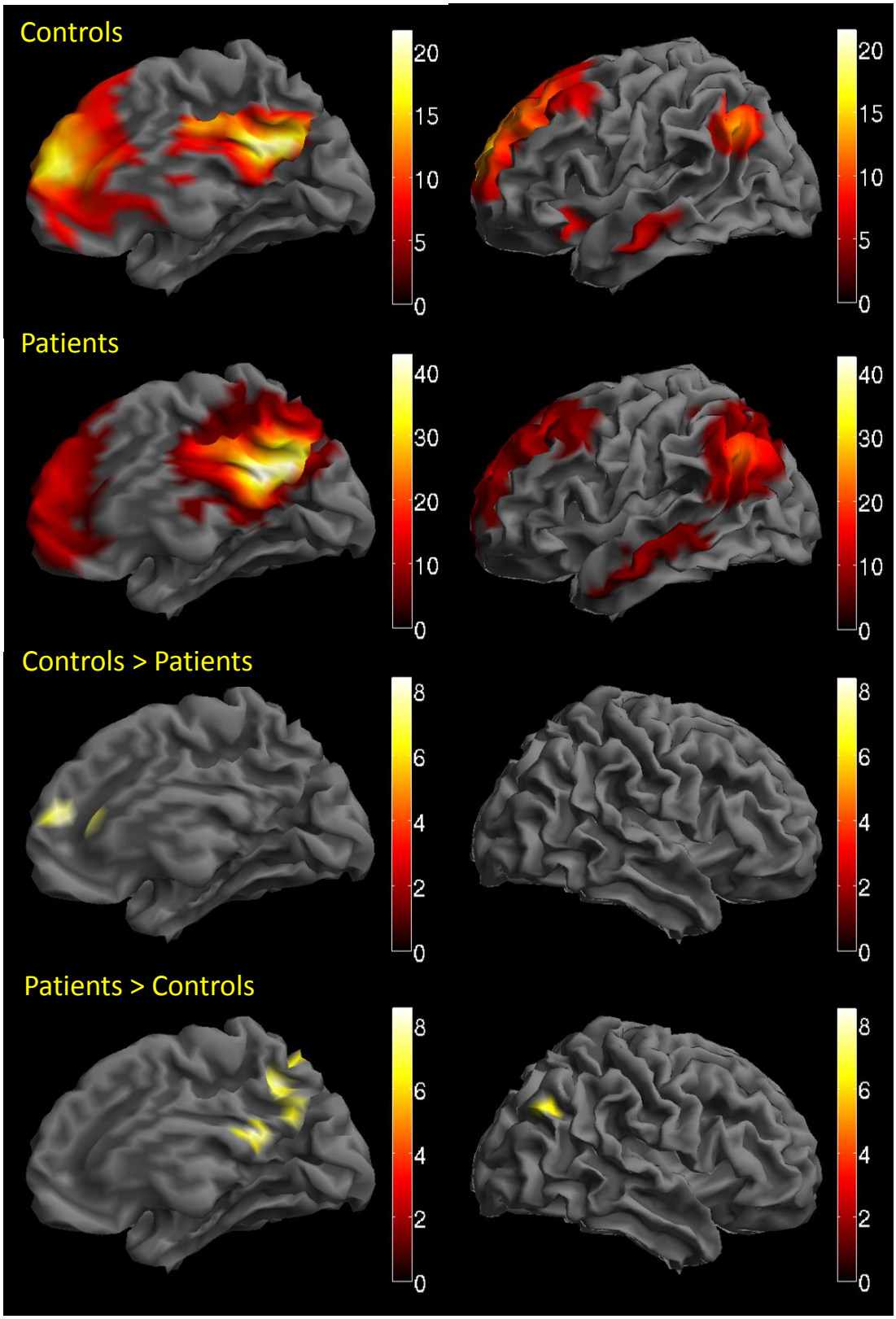

*Figure 28.*The Default Mode Network.Images are thresholded at FWE p<.05 and rendered on a normalised surface of the brain.

6.3.2 The effects of IEDs on stationary connectivity

6.3.2.1 Left Fronto-Parietal (controlling for IEDs)

Having controlled for the effects of IEDs the contrast Controls>Patients displayed there were 8 statistically significant differences: Left Inferior Frontal-Pars Triangularis (MNI coordinate = -42,38, 2), Left Precentral Gyrus (MNI Coordinate = -52, 6 ,26), Left Inferior Parietal(MNI Coordinate = -53 -46 ,44),Right Precentral Gyrus (64,14,16), Right Inferior Parietal(MNI Coordinate = -40 -44 ,46), Right Inferior Frontal-Pars Triangularis (MNI Coordinate = 44, 38,14). In the contrast Patients>Controls there were no statistically significant differences (See Figure 29).

6.3.2.2 Default Mode Network (controlling for IEDs)

Having controlled for the effects of IEDs the contrast Controls>Patients displayed 6 statistically significant differences: The Anterior Cingulate (MNI Coordinate = -4, 42, 20), Left Caudate (MNI Coordinate = -12, 12, 14), Right Caudate (MNI Coordinate = 12, 14, 16), Right l inferior orbitofrontal Cortex (22, 16,-18), Left inferior Orbitofrontal Cortex (MNI Coordinate = 12, 14, 16). In the contrast Patients>Controls there were no statistically significant differences (See Figure 30).

.

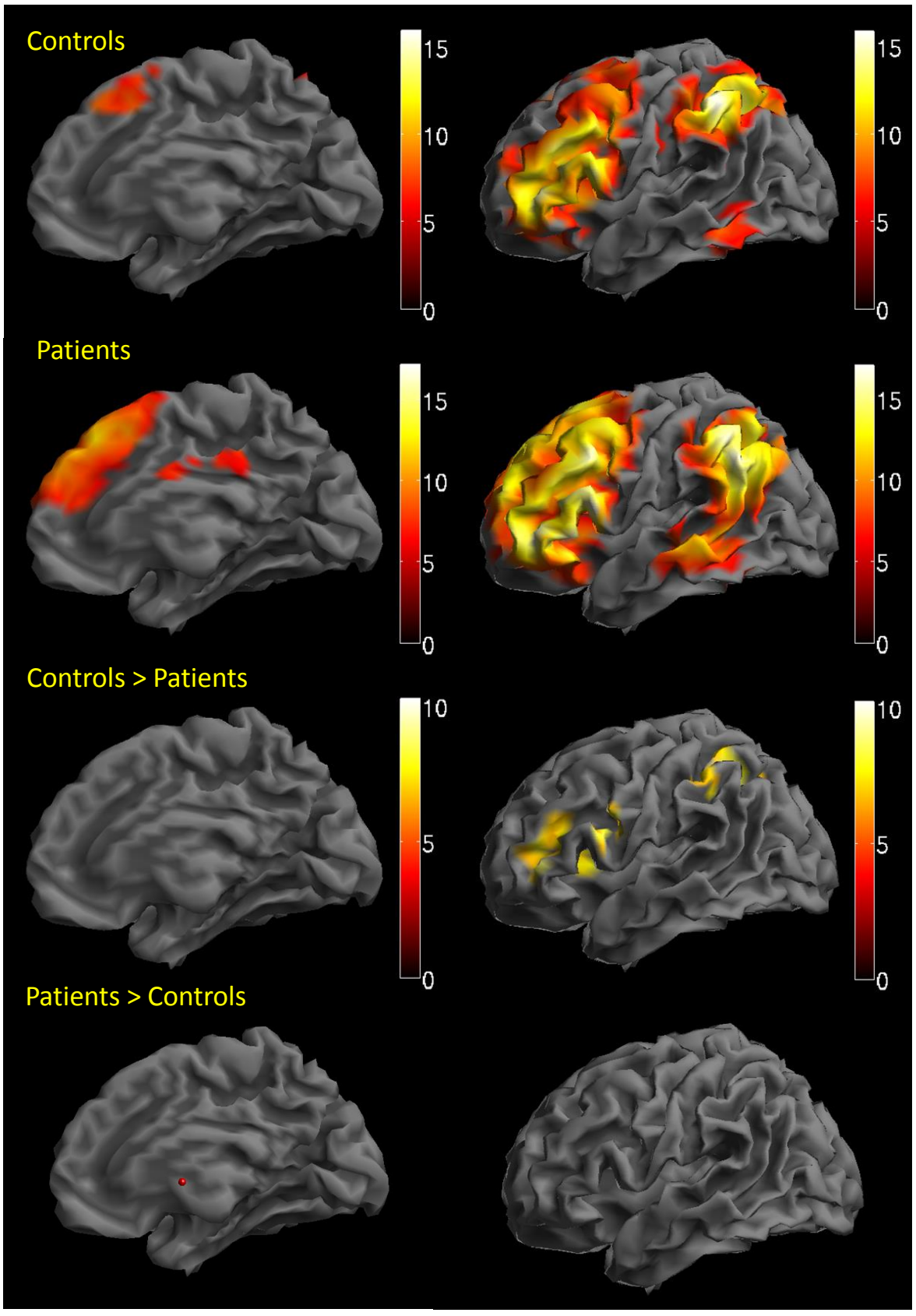

Figure 29. The Left Fronto-Parietal Network (Controlling For the effect of IEDs). Images are thresholded at FWE p<.05 and rendered on a normalised surface of the brain.

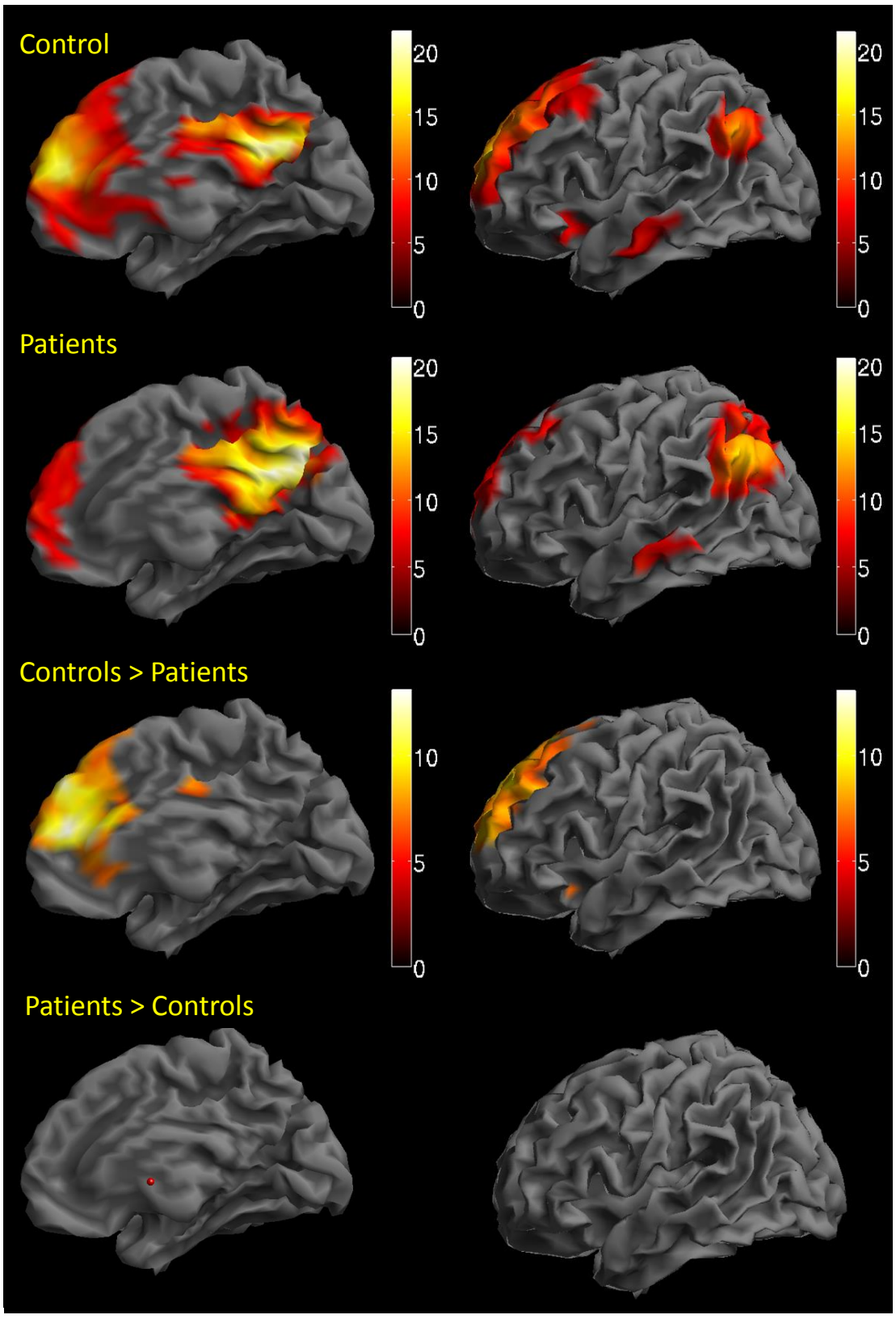

Figure 30. The Default Mode Network (Controlling for the effect of IEDs). Images are thresholded at FWE p<.05 and rendered on a normalised surface of the brain.

6.3.3 Dynamic Connectivity

Wilcoxon rank sum tests were employed to assess if metastability varied between control and patient groups across each of the seven networks identified. The test statistics are summarised in Table 5. There were no statistically significant results identified.

Network	Statistic (W)	*p*
Auditory	595	0.24
Basal Ganglia	439	0.4032
Default Mode	590	0.2672
Lateral Visual	500	0.9639
Left Fronto-parietal	548	0.5733
Primary Visual	508	0.9639
Right Fronto-parietal	496	0.9227
Sensorimotor	549	0.5645

Table 5. Metastability across ICNs. W refers to the test statistic of the Wilcoxon rank sum-test and *p* refers to the p-value associated with the statistic.

6.4 Discussion

6.4.1 Stationary Connectivity (not controlling for the effects of IEDs)

The multivariate Factor Analysis identified seven ICNs that were subsequently tested in a univariate fashion to establish the functional integrity of these networks. There were no differences observed in the sensory/ motor networks at rest in this study (Primary Visual, Secondary Visual, Auditory, Sensorimotor) regardless of whether the effects of IEDs were controlled for. This provides an interesting contrast to Shamshiri et al (2016) who demonstrated connectivity differences in the visual network in the same sample(under different experimental conditions). However the observed connectivity differences in Shamshiri et al (2016) were no longer present when the effects of IEDs were controlled for.

The key differences between the two studies is the fact that Shamshiri et al (2016) performed their experiment during a cognitively low demand natural stimulus task whereas the current study was performed at rest (eyes closed). This suggests a mechanism by which IEDs can interfere with the

brains functional organisation in a cognitive load dependent manner (i.e. the disruptive influence of IEDs increases with cognitive/behavioural demand). This should be caveated with the fact the difference in attentional load between rest and natural stimulus watching has not been determined and is not generalizable to other ICNs without the construction of tasks designed to probe the function of those networks. That being said it has previously been suggested in the field of transient cognitive impairment that less cognitively/behaviourally demanding actions are less susceptible to the performance impairment associated with IEDs (Aarts, Binnie, Smit, & Wilkins, 1984).

Interestingly, the patient group initially displayed greater connectivity between the left fronto-parietal network and the default mode network (medial frontal, precuneus and inferior parietal: Figure 27) while displaying reduced connectivity in the superior parietal cortex. This is also in line with previous work which has found greater inter-network connectivity and reduced intra-network connectivity in epilepsy patients (Ibrahim et al., 2014; Warren et al., 2016).

The results in the default mode network are perhaps less in line with previous work as increased intra-network connectivity was brain area specific (with the precuneus displaying increased connectivity and the medial frontal displaying reduced connectivity). However, as these results have not controlled for the effects of IEDs they should be interpreted with caution due to the substantial effects IED can have on network connectivity (Shamshiri et al., 2016)

6.4.2 Stationary Connectivity (controlling for the effects of IEDs)

Once the effects of IEDs were controlled for a number of changes were observed. Interestingly we no longer noted increased network connectivity between the Fronto-parietal network and the default mode network (see Figure 27). Instead a pronounced reduction in connectivity within the left fronto-parietal network was observed (see Figure 29). The regions affected included the bilateral inferior frontal gyrus, inferior parietal and precentral gyrus. These areas comprise the key brain nodes for expression of language (Price, 2012). This is perhaps unsurprising as it has been previously noted that the ventral language network is particularly at risk

of functional disruption in children with focal epilepsy (Croft et al., 2014).

Once the effects of IEDs had been controlled for in the default mode network (Figure 30) the initially observed increased patient connectivity was no longer apparent. Instead only decreased patient connectivity was observed. This decreased connectivity was apparent in the anterior cingulate and the medial frontal cortex (both nodes of the default mode network) bilaterally in the caudate and bilaterally in the inferior orbitofrontal cortex. Interestingly, the clusters in the orbitofrontal cortex are situated just anterior to the junction of the temporal and frontal lobes (the piriform cortex).

It has been postulated in humans that the anterior portion constitutes the “area tempestas” which is not anatomically defined but functionally defined as an area in the piriform cortex that can be easily chemically manipulated to produce seizures (Piredda & Gale, 1985; Vaughan & Jackson, 2014). It can also be defined functionally due to this brain regions role in olfaction (Wiesmann et al., 2006). We therefore include an image from a study on olfaction (Wiesmann et al., 2006) as a reference point for the definition of piriform cortex (See Figure 31).

The simultaneous change in caudate function is also not surprising as both the piriform cortex and the caudate are often the first sites to experience cell damage following status epilepticus (Vaughan & Jackson, 2014) and the FC of the caudate has previously been associated with IEDs (Shamshiri et al., 2016). The fact that the current cohort were not in status but producing IEDs is interesting as it suggests that even mild epileptic events are associated with increased connectivity of highly epileptogenic zones with the default mode network.

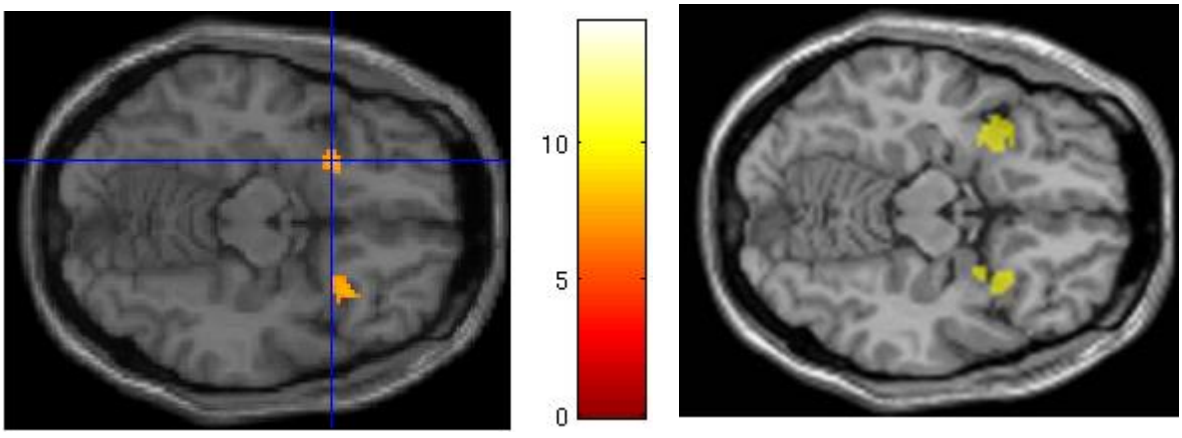

Figure 31. Regions of reduced connectivity in the priform cortex. (a) The t-

contrast of patients > controls for the Default Mode Seed thresholded at p<.05 FWE on a normalised T1-weighted template in MNI space. (b) Combined anatomical and functional definition of piriform cortex (Wiesmann et al., 2006, reproduced with permission) as a comparison for localisation of piriform cortex.

Previous work has demonstrated IEDs across focal epilepsies activate this region (Fahoum, Lopes, Pittau, Dubeau, & Gotman, 2012; Flanagan, Badawy, & Jackson, 2014; Laufs et al., 2011). However the exact region is not consistent between studies with some activations being more temporal and some being frontal. However, this is the first demonstration in a paediatric population and the first to explore how the brain's connectivity to these regions may be altered by the occurrence of IEDs. The fact that these regions (caudate and piriform have increased connectivity to the DMN when IEDs occur is of significance as it could suggest a mechanism by which propagation of IEDs to other networks occur. Alternatively it could suggest that IEDs occur preferentially when there is a particular connectivity state where the DMN is connected to the piriform and caudate.

6.4.3 Contrast between stationary and dynamic connectivity.

In contrast to the stationary connectivity no statistically significant differences were observed in the dynamic connectivity. There are a number of possible reasons for this to occur. Firstly we may be underpowered to detect the effect. However, if that is the case the effect size is most likely small. Another possibility is that the sample is simply too heterogeneous and that sub-group analysis may be more sensitive. Another possibility is that fMRI is not appropriate for detecting neural dynamics (Laumann et al., 2016). However, this is in contrast to other studies which have produced theoretically plausible results (Demirtas et al., 2016; Hellyer et al., 2015). The last explanation is that there simply is no appreciable difference in dynamic connectivity between patients and focal epilepsy and controls. If this is the case it suggests that the disease process and IEDs can produce abnormal connectivity but ICN dynamics, at least on the timescale measureable by fMRI, are normal.

6.4.4 Limitations

Subjects were recruited for the purpose of establishing the utility and feasibility of unsedated simultaneous EEG-fMRI in children (Centeno et al., 2016). As such subjects were selected from the population of focal epilepsy patients undergoing surgical evaluation. As such the conclusions of this study do not necessarily generalise to all of focal epilepsy but instead to those where the disease is severe enough to warrant surgical intervention.

The second limitation concerns the choice to study a heterogeneous population. This decision results in reduced power to detect effects that may be specific to sub-populations of children with focal epilepsy. However, the increased numbers of subjects that this approach results in offers increased power to detect effects that are common across focal epilepsies. This may offer insight into important issues such as common mechanisms of cognitive impairment or IED/seizure propagation.

Lastly all subjects were taking a variety of medications at the time of scanning which we were not able to control for in this analysis.

6.5 Conclusion

We have developed upon previous work that has identified IEDs as an important contributor to stimulus driven functional connectivity. We have extended these findings using a multivariate data driven framework to a heterogeneous population of focal epilepsy patients at rest. We have identified the FC of the default mode network and the expressive language network as being associated with changes in IEDs. We found no evidence that these differences are associated with sustained abnormal neural dynamics as measured by metastability. Interestingly IEDs were associated with increased connectivity of the piriform cortex and caudate to the default mode network. This effect appears quite general as the focal epilepsy population studied was quite heterogeneous. Moreover this suggests a canonical mechanism by which focal epileptic activity may involve intrinsic connectivity networks in humans via regions of high connectivity (caudate) and epileptogenicity.

6.6 References

Aarts, J. H. P., Binnie, C. D., Smit, A. M., & Wilkins, A. J. (1984). Selective cognitive impairment during focal and generalized epileptiform eeg activity. *Brain*, *107*(1), 293–308. http://doi.org/10.1093/brain/107.1.293

Aja-Fernández, S., & Tristán-Vega, A. (2013). A review on statistical noise models for Magnetic Resonance Imaging. *Tech Report of the LPI, TECH-LPI2013-01, Universidad de Valladolid, Spain,*.

Berg, A. T., Berkovic, S. F., Brodie, M. J., Buchhalter, J., Cross, J. H., Van Emde Boas, W., … Scheffer, I. E. (2010). Revised terminology and concepts for organization of seizures and epilepsies: Report of the ILAE Commission on Classification and Terminology, 2005-2009. *Epilepsia*, *51*(4), 676–685. http://doi.org/10.1111/j.1528-1167.2010.02522.x

Centeno, M., & Carmichael, D. W. (2014). Network connectivity in epilepsy: Resting state fMRI and EEG-fMRI contributions. *Frontiers in Neurology*, *5 JUL*(July). http://doi.org/10.3389/fneur.2014.00093

Centeno, M., Tierney, T. M., Perani, S., Shamshiri, E. a, StPier, K., Wilkinson, C., … Carmichael, D. W. (2016). Optimising EEG-fMRI for Localisation of Focal Epilepsy in Children. *PloS One*, *11*(2), e0149048. http://doi.org/10.1371/journal.pone.0149048

Croft, L. J., Baldeweg, T., Sepeta, L., Zimmaro, L., Berl, M. M., & Gaillard, W. D. (2014). Vulnerability of the ventral language network in children with focal epilepsy. *Brain*, *137*(8), 2245–2257. http://doi.org/10.1093/brain/awu154

Demirtas, M., Tornador, C., Falcon, C., Lopez-Sola, M., Hernandez-Ribas, R., Pujol, J., … Deco, G. (2016). Dynamic functional connectivity reveals altered variability in functional connectivity among patients with major depressive disorder. *Human Brain Mapping*, *37*(8), 2918–2930. http://doi.org/10.1002/hbm.23215

Fahoum, F., Lopes, R., Pittau, F., Dubeau, F., & Gotman, J. (2012). Widespread epileptic networks in focal epilepsies: EEG-fMRI study. *Epilepsia*, *53*(9), 1618–1627. http://doi.org/10.1111/j.1528-1167.2012.03533.x

Flanagan, D., Badawy, R. a B., & Jackson, G. D. (2014). EEG-fMRI in focal epilepsy: Local activation and regional networks. *Clinical Neurophysiology*, *125*(1), 21–31. http://doi.org/10.1016/j.clinph.2013.06.182

Glerean, E., Salmi, J., Lahnakoski, J. M., Jääskeläinen, I. P., & Sams, M. (2012). Functional Magnetic Resonance Imaging Phase Synchronization as a Measure of Dynamic Functional Connectivity. *Brain Connectivity*, *2*(2), 91–101. http://doi.org/10.1089/brain.2011.0068

Glorfeld, L. W. (1995). An Improvement on Horn's Parallel Analysis Methodology for Selecting the Correct Number of Factors to Retain. *Educational and Psychological Measurement*, *55*(3), 377–393. http://doi.org/10.1177/0013164495055003002

Hellyer, P. J., Scott, G., Shanahan, M., Sharp, D. J., & Leech, R. (2015). Cognitive Flexibility through Metastable Neural Dynamics Is Disrupted by Damage to the Structural Connectome. *Journal of Neuroscience*, *35*(24), 9050–9063. http://doi.org/10.1523/JNEUROSCI.4648-14.2015

Horn, J. (1965). A rationale and test for the number of factors in factor analysis. *Psychometrika*, *30*, 179–185.

Iannotti, G. R., Grouiller, F., Centeno, M., Carmichael, D. W., Abela, E., Wiest, R., … Vulliemoz, S. (2016). Epileptic networks are strongly connected with and without the effects of interictal discharges. *Epilepsia*, *57*(7), 1086–1096. http://doi.org/10.1111/epi.13400

Ibrahim, G. M., Morgan, B. R., Lee, W., Smith, M. Lou, Donner, E. J., Wang, F., … Carter Snead, O. (2014). Impaired development of intrinsic connectivity networks in children with medically intractable localization-related epilepsy. *Human Brain Mapping*, *35*(11), 5686–5700. http://doi.org/10.1002/hbm.22580

Laufs, H., Richardson, M. P., Salek-Haddadi, a., Vollmar, C., Duncan, J. S., Gale, K., … Koepp, M. J. (2011). Converging PET and fMRI evidence for a common area involved in human focal epilepsies. *Neurology*, *77*(9), 904–910. http://doi.org/10.1212/WNL.0b013e31822c90f2

Laumann, T. O., Snyder, A. Z., Mitra, A., Gordon, E. M., Gratton, C., Adeyemo, B., … Petersen, S. E. (2016). On the Stability of BOLD fMRI Correlations. *Cerebral Cortex*, 1–14. http://doi.org/10.1093/cercor/bhw265

Piredda, S., & Gale, K. (1985). A crucial epileptogenic site in the deep prepiriform cortex. *Nature*, *317*(6038), 623–625. http://doi.org/10.1038/317623a0

Price, C. J. (2012). A review and synthesis of the first 20 years of PET and fMRI studies of heard speech, spoken language and reading. *NeuroImage*, *62*(2), 816–47. http://doi.org/10.1016/j.neuroimage.2012.04.062

R Core team. (2015). R Core Team. *R: A Language and Environment for Statistical Computing. R Foundation for Statistical Computing , Vienna, Austria. ISBN 3-900051-07-0, URL http://www.R-Project.org/.*

Revelle, W. (2016). psych: Procedures for Personality and Psychological Research. *R Package*, 1–358.

Shamshiri, E. A., Tierney, T. M., Centeno, M., St Pier, K., Pressler, R. M., Sharp, D. J., … Carmichael, D. W. (2016). Interictal activity is an important contributor to abnormal intrinsic network connectivity in paediatric focal epilepsy. *Human Brain Mapping*, *00*(August), 1–16. http://doi.org/10.1002/hbm.23356

Simony, E., Honey, C. J., Chen, J., Lositsky, O., Yeshurun, Y., Wiesel, A., & Hasson, U. (2016). Dynamical reconfiguration of the default mode network during narrative comprehension. *Nature Communications*, *7*(May 2015), 1–13. http://doi.org/10.1038/ncomms12141

Tavor, I., Parker Jones, O., Mars, R. B., Smith, S. M., Behrens, T. E., & Jbabdi, S. (2016). Task-free MRI predicts individual differences in brain activity during task performance. *Science (New York, N.Y.)*, *352*(6282), 216–20. http://doi.org/10.1126/science.aad8127

Tierney, T. M., Weiss-Croft, L. J., Centeno, M., Shamshiri, E. a., Perani, S., Baldeweg, T., … Carmichael, D. W. (2016). FIACH: A biophysical model for automatic retrospective noise control in fMRI. *NeuroImage*, *124*, 1009–1020. http://doi.org/10.1016/j.neuroimage.2015.09.034

Tzourio-Mazoyer, N., Landeau, B., Papathanassiou, D., Crivello, F., Etard, O., Delcroix, N., … Joliot, M. (2002). Automated anatomical labeling of activations in SPM using a macroscopic anatomical parcellation of the MNI MRI single-subject brain. *NeuroImage*, *15*(1), 273–89. http://doi.org/10.1006/nimg.2001.0978

Van den Heuvel, M. P., Stam, C. J., Kahn, R. S., & Hulshoff Pol, H. E. (2009). Efficiency of functional brain networks and intellectual performance. *The Journal of Neuroscience : The Official Journal of the Society for Neuroscience*, *29*(23), 7619–7624. http://doi.org/10.1523/JNEUROSCI.1443-09.2009

Vaughan, D. N., & Jackson, G. D. (2014). The piriform cortex and human focal epilepsy. *Frontiers in Neurology*, *5*(DEC), 1–18. http://doi.org/10.3389/fneur.2014.00259

Warren, A. E. L., Abbott, D. F., Vaughan, D. N., Jackson, G. D., & Archer, J. S. (2016). Abnormal cognitive network interactions in Lennox-Gastaut syndrome: A potential mechanism of epileptic encephalopathy. *Epilepsia*, *57*(5), 812–822. http://doi.org/10.1111/epi.13342

Whitfield-Gabrieli, S., & Nieto-Castanon, A. (2012). Conn: A Functional Connectivity Toolbox for Correlated and Anticorrelated Brain Networks. *Brain Connectivity*, *2*(3), 125–141. http://doi.org/10.1089/brain.2012.0073

Wiesmann, M., Kopietz, R., Albrecht, J., Linn, J., Reime, U., Kara, E., … Stephan, T. (2006). Eye closure in darkness animates olfactory and gustatory cortical areas. *NeuroImage*, *32*(1), 293–300. http://doi.org/10.1016/j.neuroimage.2006.03.022

7. Conclusions and Future Research

This thesis sought to develop and apply fMRI in the context of paediatric focal epilepsy. This posed a number of challenges, the first being subject motion. In Chapter 3 we have demonstrated that the effects of motion can be controlled for in tasks that involve overt speech in children. This is an area of crucial importance because the ability to map the areas of the brain responsible for speech production is crucial to optimising surgical procedures in children with focal epilepsy. To achieve this biophysical model named FIACH was developed in order to identify spurious signal changes in fMRI data that are associated with motion. This model has been implemented at Great Ormond Street Hospital to optimise the mapping of language function in children with focal epilepsy demonstrating immediate translation.

However the model's impact has not been specific to paediatric focal epilepsy. It has been used to improve data quality in acquisitions with limited signal to noise ratio such as simultaneous intracranial EEG-fMRI, simultaneous stimulation-intracranial EEG-fMRI and fMRI studies in healthy adults studying the function of the inferior temporal lobe. It has also been used to study drug-naïve paediatric patients with generalised epilepsy. It has even been applied to the study of memory function in individuals with Alzheimer's.

Despite the success of the model's application it is not an ideal correction method for the effects of motion. If a motion event causes a signal change that has magnitude similar to a normal BOLD response it will not be corrected. This means there will still be many motion related signal changes in the data. However there will not be any signal changes capable of radically biasing parameter estimation. Ideally data should be acquired at the best quality possible. This has become more feasible due to the advent of prospective motion correction (PMC) systems which dynamically track motion at incredibly high temporal resolution (80fps) and subsequently update the scanner gradients in real time to improve the data quality. A comparison of parameter estimation using FIACH vs PMC would ideally clarify what motion events FIACH can and cannot correct.

A subsequent issue is the bias that FIACH introduces to the estimation of the standard error of the t-statistic. To calculate the standard error of the t-statistic the degrees of freedom must be known. However, FIACH essentially functions as a non-linear filter which reduces the degrees of freedom by replacing motion corrupted time points with values from an interpolation procedure. Ideally this should be accounted for. This could be possible if multiple imputation was performed (a statistical technique designed to address the issue of “missing data”). However, the development of this method in the context of fMRI was not pursued during the course of this PhD.

To address the issue of physiological noise in fMRI in chapter 3 we have extended FIACH to identify areas of the brain with high blood volume (large vessels) which contribute substantially to physiological noise. Having automatically identified these areas we model their effects on the fMRI time series using principal components analysis to derive a parsimonious model. This model was validated in a comparison with six other methods of retrospective noise control. However the model is not specific to identifying areas of high blood volume capable of producing physiological noise. There are a number of other factors that can contribute to large changes in signal variance in fMRI. Most notably increased Iron content in the basal ganglia would elevate signal variance. Ideally the model should be adapted to be more specific to identifying areas of high blood volume.

The issue of quality assurance in the application of simultaneous EEG-fMRI is an important one. In Chapter 4 we have identified what metrics can and cannot predict clinical utility (defined here as obtaining a localisation of the presumed epileptogenic zone) of simultaneous EEG-fMRI before the analysis is performed. We were able to identify design efficiency as an important predictor of clinical utility. We have also quantified the reduction in subject motion that can be achieved by utilising a natural stimulus (cartoon watching) without reducing epileptic discharge rate. Both of these results are important due to their impact in the clinical and research setting. Firstly, in the research setting statistical power can be realistically determined prior to analysis by calculating design efficiency. In the clinical setting we can display

low level stimuli with confidence knowing that compliance can be improved without the risk of reducing epileptic activity and thus negatively affecting statistical power.

In chapter 4 it was noted that Bonferroni correction was always a more sensitive correction for multiple comparisons than Random Field Theory (RFT). Therefore in chapter 5 we characterised sensitivity when RFT is employed to analyse fMRI data. Furthermore this sensitivity issue was found to be a widespread problem in the current literature and largely reflects poor understanding of the current methods utilised for statistical analysis of fMRI data. We provide simulations that can be used to determine the parameters necessary to avoid this loss in sensitivity and to identify regimes in which the parametric methods should and should not be used.

Future work will centre on trying to develop Random Field Theory in the regimes identified in this thesis where its application resulted in poor sensitivity (low smoothness). This will be important for clinical studies utilising fMRI as it means that optimal sensitivity will be achieved for identifying the epileptogenic zone or mapping the brain areas responsible for speech and language. Furthermore this work will also be extended to examine high resolution fMRI where the high levels of smoothness required by RFT are not plausible to achieve.

Finally, in chapter 6 having focused heavily on data quality and statistical analysis throughout the thesis, we were capable of characterising how the brain's functional organisation at rest is influenced by the occurrence of Interictal Epileptiform Discharges (IEDs) in paediatric focal epilepsy. A novel finding was that the piriform cortex (an epileptogenic trigger zone) and caudate (an area of high connectivity) were commonly found to increase their functional connectivity to the Default Mode Network (DMN) as a function of IEDs. This suggests a common basis for the widespread effects of focal IEDs from different brain regions whereby the DMN and epileptic network appear to interact via the piriform cortex and caudate.

Ultimately this thesis outlines the challenges faced when one attempts to apply fMRI in the context of paediatric focal epilepsy. However, this thesis

also provides methods/practical advice to address these challenges. This thesis therefore highlights the potential of applying fMRI in the context of paediatric focal epilepsy despite the challenges faced.